POLYTECHNIQUE MONTRÉAL

affiliée à l'Université de Montréal

Imaging cerebral oxygenation alterations in an Alzheimer mouse model

XUECONG LU

Institut de génie biomédical

Thèse présentée en vue de l'obtention du diplôme de *Philosophiæ Doctor*

Génie biomédical

Juin 2019

POLYTECHNIQUE MONTRÉAL

affiliée à l'Université de Montréal

Cette thèse intitulée :

Imaging cerebral oxygenation alterations in an Alzheimer mouse model

présentée par **Xuecong LU**

en vue de l'obtention du diplôme de *Philosophiae Doctor*

a été dûment acceptée par le jury d'examen constitué de :

Farida CHERIET, présidente

Frédéric LESAGE, membre et directeur de recherche

Christos BOUTOPOULOS, membre

Hui WANG, membre externe

DEDICATION

To my family

ACKNOWLEDGEMENTS

First and foremost I would like to express my sincere thanks to my doctoral supervisor, Professor Frédéric Lesage, for supervising and guiding me as a Ph. D. student in his research group. His immense knowledge and expertise in my research project have contributed tremendously to the completion of this thesis. Discussion with Prof. Lesage is always enjoyable and encouraging, thanks to his kindness, patience, confidence, and profound knowledge in biomedical brain imaging. Whenever I have difficulty in formulating my ideas, conducting experiments, or article writing, Prof. Lesage would always be there to offer me valuable advice and help me solve these problems during my study. Without his support and great assistance, my research project would not be completed, and this thesis would not be finished. I owe a debt of gratitude to his sustained assistance, patient guidance, and charming personality during my study here and in the rest of my life.

I also would like to express my gratitude all staff from the Montreal Heart Institute animal facility, especially Marc-Antoine Gillis and Natacha Duquette, who were kind mentors and tought me necessary experimental skills. They also assisted me with animal preparation and experiments, thus facilitating my data collection for this thesis.

I would like to sincerely thank Dr. Philippe Pouliot who gave me great comments and advice during my study. This thesis also benefits from his in-depth knowledge in MRI imaging, and I very much appreciate Dr. Philippe Pouliot's kind support to data collection and analysis in my projects.

I am also thankful for the coauthors of my papers: Yuankang Lu, Rafat Damseh, Mohammad Moeini, Baoqiang Li, Samuel Bélanger, Olivia de Montgolfier, Éric Thorin, Philippe Pouliot, and Sava Sakadžić, who have greatly assisted me in my doctoral study and improved the overall quality of the papers. I am grateful to know all the members at the LIOM lab at Polytechnique of Montreal: Hanieh Mohammadi, Parikshat Sirpal, Cong Zhang, Ke Peng,

Mehran Sharafi, Alexandre Castonguay, Clément Bonnéry, Michèle Desjardins, Edgar Guevara, Samuel Bélanger, Mahnoush Amiri, Maxime Abran, Joël Lefebvre, Yuankang Lu, Ghada Jerbi, Maryam Tabatabaei, Rafat Damseh, Pier-Luc Tardif, Luis Akakpo, Azadeh Naderian, Mohammad Moeini, and Baoqiang Li. It is great to know these nice people who bring fun to my study and life.

I would like to express my endless thankfulness to my family members who always support and encourage me. Whatever challenges I meet during my study, you always have confidence in me and give me constant assistance. I am gratefully that you share all my happiness and sorrow all the time with me in my study and in the rest of my life.

Finally, I would like to wholeheartedly express my appreciation and gratitude to my doctoral supervisor, Prof. Frédéric Lesage, for his enormous assistance and generous support during my doctoral study and life. His patient guidance and direction in my research projects have always sparked my interests in this field and will benefit my future research career.

RÉSUMÉ

Cette thèse a pour objectif d'explorer l'oxygénation cérébrale en exploitant un système de microscopie à deux photons combiné à un colorant phosphorescent sensible à la pression d'oxygène, le PO_2. La combinaison du colorant phosphorescent au système à deux photons permet une mesure de l'oxygène avec une excellente résolution spatiale et temporelle, facilitant la recherche de sur l'oxygénation des tissus, en particulier dans les situations pathologiques. À cette fin, la microscopie laser à deux photons a d'abord été associée au colorant phosphorescent, tandis que d'autres techniques d'imagerie, y compris l'imagerie optique de signaux intrinsèques (ISOI), l'imagerie par résonance magnétique (IRM) et la tomographie par cohérence optique ont pu fournir des informations complémentaires dans les études qui ont été faites. Nos travaux ont visé l'étude de modèles murins de la maladie d'Azheimer (AD) pour explorer les altérations de l'oxygénation cérébrale dans ces modèles. Les résultats accumulés ont fait l'objet de publications qui ont été soumises à trois revues avec comité de lecture.

Dans le premier travail, nous avons cherché à examiner 1) si l'oxygénation du cerveau est compromise par l'apparition de la maladie d'Alzheimer et 2) comment l'exercice physique volontaire module l'influence de la maladie d'Alzheimer sur l'oxygénation du cerveau. Bien que les contributions vasculaires à la démence et à la maladie d'Alzheimer soient de plus en plus reconnues, la perturbation potentielle de l'oxygénation du cerveau associée à la maladie et le fait que les stratégies de prévention visant à maintenir l'oxygénation des tissus soient bénéfiques ont des causes qui restent largement inconnues. Nos résultats montrent que la pression partielle d'oxygène du tissu cérébral (PO_2) a diminué avec l'apparition de la maladie d'Alzheimer. Cette réduction de la PO_2 était associée à la présence de petites zones spatiales presque hypoxiques, à une fraction accrue d'extraction d'oxygène et à une réduction du débit sanguin, observations qui ont toutes été annulées par l'exercice. L'Alzheimer et l'âge ont également accru l'hétérogénéité spatiale de l'oxygénation du tissu cérébral, qui fut par ailleurs

normalisée par l'exercice. Une coloration ex vivo du tissu cérébral a également montré moins de dépôts d'amyloïde-β (Aβ) dans le groupe d'exercice. Enfin, nous avons observé des corrélations entre la distance de course volontaire et l'oxygénation des tissus cérébraux / le flux sanguin, suggérant une relation dose-réponse de l'exercice sur le cerveau.

Le deuxième article avait pour objectif de caractériser, dans une seconde cohorte de souris, les modifications de l'hémodynamique capillaire avec l'Alzheimer et le rôle modulateur de l'exercice, étant donné le rôle fondamental des capillaires dans le transport de l'oxygène vers les tissus et les bénéfices proposés de l'exercices pour la maladie d'Alzheimer. Nous avons constaté des altérations hémodynamiques et une densité vasculaire plus faible chez la souris Alzheimer, inversées par l'exercice. Nous avons en outre observé que les propriétés des capillaires étaient dépendantes de l'ordre des branches et que la stimulation évoquait des changements atténués par l'Alzheimer mais augmentés par l'exercice. Notre étude fournit de nouvelles informations sur les perturbations de la microcirculation cérébrale avec la maladie et sur le rôle modulateur de l'exercice volontaire sur ces altérations.

Le dernier article avait pour objectif d'explorer les modifications de l'oxygénation des tissus évoquées par un stimulus dans le même modèle animal, et d'explorer plus avant les facteurs modulateurs, notamment l'exercice et l'hypertension, responsables de ces modifications. La microscopie à deux photons in vivo a été utilisée pour étudier les modifications locales de l'oxygénation du tissu cérébral avec la maladie et sa modulation par l'exercice et l'hypertension chez la souris transgénique suivant une stimulation des moustaches. Nous avons observé une décroissance plus rapide de la PO_2 tissulaire entourant les artérioles et une plus grande hétérogénéité de la PO_2 dans le groupe de pathologies doubles (AD et hypertension). Nos résultats ont également montré une valeur de base inférieure de la PO_2 dans le groupe AD, exacerbée par l'hypertension artérielle alors qu'elle était inversée par l'exercice.

Globalement, ces études suggèrent que l'oxygénation cérébrale compromise est un indicateur de l'apparition de l'Alzheimer, avec l'apparition de mécanismes délétères potentiels associés à l'hypoxie. L'exercice volontaire a amélioré le processus d'oxygénation neurovasculaire, offrant

potentiellement un moyen de retarder ces changements dans la maladie, alors que des maladies vasculaires telles que l'hypertension pourraient exacerber la perturbation de l'oxygénation.

ABSTRACT

This thesis aims to explore the cerebral oxygenation by eploiting two photon microscopywith a phosphorescence PO_2 sensitive dye. Combining the phosphorescence dye to the two-photon system enables better spatial and temporal resolution compared to other oxygen measurement methods (e.g., mass spectroscopy and polarography), facilitating the investigation of oxygenation in tissues especially in pathological situations. Toward this end, two-photon laser microscopy was combined with the phosphorescence dye first, while other imaging techniques, including intrinsic signal optical imaging (ISOI), magnetic resonance imaging (MRI), and optical coherence tomography (OCT) were also used to provide complementary information (e.g., changes of oxygenated hemoglobin, blood perfusion, and blood flow). All imaging methods were used to investigate a mouse model of Azheimer's disease (AD) to explore the oxygenation alterations in the brain. Results from these studies have been submitted to three peer-reviewed journals.

In the first endeavor, we aimed to examine 1) whether brain oxygenation is compromised by the onset of AD and 2) how voluntary exercise modulates the influence of AD on brain oxygenation. While vascular contributions to dementia and AD are increasingly recognized, the potential brain oxygenation disruption associated with AD and whether preventive strategies to maintain tissue oxygenation are beneficial remain largely unknown. Our results show that cerebral tissue oxygen partial pressure (PO2) decreased with the onset of AD. Reduced PO2 was associated with the presence of small near-hypoxic areas, an increased oxygen extraction fraction, and reduced blood flow. The observations were all reverted by exercise. AD and age also increased the spatial heterogeneity of brain tissue oxygenation, which was homogenized by exercise. Immunohistological staining also showed fewer amyloid-β (Aβ) deposits in the exercise group. Finally, we observed correlations between voluntary running distance and cerebral tissue oxygenation/blood flow, suggesting a dose-response relationship of exercise on the brain.

The second article aimed to characterize the changes in capillary hemodynamics with AD and the modulating role of exercise, given the fundamental role of capillaries in the oxygen transport to tissue and the propoosed benefits of exercise to AD. We found hemodynamic alterations and lower vascular density with AD, reversed by exercise. We further observed that capillary properties were branch order dependent and that stimulation evoked changes were attenuated with AD but increased by exercise. Our study provides novel insights into cerebral microcirculatory disturbances with AD and the modulating role of voluntary exercise on these alterations.

The last paper aimed to explore the stimulus-evoked tissue oxygenation changes in the model of AD and further explore modulating factors, including exercise and hypertension, for these changes. In vivo two-photon phosphorescence lifetime microscopy was used to investigate local changes of brain tissue oxygenation with AD and its modulation by exercise and hypertension in the transgenic AD mice under whisker stimulation. We observed faster decay of tissue PO_2 surrounding arterioles and more PO2 heterogeneity in the group of dual pathology (both AD and hypertension). Our results also showed lower baseline tissue PO2 value in the AD group, exacerbated by hypertension but reversed by exercise.

Overall, this these studies suggest that compromised brain oxygenation is an indicator of the onset of AD, with the emergence of potential deleterious mechanisms associated with hypoxia. Voluntary exercise enhanced the neurovascular oxygenation process, potentially offering a means to delay these changes in AD, whereas vascular disease such as hypertension could exacerbate the oxygenation disruption in AD.

TABLE OF CONTENTS

LIST OF TABLES

LIST OF FIGURES

LIST OF SYMBOLS AND ABBREVIATIONS

AD Alzheimer's disease

MRI Magnetic resonance imaging

IOSI Intrinsic optical signal imaging

OCT Optical Coherence Tomography

RBC Red blood cells

CBF Cerebral blood flow

VSMC Vascular smooth muscle cell

BBB Blood brain barrier

PO_2 Partial pressure of oxygen

Δ[HBO](t) Changes in oxy-hemoglobin concentration

Δ[HBR](t) Changes in deoxy-hemoglobin concentration

Δ[HBT](t) Changes in total hemoglobin concentration

Aβ Beta-amyloid

EPR Electron parametric resonance

APP-PS1 Amyloid precursor protein and presenilin 1

CHAPTER 1 INTRODUCTION

1.1 Overview

Alzheimer's disease (AD) is a chronic neurodegenerative disease whose symptoms slowly occur and gradually worsen over time (Gaugler et al., 2018). According to a recent report ("Latest information and statistics," 2018), half a million Canadians live with AD-related dementia, and this number is expected to get doubled in the next ten years. Since AD brings significant burden to patients, their family members and caregivers, and the national health care system, understanding the mechanism of AD progression and potential treatment to delay or even cure AD patients is of great interest to healthcare practitioners and researchers.

From a neurovascular perspective, AD can cause cerebral hypoperfusion and cerebrovascular disorders, which, in turn, impair normal neuron functioning and cognitive function (Grammas, 2011; Iadecola, 2017, 2010a, 2004; Sweeney et al., 2011). The reduced supply of oxygen to brain tissue may not support the metabolic and oxidative demand of neuron cells, leading to cognitive malfunction. Beyond deleterious consequences on cognition (Iadecola, 2010a), AD has been associated with changes in brain vascular characteristics including thickening of endothelial basement membranes, variable capillary diameters and reduced capillary density, and pericyte loss. In addition, cerebral blood flow (CBF) may become uncoupled with the underlying tissue metabolic needs, leading to homeostatic imbalance and brain dysfunction (Devor et al., 2011). Since oxygen supply is essential for normal functioning of the brain and CBF needs to be finely regulated to meet neural metabolic demand, cerebral oxygenation represents an important marker of healthy versus unhealthy aging. Therefore, alterations of brain tissue oxygenation can indicate the functioning of brain and shed light on the mechanisms of neurovascular diseases from the perspective of oxidative metabolism.

Combining a novel two-photon enhanced phosphorescent dye, PtP-C343, to the two-photon laser system enables better spatial and temporal resolution reaching depths of hundreds of

micrometers under the brain surface, facilitating the investigation of oxygenation in tissues especially in pathological situations. Therefore, two-photon laser microscopy was combined with the phosphorescence dye to quantify the cerebral oxygenation in neurovascular diseases, while other imaging techniques, including intrinsic signal optical imaging (ISOI), magnetic resonance imaging (MRI), and optical coherence tomography (OCT), were also used to provide complementary measurements.

1.2 Organization of the thesis by objectives

There are three objectives in this thesis, and each objective is associated with an article and relevant hypotheses.

Objective 1: Monitor the changes of brain tissue oxygenation in a mouse model of AD (APP-PS1) and explore the modulating effect of voluntary exercise on oxygenation.

Hypothesis 1-1: Brain tissue oxygenation is compromised by the onset of AD, expressed by attenuated tissue PO2, the presence of hypoxia, and heterogeneity of tissue PO2.

Hypothesis 1-2: Exercise modulates tissue oxygenation alterations in AD, thus alleviating oxidative stress.

Article 1: **Lu X**, Moeini M, Li B, de Montgolfier O, Lu Y, Bélanger S, Thorin E, Lesage F, Voluntary exercise increases brain tissue oxygenation and spatially homogenizes oxygen delivery in a mouse model of Alzheimer's Disease. Neurobiology of Aging, (Provisional acceptance).

Objective 2: Quantify the changes in capillary red-blood-cell (RBC) dynamics with AD and the modulation of exercise on cerebral capillaries to explore microvascular alterations in AD.

Hypothesis 2-1: Capillary hemodynamic changes are associated with the presence of AD, expressed through capillary diameter, RBC flux, velocity, hematocrit variations, and the overall RBC flow.

Hypothesis 2-2: Exercise plays a modulating role on the alterations of capillary RBC

dynamics.

Article 2: **Lu X**, Moeini M, Li B, Lu Y, Damseh R, Pouliot P, Thorin E, Lesage F, Changes in capillary hemodynamics and its modulation by exercise in the APP-PS1 Alzheimer mouse model. Frontiers in Neuroscience (First-round review).

Objective 3: Investigate the stimulus-evoked tissue oxygenation changes in a model of AD and further explore the modulating factors, including exercise and hypertension, for these changes.

Hypothesis 3-1: The stimulus-evoked tissue oxygenation changes differ between AD mice and control mice.

Hypothesis 3-2: Hypertension has modulating effects on the stimulus-evoked tissue oxygenation changes in AD.

Article 3: **Lu X**, Moeini M, Li B, Thorin E, Lesage F, Hypertension accelerates cerebral tissue PO2 disruption in Alzheimer's disease during stimulation. Neuroscience Letters, Under review.

Beyond the above three peer-reviewed articles, my word directly, or through collaborations, led to other conference papers and co-authored journal articles published during the doctoral study. These publications resulted from my implication in performing experiments using two-photon microscopy or cerebral tissue oxygenation and are listed below for reference.

- Moeini M, **Lu X**, Bélanger S, Picard F, Boas D, Kakkar A, Lesage F. Cerebral tissue pO2 response to stimulation is preserved with age in awake mice. Neuroscience letters. 2019, 699 (160-166).
- Moeini M, **Lu X**, Avti PK, Damseh R, Bélanger S, Picard F, Boas D, Kakkar A, Lesage F. Compromised microvascular oxygen delivery increases brain tissue vulnerability with age. Scientific reports. 2018 May 29;8(1):8219.
- **Lu X**, Moeini M, Li B, de Montgolfier O, Lu Y, Bélanger S, Thorin E, Lesage F. Brain

tissue oxygenation is modulated by voluntary exercise in AD awake mice. Brain & Brain Pet 2019 Conference, July 2019, Japan.

- **Lu X**, Moeini M, Li B, Lu Y, Damseh R, Pouliot P, Thorin E, Lesage F, Effect of exercise on capillary red blood cell dynamics in transgenic AD mice. Brain & Brain Pet 2019 Conference, July 2019, Japan.
- **Lu X**, Moeini M, Li B, Zhang C, Sakadžić S, Lesage F. 3D brain oxygenation measurements in awake hypertensive mice using two photon phosphorescence lifetime imaging. InMultiphoton Microscopy in the Biomedical Sciences XVIII 2018 Feb 23 (Vol. 10498, p. 104981Y). International Society for Optics and Photonics.
- **Lu X**, Moeini M, Li B, Sakadžić S, Lesage F. Voluntary exercise confers protection against age-related deficits in brain oxygenation in awake mice model of Alzheimer's disease. InNeural Imaging and Sensing 2018 2018 Feb 12 (Vol. 10481, p. 104811G). International Society for Optics and Photonics.
- Zhang C, Tabatabaei M, Bélanger S, Girouard H, Moeini M, **Lu X**, Lesage F. In vivo measurement of astrocytic endfoot Ca 2+ and parenchymal vessel responses during 4-AP induced epilepsy using two-photon fluorescence lifetime microscopy. InMultiphoton Microscopy in the Biomedical Sciences XVIII 2018 Feb 23 (Vol. 10498, p. 104980X). International Society for Optics and Photonics.
- Zhang C, Tabatabaei M, Bélanger S, Girouard H, Moeini M, **Lu X**, Lesage F. Astrocytic endfoot Ca2+ correlates with parenchymal vessel responses during 4-AP induced epilepsy: An in vivo two-photon lifetime microscopy study. Journal of Cerebral Blood Flow & Metabolism. 2017 Feb;39(2):260-71.
- Moeini M, **Lu X**, Tam T, Bélanger S, Kakkar A, Lesage F. Brain tissue oxygenation changes with age in awake mice. Cerebral Blood Flow and Metabolism. 37(57), 2017.
- **Lu X**, Li B, Moeini M, Lesage F. Simultaneous two-photon imaging of cerebral oxygenation and capillary blood flow in atherosclerotic mice. InNeural Imaging and Sensing 2017 Feb 8 (Vol. 10051, p. 100510O). International Society for Optics and

Photonics.

This thesis is structured as follows. The second chapter provides a literature review of brain function changes in pathology and the mechanisms by which such changes occur. The third chapter reviews various methods that can be sued to quantify brain oxygenation and elucidate the principles of the methods used in our studies and their advantages. The fourth, fifth, and sixth chapters present the articles submitted to peer-reviewed journals. The seventh chapter discusses these studies in general in the context of the objectives set, and the last chapter provides a brief conclusion over these studies.

CHAPTER 2 LITERATURE REVIEW

2.1 Alzheimer's pathology

AD is characterized as a neurodegenerative disease and can lead to dementia whose symptoms include difficulties with memory, language, and other cognitive abilities for everyday activities (Gaugler et al., 2018). AD begins years before the dementia occurs, and people with AD experience various symptoms over different stages. In the early stage of AD, memory loss and cognitive impairments are sporadic, but becomes increasingly noticeable. However, most people are still capable to function independently. In the moderate stage, individuals experience more mental, personality, and physical changes, such as unpredictable mood swings and disorientation. In the severe stage, individuals depend on caregivers for basic activities of daily life, such as bathing, walking, and dressing. Eventually, their capacity to breathe, swallow, and verbally communicate is deteriorated, and AD is fatal in the final stage. Table 2.1-1 gives a summary of symptoms in different stages of AD. Currently, no effective treatment for AD exists, and much is yet to be explored about the early diagnosis of AD, and how AD could be treated or delayed for its progression (Gaugler et al., 2018).

Table 2-1. Summary of symptoms in different stages of AD.

Stages of AD	Symptoms
Early	Sporadic memory loss and cognitive impairments
Moderate	Mental, personality, and physical changes, such as unpredictable mood swings and disorientation
Severe	Incapability of engaging basic activities, such as bathing, dressing, and walking
Final	Loss of capability to breath, swallow, and communicate

AD leads to progressive cognitive decline and irreversible damage to brain (Bero et al., 2012; Wang et al., 2012). A healthy adult brain has around 100 billion neurons to transmit signals through the brain's neuronal network (Gaugler et al., 2018). However, toxic molecules accumulate in AD brains: beta-amyloid plaques deposit outside neurons cells and abnormal proteins tau accumulate inside neurons in the cortical area (Mueggler et al., 2003), an energetically demanding component of the brain for advanced cognitive functioning (Sakadžić et al., 2014). Beta-amyloid plaques interfere with the neuronal communication, whereas abnormal tau proteins block the transportation of nutrients inside neurons (Gaugler et al., 2018), thus leading to neuronal injury and neurodegeneration.

Besides toxic molecules deposited in the cortex of the brain, cerebral blood flow (CBF), through which oxygen and glucose are delivered to neurons, is also found to be disrupted in the early stages of AD (Kisler et al., 2017a; Zlokovic, 2011). The blood flow changes may develop independently of those toxic molecules and precede neuronal dysfunction in AD that develops later (Kisler et al., 2017a), and thus CBF could serve as an early biomarker for AD. .Compromised CBF leads to disrupted supply to neuronal cells and limited clearance of toxic molecules deposited in the brain (Zlokovic, 2011). In the next section, CBF regulation and neurovascular dysfunction in AD is further discussed.

2.2 Neurovascular coupling dysfunction in AD

2.2.1 Neurovascular coupling

The tight interactions between neuronal activity and CBF control is characterized as neurovascular coupling (Iadecola, 2004; Kisler et al., 2017a). Under physiological conditions, the neurovascular coupling enables efficient supply of CBF to functioning brain areas and diffusion of nutrients and oxygen to neuronal cells distant from sourcing vessels (Iadecola, 2004). CBF is regulated by a coordinated vascular network from artery to vein. Within this vascular network, the cerebral arterioles and capillaries ensure supply of oxygen, glucose and

other nutrients to brain cells, while the venous network facilitates the clearance of waste from the tissue.

Figure 2-1 provides a representation of microvascular unit with cellular and vascular elements that regulate CBF. The arteriole consists of the endothelial cells and the vascular smooth muscle cell (VSMC). The capillary consists of the pericyte and the endothelial cells. The endothelial cells make up the inner layer of the vessel walls, layers of VSMCs ring the arteriole, and the pericyte is attached to capillaries. Neurons innervate VSMCs and pericytes to adjust the dilation of arterioles or capillaries for CBF regulation. There are different types of pericytes depending on their position in the vascular network: transitional pericytes, mid-capillary pericytes, and stellate pericytes. The capillaries branch off the arteriole, and can be labelled by their branching orders (Rungta et al., 2018), such as up-stream capillaries which directly derives from the arterioles and down-stream capillaries which transmit blood to venules. It is critical to label these different vascular compartments, as they may differ in the timing of their dilation during demand and the red blood cell (RBC) velocity to adjust the CBF (Hall et al., 2014; Rungta et al., 2018). Finally, blood returns from downstream capillaries to venules to remove metabolic end products from the neuron cells.

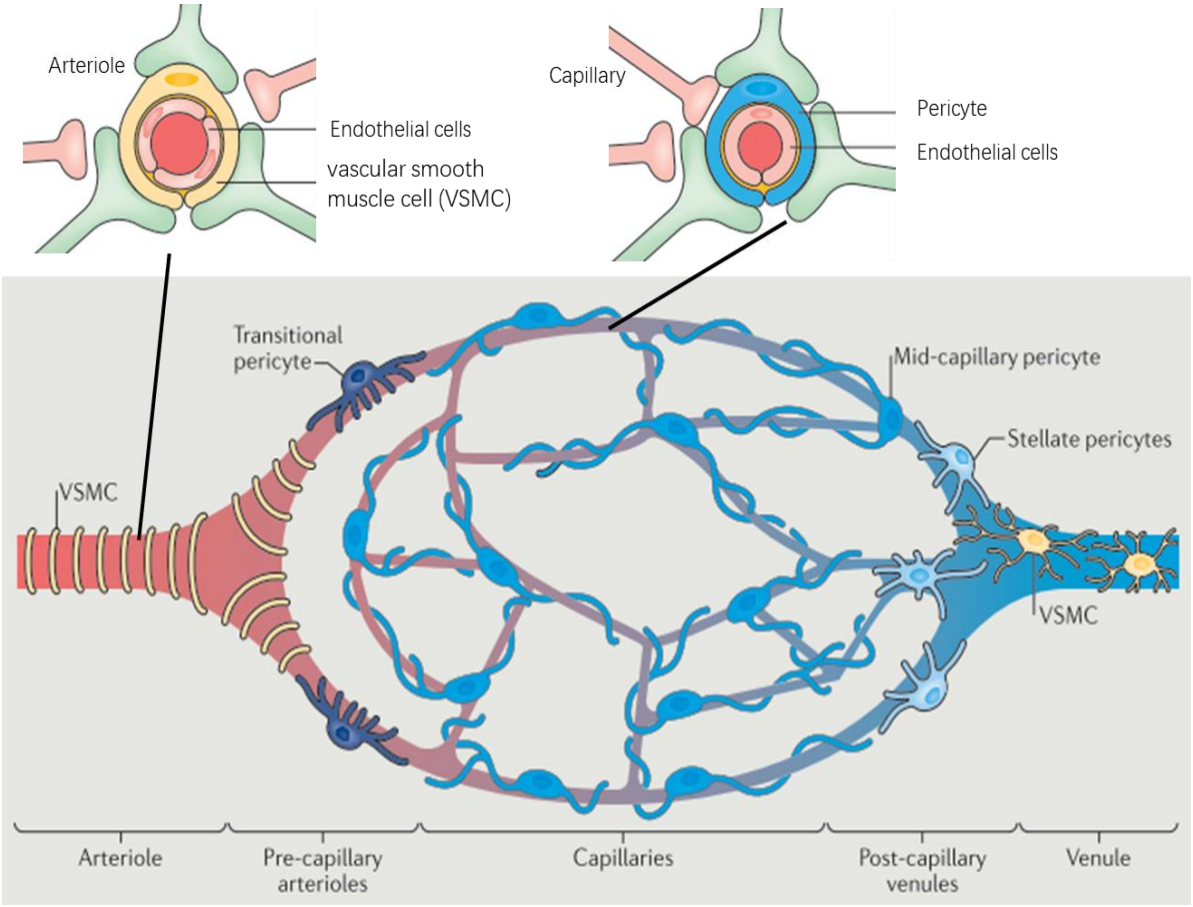

Figure 2-1 Representation of microvascular unit showing vascular and cellular elements regulating CBF (Kisler et al., 2017a).

2.2.2 Neurovascular uncoupling in AD

Prior studies documented that vascular damage and Aβ accumulation both contribute to the onset of AD and dementia (Iadecola, 2010b; Iturria-Medina et al., 2016; Kisler et al., 2017a; Sweeney et al., 2011; Zlokovic, 2011), as illustrated in figure 2-2. On the one hand, vascular damage of the brain has been estimated to contribute to major dementias, including 80% in AD (Hachinski, 2015; Toledo et al., 2013). Multiple risk factors influence vascular functioning, including genetics, vascular disease, and environment (Iadecola, 2013; Kisler et al., 2017a). Vascular damage can lead to neurovascular dysfunction due to constricted arterioles, hypoperfusion, and blood brain barrier (BBB) breakdown (Sweeney et al., 2011;

Zlokovic, 2011). For example, hypertension has been shown to accelerate the progression of AD (Cifuentes et al., 2015), and thus should be jointly considered in the AD pathology. Neurovascular dysfunction can directly lead to neuronal dysfunction due to CBF reduction and toxic accumulation. Additionally, neurovascular dysfunction also contributes to neuronal dysfunction through the mediation effect of Aβ accumulation. CBF dysregulation and impaired toxic clearance could facilitate the deposit of Aβ that is toxic to neuronal cells (Laurent et al., 2012). Vascular changes could even precede neuronal dysfunction and neurodegeneration that develops later on (Kisler et al., 2017a), thus offering a potential diagnostic target for identifying AD in early stages (Farkas andLuiten, 2001; Nielsen et al., 2017). Furthermore, lifestyle, such as exercise, has been found to modulate the influence of vascular damage on cognitive decline and dementia (Adlard et al., 2005; Cahill et al., 2017; Heyn et al., 2004; Larson et al., 2006; Radak et al., 2010; Wong-Goodrich et al., 2010). A biological mechanism associated with positive effects of exercise involves improved cerebral perfusion and CBF (Cahill et al., 2017; Dorr et al., 2017; R.L. et al., 1990).

On the other hand, Aβ accumulation can lead to neuronal deficit independently and synergistically influence neurons through vascular changes (Kisler et al., 2017a). The accumulation of the protein fragment Aβ outside neurons contribute to neuronal injury by disrupting the neuronal communications through synapses (Gaugler et al., 2018; Sweeney et al., 2011). The presence of toxic proteins activates the immune system to clear these toxic fragments as well as debris from dying neurons, leading to chronic inflammation to occur when the immune system cannot keep up with the toxins to be cleared (Nazem et al., 2015). In addition, Aβ accumulation at a low level could lead to an impairment of vascular responses (Kisler et al., 2017a). Previous study using transgenic mice expressing amyloid precursor protein (APP) Swedish mutation found that APP overexpression increased the susceptibility to cerebral ischemic damage due to the Aβ-induced disruption in the functioning of vascular endothelial cells (Zhang et al., 1997). Previous study also found that transgenic mice overexpressing APP and Aβ had a significant decrease in the increase of cerebral blood flow

in response to somatosensory activation, producing a deleterious mismatch between nutrients delivery and energy consumption by neurons (Niwa et al., 2000). CBF decrease was also found in transgenic mice expressing human apolipoprotein E which is a significant risk factor for developing AD (Alata et al., 2015). These studies suggest that Aβ deposition could further deteriorate vascular function and neurovascular coupling, whose dysfunction further facilitates Aβ accumulation and neuronal damage in the brain. Taken together, both pathways, including vascular damage and Aβ production can independently or synergistically lead to neuron damage, contributing to dementia.

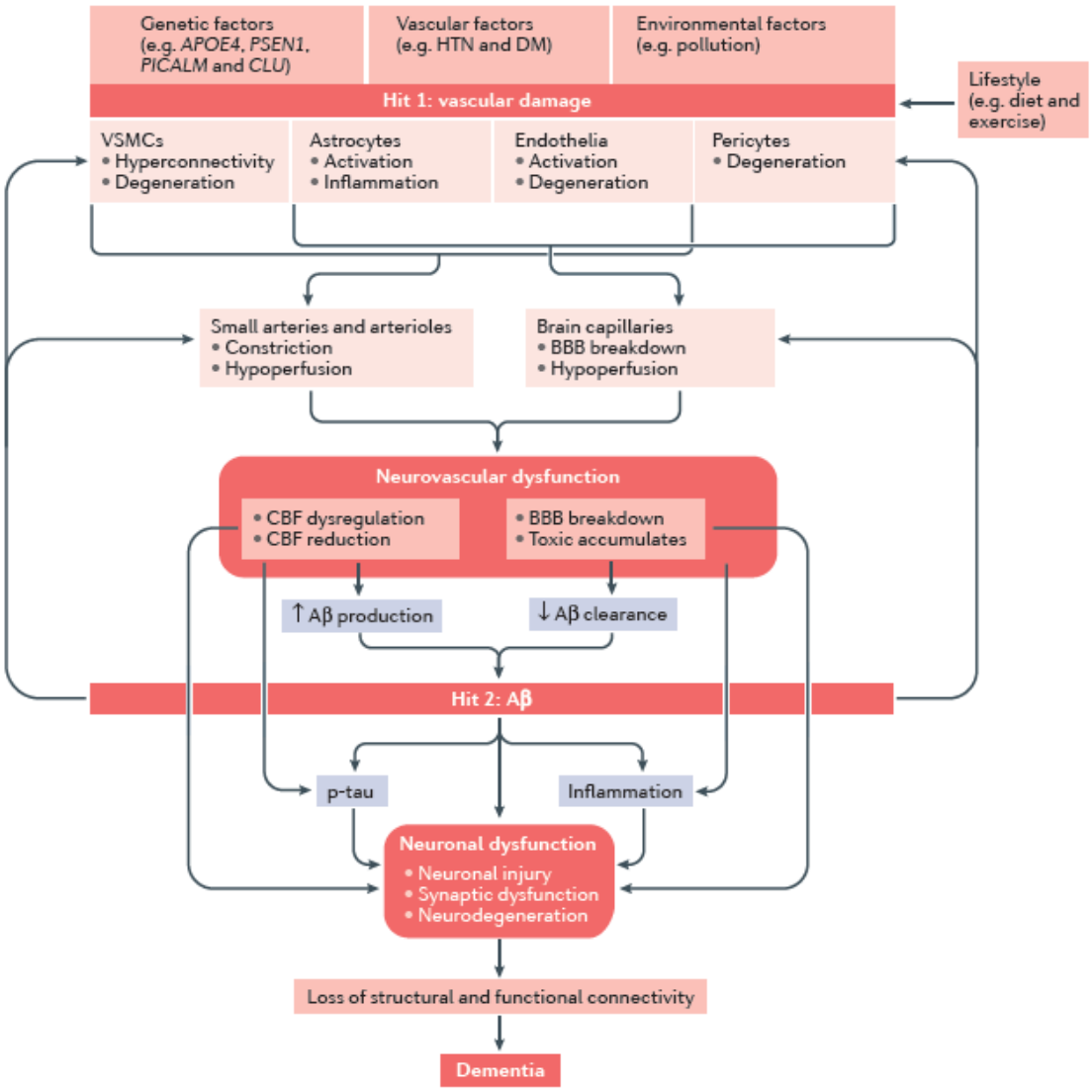

Figure 2-2 Neurovascular uncoupling in AD: two hit mechanism (Kisler et al., 2017a).

2.3 Compromised cerebral tissue oxygenation

Although CBF gives essential information on how the brain functions in AD, cerebral tissue oxygenation offers extra information regarding the functioning of the brain, especially in pathological condition of AD due to the following reasons. Firstly, CBF regulation ensures sufficient supply of oxygen to tissue in normal condition, but the connection between CBF and oxygen supply to tissue could be compromised in AD (Kisler et al., 2017a, 2017b; Zlokovic, 2011). Hence, CBF alone may not directly reflect the tissue oxygenation state in AD. Secondly, brain neurons are highly dependent on oxygen to meet their oxidative metabolic demands (Chance, 1957; Chance et al., 1962), and thus the oxygenation level of cerebral tissue has been recommended as a biomarker in models of neurodegenerative diseases (Devor et al., 2011; Sakadžić et al., 2014). Thereby, the link between AD and cerebral tissue oxygenation is critical for our comprehension of the progression of neurovascular dysfunction and neurodegeneration in AD. In the following sections, the mechanism of oxygen supply from vasculature to tissues is discussed and the potential oxygenation changes in AD is provided.

2.3.1 Mechanisms of oxygen supply

Traditionally, it was believed that blood flow was largely regulated by arterioles on the pial surface of the brain (Nippert et al., 2018). However, recent studies document that penetrating arterioles supply 50% of the extracted oxygen at resting state (Sakadžić et al., 2014), which offer a secure margin to maintain brain function. Capillaries also play a crucial role in supplying oxygen to support neuronal activity (Hall et al., 2014; Kisler et al., 2017b; Santisakultarm et al., 2014; Stefanovic et al., 2008), since they are the vessels most proximal to neurons. Thus, this thesis focusses on the role of penetrating arterioles and capillaries on oxygen supply to neurons, due to their essential role in regulating CBF (Kisler et al., 2017b; Nippert et al., 2018; Sakadžić et al., 2014).

To transmit from blood to tissues, oxygen molecules firstly unbind from hemoglobin and diffuse from the red blood cells (RBC) to plasma, across the vascular wall, and finally into the tissues. Partial pressure of oxygen (PO_2) represents the amount of oxygen gas and can diffuse from blood to tissue. The intravascular and extravascular PO_2 are the most basic physiological parameters with great variability that may originate from dynamics in regional CBF and metabolic needs for different brain areas (Masamoto et al., 2003; Sakadži et al., 2010). Under normal physiological conditions, oxygen supply enabled by increased CBF exceeds the neuron cells' metabolic demand, thus ensuring a large PO_2 gradient for oxygen diffusion to cells even furthest from capillaries (Attwell et al., 2010; Buxton, 2010; Lin et al., 2010).

Diffusion of oxygen to neuronal cells can be boosted with external stimulation for more computationally demanding neuronal activities (Beau M.Ances et al., 2001; Vazquez et al., 2010). During functional stimulation, tissue locations far from the vascular feeding source were also observed to have an overshoot in oxygenation (Devor et al., 2011). Low level of cerebral tissue PO_2 may lead to hypoxia and affect the survival of neuronal cells far from vascular sources (Moeini et al., 2019, 2018). During functional stimulation, the increased oxygen supply results from the increased CBF (Moeini et al., 2019), which creates large PO_2 gradient for oxygen delivery. Because of the close relationship among PO_2, CBF, and neuronal activity (B.M.Ances et al., 2001), PO_2 can serve as an effective marker in neurodegenerative disease, such as AD, either to detect if a departure from normal PO_2 occurs in the disease model or to determine the efficiency and effectiveness of potential preventive therapies (Devor et al., 2011).

2.3.2 Compromised CBF and cerebral tissue oxygenation with AD

Previous research have documented neurovascular deficits in AD (Delafontaine-Martel et al., 2018; Gorelick et al., 2011; Kitaguchi et al., 2007; Montine et al., 2014; Snyder et al., 2014; Wardlaw et al., 2013). Findings in transgenic mice APPSwDI have shown that arterial

VSMCs exhibited an impaired ability to clear Aβ (Bell et al., 2009), thus leading to Aβ accumulation in the vascular walls and blocking the exchange of oxygen between blood and tissues. An earlier large population-based study showed that cerebral hypoperfusion preceded and possibly contributed to onset of clinical dementia with transcranial Doppler (Ruitenberg et al., 2005). By contrast, individuals exhibiting higher CBF were less inclined to develop dementia and had larger brain areas (e.g., hippocampal & amygdala volumes) for cognitive functioning (Ruitenberg et al., 2005). Using pseudo-continuous arterial spin labeling MRI, previous studies also showed global CBF was lower in patients having moderate cognitive impairment, as compared to normal control (Michels et al., 2016). Collectively, these findings demonstrate that changes in CBF are an essential feature of AD and adding vascular changes into diagnosis of AD could further improve the accuracy of AD diagnosis in early stages.

Due to the tight connection between CBF and tissue oxygenation (Devor et al., 2012; Moeini et al., 2018; Sakadžić et al., 2014), disturbance of CBF in AD may drop cerebral tissue PO_2, and disrupt the normal cerebral PO_2 gradients between microvasculature and tissue, resulting in lack of oxygen diffusion from microvasculature to the neuronal cells (Masamoto et al., 2003). Since neurons are highly sensitive to oxygen supply (Girouard andIadecola, 2006; Iadecola, 2004; Østergaard et al., 2013), slight variations in CBF may lead to hypoxia and neuron damage in regions with low tissue PO_2. The spatial heterogeneity of tissue PO_2 which depends on CBF properties could thus be altered with factors such as aging and neurodegenerative diseases (Moeini et al., 2018). However, existing research mostly focus on the vascular changes in AD and neglect the importance of tissue oxygenation as a biomarker for AD. Tissue oxygenation is essential to understand and monitor the progression of AD, since 1) tissue oxygenation directly influence neuron survival due to the high demand for oxygen in neuronal cells (Devor et al., 2012; Kisler et al., 2017a; Moeini et al., 2018; Østergaard et al., 2013), 2) tissue oxygenation is both closely related by CBF regulation and neuronal activity (Iadecola, 2004; Kisler et al., 2017a). Due to the heterogeneity and dynamics of tissue PO_2, new technology for in vivo measurement of PO_2 in the cerebral

cortex based on non-invasive optical method can play a key role in recording images with high spatial resolution (Sakadži et al., 2010; Sakadžic et al., 2016; Sakadžić et al., 2014). In the next chapter, imaging techniques that can record oxygenation parameters are discussed.

CHAPTER 3 METHODOLOGY REVIEW FOR PO_2 MEASUREMENTS

Multiple approaches have been used to quantify tissue oxygenation, each with a different mechanism to measure PO_2. In this chapter, numerous imaging techniques on tissue oxygenation will be reviewed and assessed.

3.1 Mass spectroscopy

Mass spectroscopy has been used to analyze cerebral blood gas and cerebral PO_2 in early animal research (Brantigan et al., 1972; Rigaud-Monnet et al., 1994). A gas-sampling cannula needs to be implanted chronically into the brain to withdraw minor quantities of physiological tissue gasses. A specially designed Teflon diffusion membrane (see Fig. 3-1) is inserted at the end of the implantable cannula with the membrane end into the tissue or blood and the opposite end connecting to the vacuum of the mass spectrometer. The membrane ensures that only dissolved gases with no blood are aspirated through the membrane in proportion to their partial pressures.

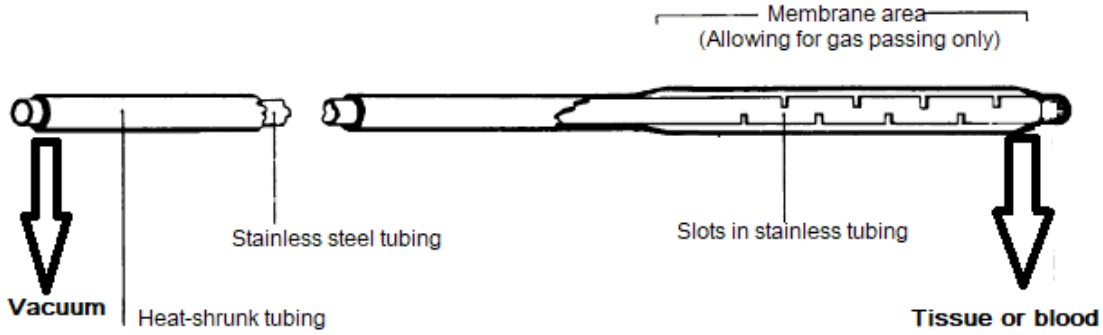

Figure 3-1 Design of Teflon membrane and cannula.

These gases are then analyzed in the chamber of mass spectrometer. The oxygen molecules are identified by ionization, acceleration and separation based on their molecular weight, allowing for quantitative measurement of tissue PO_2 (Reusch, 2013). To measure the characteristics of oxygen molecules, the mass spectrometer converts the gases into ions

which can be manipulated by magnetic fields. As shown in Fig. 3-2, firstly, a sample gas is collected by a high vacuum (e.g., 10^{-2} torr pressure in contrast to the atmospheric pressure of 760 torr). Due to the short-lived nature of ions, this sample is handled under the pressure of 10^{-7} torr, and ionization is achieved by a high energy beam of electrons enabled by a filament. The ion separation is effected by accelerating and focusing the beam through the accelerating slits and bending the beam by a magnetic field. By adjusting the strength of the magnetic field, ions of different mass can be collected by the detector progressively. Lastly, a computer analyzes the character of the ions by its specific mass-to-charge ratio (m/z). For example, oxygen (O_2) has a mass-to-charge ratio of 32, and carbon dioxide has a ratio of 28.

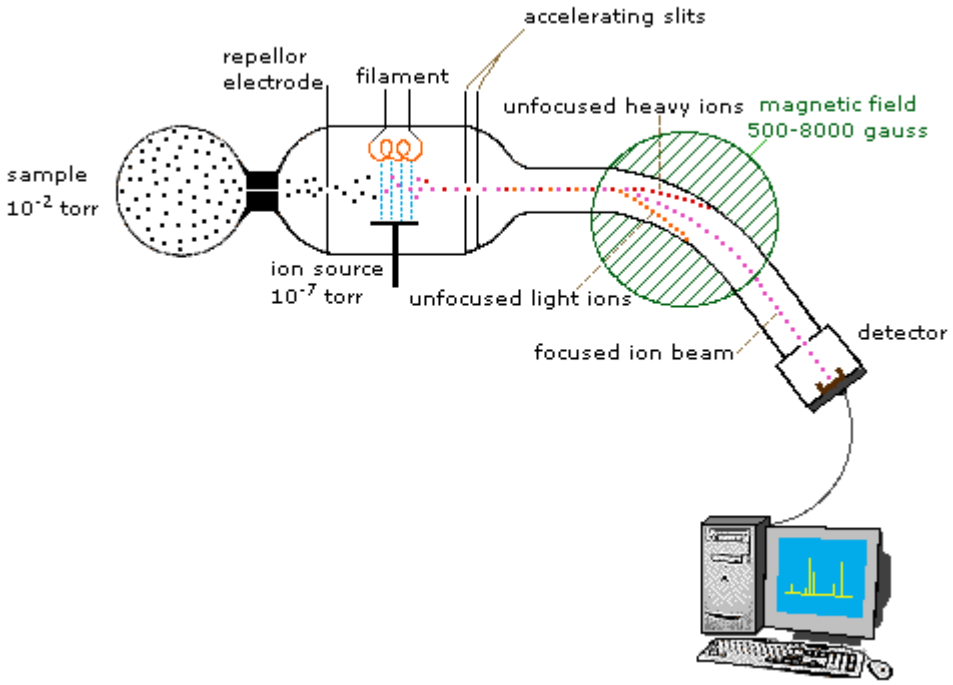

Figure 3-2. A sample design of spectrometer (Reusch, 2013).

However, there are several drawbacks with this method. Firstly, this method is invasive due to the need for implantation of the cannula which connects to the vacuum and analysis chamber of mass spectrometer on the one end and the blood vessels in the other end (Weaver andLiu, 2017). The cannula usually needs to be inserted into the vessels for 1 or 2 days

(Brantigan et al., 1972), so that there is inflammation concerns at the site of implantation which may delay the experimental process (Weaver andLiu, 2017). Secondly, measurements of tissue PO_2 can be obtained only at the site of implantation, limiting its capability to offer oxygen information in other regions of the brain (Lyons, 2015). Thirdly, although oxygen parameters can be collected in vivo, the animals need to be anesthetized, which may influence the physiological parameters of the animals. Hence, the accuracy of oxygen measurement may be compromised due to anesthesia.

3.2 Polarography

Polarography has been used for *in vivo* measurements of cerebral PO_2 for decades and established major findings to shape our current understandings of the cerebral tissue oxygenation (see review (Ndubuizu andLaManna, 2007)). Polarography is based on the reduction of oxygen at the surface of a noble metal (e.g., platinum) affected by the negative polarizing voltage. The polarographic electrode consists of a cathode covered by a membrane for oxygen reduction and a nearby reference electrode. The tip of the cathode electrode is inserted into the tissue of interest for oxygen measurements by producing a current in proportion to the concentration of oxygen adjacent to the electrode, inducing the reduction of oxygen by transforming O_2 to H_2O.

Among the polarographic sensors, the Clark electrode (see Fig. 3-3), developed by Dr. Leland Clark in 1956, was commercially produced and has been used to measure dissolved oxygen in recent research (for example in the work of (Lecoq et al., 2009)) due to its time-efficiency and less susceptibility to interference (see the review (Ndubuizu andLaManna, 2007)). The dissolved oxygen molecules diffuse through the specially-designed membrane and are reduced at the cathode, based on the following reaction (Nguyen et al., 2014):

$$\mathbf{O_2 + 2H_2O + 2e^- \rightarrow H_2O_2 + 2OH^-}$$

$$\mathbf{H_2O_2 + 2e^- \rightarrow 2OH^-}$$

The PO_2 versus the electrode current generated through oxygen reduction can be calibrated due to the oxygen diffusive flux in proportion to the PO_2 in the sampled region (YSI, 2009).

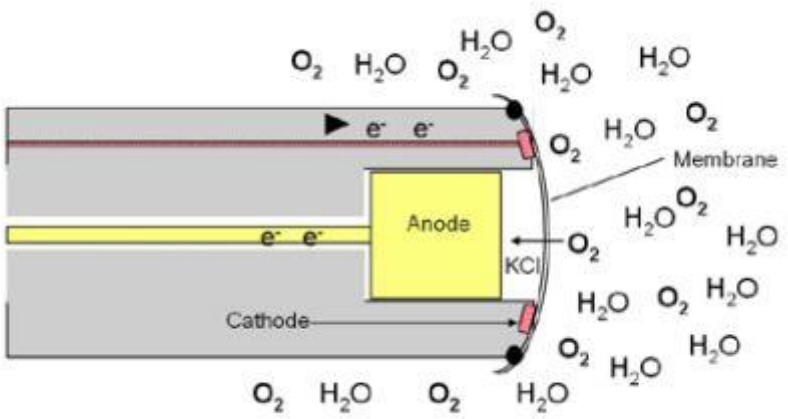

Figure 3-3 An explanation of the Clark sensor (YSI, 2009).

However, there are several limitations of the polarographic electrode (see reviews (Ndubuizu andLaManna, 2007) and (Weaver andLiu, 2017)). Firstly, this method is invasive, since the reduction of oxygen at the cathode may alter the physiological environment around the sampling area which may further influence the measurements. Secondly, this technique gives point measurement rather than a 2D mapping of tissue PO_2, as it only gives oxygen information nearby the electrode. To obtain oxygen distribution, multiple probes may be used for simultaneous measurement or multiple sequential repositioning of the electrodes are required. Thirdly, this method cannot offer repetitive measurements over prolonged periods (e.g., for days). The ions in the electrolyte are not stable over time and need to be replaced.

3.3 Electron Parametric Resonance (EPR) oximetry

Electron paramagnetic resonance (EPR) is a magnetic resonance technique that measures only species with unpaired electrons (see reviews (Gallez et al., 2004) and (Weaver andLiu,

2017)). Molecular oxygen has two unpaired electrons which represents its paramagnetic property, and thus can be measured by EPR. To directly measure oxygen in biological systems, EPR oximetry is designed based on the biomolecular collisions between oxygen and free radicals, given that this interaction can alter the resonance characteristics of the radical and consequently the EPR spectrum (see review (Gallez et al., 2004)). The most common method is to apply the oxygen dependent broadening of the EPR linewidth (LW) of a paramagnetic oxygen sensor implanted in tissues. As shown in Fig. 3-4, the oxygen sensor has a higher LW response at low PO_2, and thus EPR has high sensitivity to detect hypoxic areas (e.g., regions with low PO_2 values (e.g., 0.5 mmHg)). The sensor also has quick response to the variation of tissue PO2, see Fig. 3-4. Due to these characteristics, EPR oximetry has been used to measure oxygenation in tumor studies. A recent study (Langan et al., 2016) used EPR oximetry to quantify oxygen gradients in spheroids, ball-shaped models representing liver or tumor. Since regions with tumor are often associated with hypoxia, EPR provides the sensitivity to detect these areas and the variations of PO_2 in these regions.

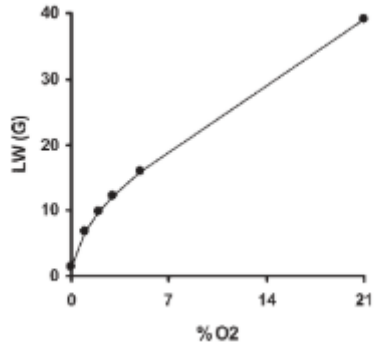

Figure 3-4. The calibration curve based on linewidth as a function of the PO2 (Adapted from the review (Gallez et al., 2004)).

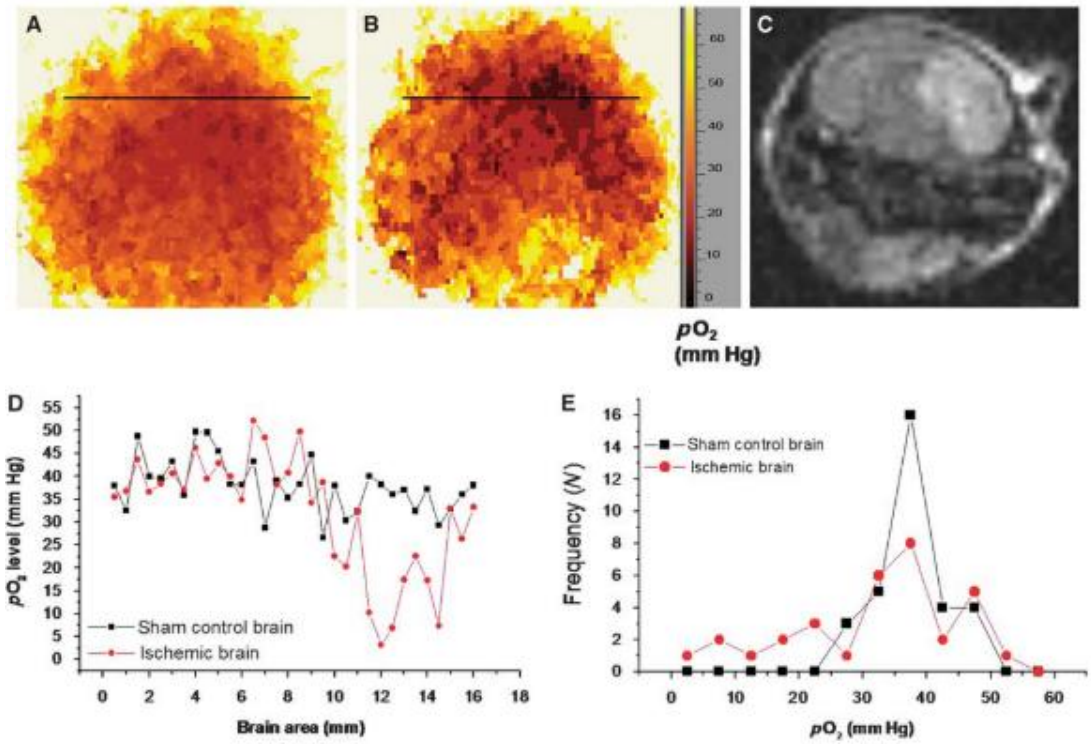

Figure 3-5 PO_2 distribution in ischemic mouse brain recorded by EPR 2D spectral-spatial linewidth imaging (Shen et al., 2009). A) PO_2 map in the sham control mouse head, B), PO_2 map in the same mouse after ischemia, C) MR diffusion image in the mouse after ischemia. D) Representative spatial profiles of PO_2 in both groups. The PO_2 values were recorded along the black lines in A and B. E) Frequency of PO_2 values in the sham control head and the ischemic head.

Suitable paramagnetic probes are needed in the tissue regions of interes for ERP line-broadening measurements (Swartz et al., 2014). Two typical types of probes for EPR include particulate and soluble probes (Weaver andLiu, 2017). However, both probes have their limitations. There are concerns about biocompatibility with exposure to particulate probes in long periods of time, since these particulate probes may have chemical reactions in the biological systems and produce toxic chemicals. Considering the sensitivity of cerebral neuronal cell, it is reasonable to evaluate the risk of implanting particulate probes into the

brains. Soluble probes can also be used for EPR oximetry for mapping of oxygen, but are used in *ex vivo* environment more frequently due to the difficulty to delivery this type of probe through the BBB. In addition, the soluble proble responds to the disolved oxygen in tissue, which is more heterogeneous than tissue PO_2, thus weakening the sensitivity of the soluble probe.

3.4 Two-photon phosphorescence optical method

3.4.1 Oxygen-dependent quenching of phosphorescence

The mechanism of oxygen-dependent quenching of phosphorescence (Quaranta et al., 2012; Shonat andKight, 2003) can be represented by the Perrin-Jablonski diagram, as shown in Fig. 3-6. Specifically, in the absorbance stage, the luminescent molecule is excited from the ground state (S_0) to the first singlet excited state (S_1) or the second singlet excited state (S_2), which takes about 10^{-15} s. Next, the luminescent molecule undergoes internal conversion which involves an intermolecular process that transitions a higher electronic state (S_2) to a lower electronic state (S_1) without radiation. This internal conversion process takes about 10^{-12} s (denoted as the rate constant k_{ic}). This transition occurs rapidly and before the de-excitation process.

There are two radiative approaches for de-excitation, including fluorescence and phosphorescence. One the one hand, fluorescence emission occurs at the first singlet excited state (S_1), which does not involve changes in multiplicity (e.g., from singlet to triplet), thus having a high possibility to occur. The fluorescence lifetimes are usually around 10^{-8} s. One the other hand, phosphorescence emission occurs from the lowest excited triplet state (T_1), which requires transition between different multiplicities ($S_1 \rightarrow T_1$) that is less likely to occur. Likewise, the transition from triplet (T) to singlet (S) is also less likely to occur than singlet to singlet transition (the case in fluorescence), and thus phosphorescence emission requires more time (from 10^{-6} s to several seconds) to decay than fluorescence. However, the

presence of heavy atom in the phosphorescent molecular probe could increase the probability of crossing between the triplet and singlet state, thus making phosphorescence highly efficient by shortening the decay time. Since phosphorescence emission occurs at a lower energy state (T_1), it emits lower energy compared to the fluorescence. Compared to fluorescence de-excitation, phosphorescence quenching is preferred due to its relatively longer triplet lifetime, and thus offering higher oxygen sensitivity (Finikova et al., 2008).

When interacting with oxygen, the luminescent molecules are quenched in a non-radiative de-excitation process involving collisions between quenchers and luminescent molecules. One potential mechanism indicates that the paramagnetic oxygen facilitates the intersystem crossing of luminescent molecules from singlet to triplet, and oxygen molecule transitions to excited state and then returns to ground state (Quaranta et al., 2012; Shonat andKight, 2003).

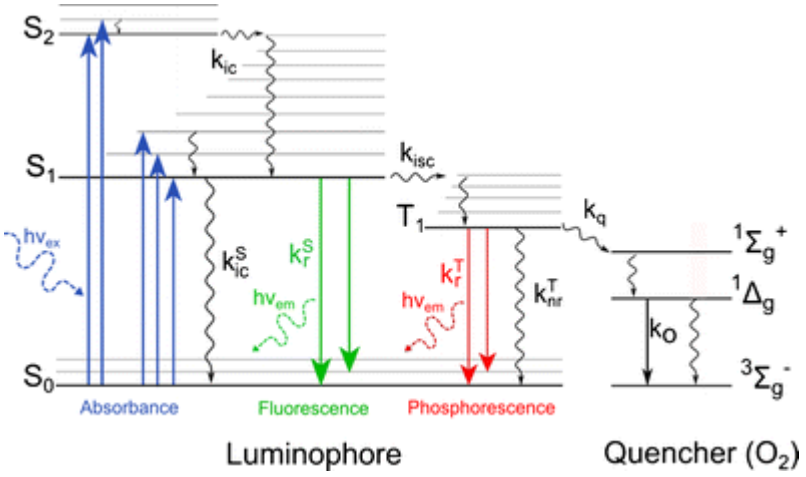

Figure 3-6. Perrin-Jablonski diagram (Quaranta et al., 2012).

In addition to the above figure, this quenching process can also be denoted in expressions. When a large quantity of phosphorescence dye is excited simultaneously, the phosphorescence emission can be represented by the exponential decay function:

$$(t)=I_0 \exp(-t/\tau) \qquad (1)$$

where $I(t)$ represents the intensity of phosphorescence as a function of time, I_0 represents the maximum intensity at time 0, and τ is the apparent lifetime of the decay. In the presence of a quenching agent, in our case the oxygen, the decay time of phosphorescence is shortened due

to the quenching by energy transfer to oxygen, described by the Stern-Volmer function:

$$\tau_0 / \tau = 1 + K_Q \tau_0 [PO2] \quad (2)$$

where τ_0 is the lifetime when no oxygen is present, K_Q is the bimolecular rate constant, and [PO2] is the concentration of PO2.

Using Stern-Volmer calibration plots, phosphorescence decay lifetimes can be converted into PO2 values. A calibration plot of conversion of phosphorescence lifetime to PO2 values (see the example in Fig. 3-6) can be achieved via oxygen titration analysis (Khajehpour et al., 2003).

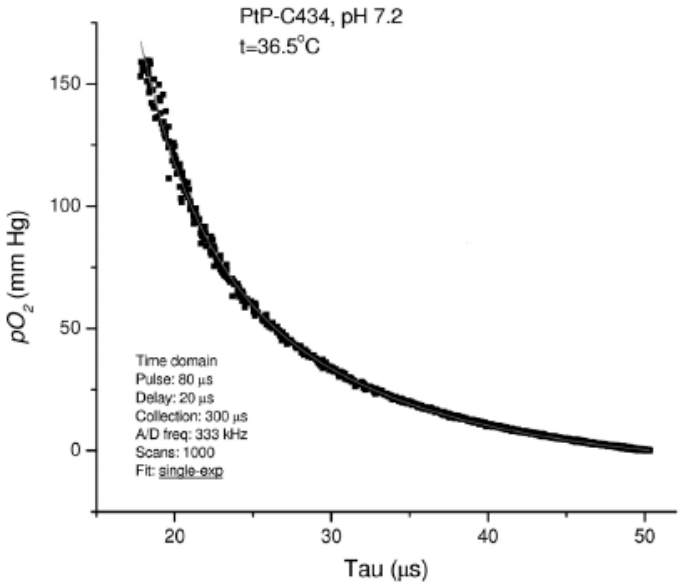

Figure 3-7. An example of calibration plot of PtP-C343 for conversion of phosphorescence lifetimes into PO2 values with the system and environment specified (Adapted from the supplementary materials of (Sakadži et al., 2010)).

3.4.2 Two-photon enhanced phosphorescent probe

Oxygen imaging approach combining the oxygen dependent phosphorescence quenching method and the two-photon laser scanning microscopy represents a natural extension, considering the depth resolution for 3D imaging and the low probability of photo damage enabled by two-photon microscopy (Finikova et al., 2008). The phosphorescent dye is

capable of phosphorescence emission in the excited state when illuminated by two-photon lasers. When interacting with oxygen molecules, the energy of phosphorescent photon is transmitted to oxygen and thus the phosphorescent photon is quenched by the oxygen.

The specific structure of probe PtP-C343 is shown in Fig. 3-8. This probe is mainly designed for intravascular and interstitial applications through injection, providing suitable pathways in biomedical research. Adding C343 as energy receptor helps avoid the drawback of low two-photon absorption of probes based only on PtP. The high fluorescence production of C343 after excitation enables efficient fluorescence resonance energy transfer (FRET). The C343 components in the probe enhances the phosphorescence intensity in a large extent, reducing the demand for extremely high excitation powers. A polyarylglycine dendrimer (PD) surrounds the PtP core to increase its solubility in the biomolecular system, prevents aggregation of the probes, and attenuate the oxygen diffusion rate by folding and restricting oxygen diffusion for more efficient oxygen measurements in the core vicinity. When the PtP core is not protected by PD, the constant rate would be too high, >1500 $mmHg^{-1}s^{-1}$ to quantify oxygen at physiological values (e.g., 100-160 mmHg) (Finikova et al., 2008; Rozhkov et al., 2002; Vinogradov et al., 1999). A concern for PtP-C343 is the residual fluorescence produced in the FRET process which may bring compounding effect to the phosphorescence response to PO2. However, the residual fluorescence is insensitive to oxygen due to its short lifetime and experiments at different oxygen concentration only show phosphorescence response to PO2 dynamics (Finikova et al., 2008).

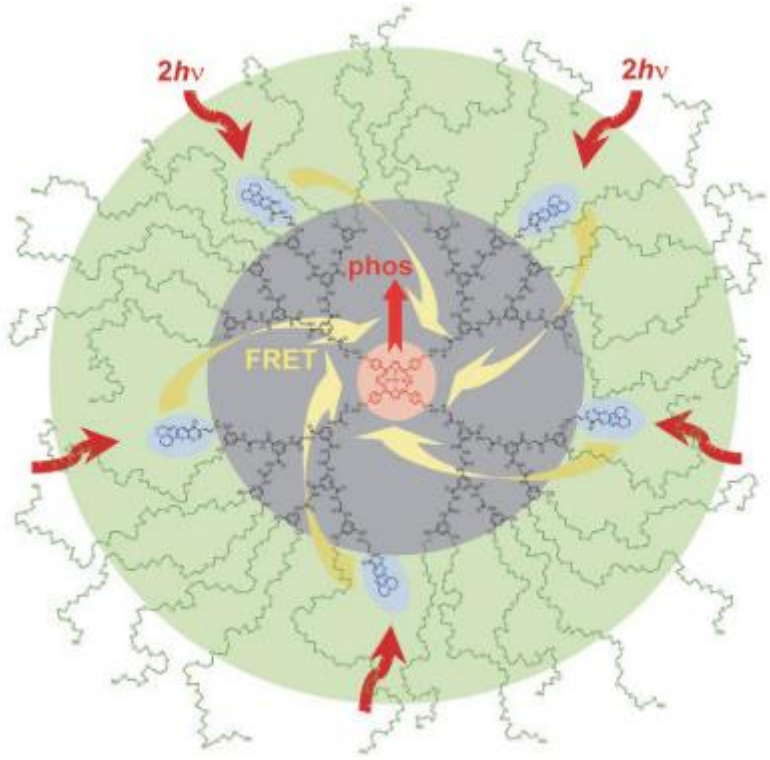

Figure 3-8. Two-photon enhanced oxygen probe PTP-C343 that consists of the Pt meso-tetraarylporphyrin core (PtP, in pink), the coumarin-343 units (C343, in blue), the peripheral oligoethyleneglycol residues (POR, in green), and the polyarylglycine dendrimer (PD, in black). The C343 is excited as the antenna through the two-photon absorption and then transmits the energy to the PtP core (in pink) through Fluorescent resonance energy transfer (FRET). After receiving energy from the C343, the core emits phosphorescent photons (Finikova et al., 2008).

The phosphorescent proble used in my study was obtained from Oxygen Enterprises Ltd (Philadelphia, USA). Before experiments, the probe was calibrated with room air (with 21% oxygen) and with deoxygenated solution in different temperatures. The parameters ($K_{Q,}$ τ_0) were choosed at physiological temperature 37ºC, as shown in the following figure.

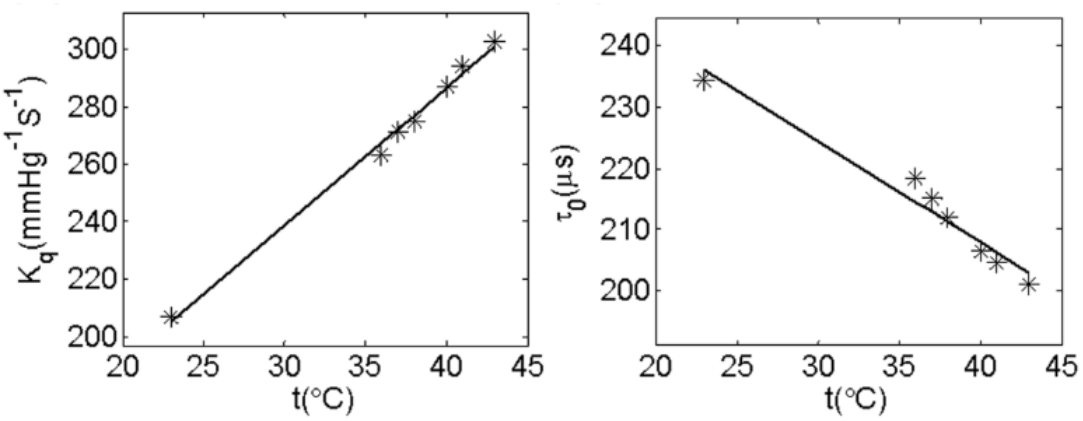

Figure 3-9. The quenching parameters ($K_{Q,}$ τ_0) obtained at different temperatures (Zhang, Cong et al., 2015). The probe was dissolved in solution with pH 7.23.

3.4.3 Advantages of two-photon phosphorescence imaging

There are several advantages of two-photon phosphorescence imaging. Firstly, the combination of phosphorescence dye (PtP-C343) with two-photon microscopy enables non-invasive and direct measurements of PO2 (Devor et al., 2012; Lecoq et al., 2011; Sakadžić et al., 2014). In this approach, the molecular phosphorescent probe is inserted into the vascular or interstitial fluid directly, with signals retrieved by the external two-photon excitation. The PtP-C343 probe is non-toxic and compatible with the biomolecular system with no documentation of inflammation. Secondly, among optical approaches, phosphorescence lifetime imaging of oxygen excels in its capacity to offer direct measurements of PO2 and avoid any influence from optical properties in tissue (Sakadži et al., 2010). The phosphorescence lifetime imaging of oxygen depends on measuring the phosphorescence lifetime which is oxygen-dependent. The signal measured is the phosphorescence lifetime, instead of the intensity of probe or optical properties, thus removing the effect of probe concentration and the optical characteristics of tissues or vasculature. Thirdly, this approach allows for measurements with hundreds of micrometer in

depth below brain surface with high temporal and spatial resolution, (Lévy et al., 2018; Sakadži et al., 2010)). The PtP-C343 probe is two-photon enhanced probe which has high absorption rate for the two-photon laser beam. Two-photon microscopy has the capacity to constrict excitation to a focal beam, ensuring the possibility of high spatial resolution and enough photon density to excite the probe deeper under brain surface. The PtP-C343 proble has a long half life with around 2 hours in tissue with the possibility of achieving high temporal resolution for repetitive measurements at a local point. Due to these advantages of two-photon phosphorescence laser microscopy, this technique was used to investigate tissue oxygenation in the following article.

CHAPTER 4 ARTICLE 1: VOLUNTARY EXERCISE INCREASES BRAIN TISSUE OXYGENATION AND SPATIALLY HOMOGENIZES OXYGEN DELIVERY IN A MOUSE MODEL OF ALZHEIMER'S DISEASE

Xuecong Lu[1,2], Mohammad Moeini[4], Baoqiang Li[5], Olivia de Montgolfier[2,3], Yuankang Lu[1,2], Samuel Bélanger[1,2], Éric Thorin[2,3], Frédéric Lesage[1,2*]

1 Biomedical Engineering Institute, École Polytechnique de Montréal, Montréal, QC, Canada

2 Montreal Heart Institute, Research Center, Montreal, Quebec, Canada.

3 Department of Surgery and Pharmacology, Faculty of Medicine, Université de Montréal, Montreal, Quebec, Canada.

4 Department of Biomedical Engineering, Amirkabir University of Technology (Tehran Polytechnic), Tehran, Iran

5 Athinoula A. Martinos Center for Biomedical Imaging, Massachusetts General Hospital, Harvard Medical School, Charlestown, MA 02129, USA

*Corresponding author: Frédéric Lesage, PhD

Address: Biomedical Engineering Institute, École Polytechnique de Montréal, P.O. Box 6079, Succursale Centre-ville, Montréal (QC), H3C 3A7, Canada

Email: frederic.lesage@polymtl.ca, Tel: +1-514-340-4711 ext. 7542, Fax: +1-514-340-4611

Running headline: Voluntary exercise modulates tissue PO2 and AD

This article was submitted to the journal "Neurobiology of Aging" on February 28, 2019 and received the provisional acceptance.

4.1 Abstract

While vascular contributions to dementia and Alzheimer's Disease (AD) are increasingly recognized, the potential brain oxygenation disruption associated with AD and whether

preventive strategies to maintain tissue oxygenation are beneficial remain largely unknown. This study aimed to examine 1) whether brain oxygenation is compromised by the onset of AD and 2) how voluntary exercise modulates the influence of AD on brain oxygenation. *In vivo* two-photon phosphorescence lifetime microscopy was used to investigate local changes of brain tissue oxygenation with the progression of AD and its modulation by exercise in the barrel cortex of awake transgenic AD mice. Our results show that cerebral tissue oxygen partial pressure (PO_2) decreased with the onset of AD. Reduced PO_2 was associated with the presence of small near-hypoxic areas, an increased oxygen extraction fraction, and reduced blood flow, observations that were all reverted by exercise. AD and age also increased the spatial heterogeneity of brain tissue oxygenation, which was normalized by exercise. *Ex vivo* staining also showed fewer amyloid-β (Aβ) deposits in the exercise group. Finally, we observed correlations between voluntary running distance and cerebral tissue oxygenation/blood flow, suggesting a dose-response relationship of exercise on the brain. Overall, this study suggests that compromised brain oxygenation is an indicator of the onset of AD, with the emergence of potential deleterious mechanisms associated with hypoxia. Furthermore, voluntary exercise enhanced the neurovascular oxygenation process, potentially offering a means to delay these changes.

4.2 Key words

Brain tissue oxygenation, Two-photon microscopy, Alzheimer’s disease (AD), Voluntary exercise, Awake imaging

4.3 Introduction

Alzheimer's disease (AD) is a typical neurodegenerative disease which leads to dementia and cognitive impairment (Farkas and Luiten, 2001; Selkoe and Schenk, 2003). The incidence of sporadic AD increases with age, affects people's capability to maintain social function (Farkas and Luiten, 2001; Larson et al., 2006) and is associated with major public health problems. AD is characterized by the extracellular deposition of amyloid-β (Aβ) peptides in the brain and in cerebral blood vessels, and by accumulation of the hyperphosphorylated tau protein in neurons (Selkoe and Schenk, 2003). Neurovascular coupling, which refers to the tight connection between neuronal activities and cerebral blood flow (CBF) is suggested to be compromised in AD (Girouard and Iadecola, 2006). Cerebral micro-vessels are decreased in number, endothelial cells are flattened, and smooth muscle cells undergo degeneration (Farkas and Luiten, 2001), thus potentially contributing to dysfunction of brain homeostasis. While vascular and cellular contributions to dementia and AD are increasingly recognized (Montagne et al., 2016; Zlokovic, 2011), we have limited knowledge about whether cerebral oxygenation is compromised with the onset of AD. Given that the cognitive functioning of the brain essentially depends on oxygen supply (K.A. Kasischke et al., 2011; Karl A. Kasischke et al., 2011; Sakadžić et al., 2014a), such information is critical not only to understand the oxidative metabolism alterations in AD brains, but also to shed light on the diagnosis of AD with potential novel biomarkers. Additionally, given the devastating nature of AD, effective prevention strategies are pivotal. Among these approaches, voluntary exercise has been identified as one of the effective means for preserving brain cognitive function in both preclinical models and clinical settings (Adlard et al., 2005; Dorr et al., 2017; Heyn et al., 2004; Larson et al., 2006; Radak et al., 2010). Voluntary exercise, such as walking, has been found to correlate with considerable decrease in loss of capability in the elderly (Singh, 2002; Yaffe et al., 2001). It has also been demonstrated to be of great benefit to alleviate cognitive impairments (Naylor et al., 2008; Wong-Goodrich et al., 2010) and data

from longitudinal studies and randomized trials suggest that physical exercise benefits cognitive function (Barnes et al., 2003; Geda et al., 2010; Kramer et al., 1999; Voss et al., 2016). Despite its preventive role on cognitive decline, the oxygenation mechanism through which voluntary exercise affects AD remains under-explored. Investigating how cerebral tissue oxygenation is altered with AD and how exercise can modulate this change can help understand how exercise offers a means to slow the rate of neurodegeneration in the clinical settings. Thus, this study aimed to examine 1) whether brain oxygenation is compromised by the onset of AD and 2) how voluntary exercise modulates the influence of AD on brain oxygenation. Voluntary treadmill running was used in our experiments as it has been appplied commonly as a rehabilitation strategy in clinical research (Ke et al., 2011).

To quantify oxygen supply, we measured tissue oxygen partial pressure (PO_2), which is affected by variations in blood flow and metabolic demand in different regions (Sakadži et al., 2010). A custom-built two-photon microscopy system with a phosphorescent lifetime arm to measure PO_2 was developed and used to provide maps of PO_2 in brain tissue with sub-capillary resolution around cortical arterioles, capillaries and venules and to obtain microvascular morphology (Sakadži et al., 2010; Sakadžić et al., 2014b). Doppler Optical Coherence Tomography (OCT) was also used to acquire cerebral blood flow (CBF) estimates in penetrating vessels.

We found that cerebral tissue PO_2 decreased after the onset of AD, but that this decrease was reversed by exercise. We further observed the presence of sparse near-hypoxic areas (PO_2 < 10 mmHg) that increased in number with AD but decreased with exercise, suggesting an association between insufficient oxygenation and the onset of neurodegeneration. Fewer Aβ deposits in the exercise group further confirmed this association. Doppler Optical Coherence Tomography (OCT) data showed that CBF decreased with AD but increased with exercise and significant correlations were established between running distance and tissue oxygenation / blood flow properties. Overall, this study indicates that brain oxygenation could serve as a biomarker of the onset of AD. Furthermore, voluntary exercise enhanced

brain oxygenation, thus offering a potential mechanism to delay brain tissue hypoxia with AD.

4.4 Methods

4.4.1 Function and property of the PtP-C343 probe.

The PtP-C343 probe was synthesized on the basis of the procedures proposed in Finikova et al.(Finikova et al., 2008) and Vinogradov et al. (Vinogradov, 2005). This proble enabled measurement of oxygen based on the phosphorescence quenching mechanism due to its enhanced absorption for two-photon. The probe was calibrated at 37 ℃ and 7.2 pH from oxygen titration experiments (Rozhkov et al., 2002; Zhang, Cong et al., 2015).

4.4.2 Experimental groups.

Animals were handled conforming to the ARRIVE guidelines and the recommendations of the Canadian Council on Animal Care. Animal surgical procedures and handling were approved by the ethics committee of the research center of the Montreal Heart Institute. Experiments were performed on male wild type mice at 3 and 6-month-old (WT3: n=8, WT6: n=8), transgenic Amyloid Precursor Protein Presenilin-1 (APP/PS1) mice at 3 and 6-month-old (AD3: n=8, AD6: n=8), and APP/PS1 mice at 6-month-old for which voluntary exercise was initiated at 3-month-old (AD6&EX: n=7) under awake and stress minimization condition. Previous work (Cifuentes et al., 2015) showed a clear onset of cognitive deficit in APP/PS1 mice at 4.5 months, and thus we conducted imaging prior to and after this time point focusing on the early AD onset. Specifically, we collected imaging data at the age of 3 month and at the age of 6 month. We expected these groups to provide a sufficient range to observe oxygenation changes associated with the AD mice model. The time interval of 3 months was also sufficient to observe the effects of voluntary running (Adlard et al., 2005; Pedersen et al., 2016).

For the AD6&EX group, mice started voluntary exercise on running wheels at 3-month-old,

and continued the exercise till 6-month-old when brain imaging was performed. The wheel (diameter 15 cm, recorded by easy matrix 16 EMKA) was attached to the cage to preserve living space for the experimental animals. The number of wheel rotations was recorded using the external counter (LE907) on a daily basis for the whole exercise periods. Wheel running is widely used as voluntary exercise for mouse, since it involves with different neural and physiological mechanisms from spontaneous activity.

4.4.3 Experimental preparation.

One week before the surgery, physiological parameters, such as heart rate and blood pressure, were measured and recorded while awake. During the surgery, animals were under anesthesia with 1.5-2.0% isoflurane in pure oxygen, and the body temperature was kept at 37C with a feedback control. 1% Ketaprofen (SC, 5 mg/Kg, MERIAL Canada Inc) and 0.015 mg/ml Buprenorphine (SC, 0.05 mg/Kg, Reckitt Benckister Healthcare, UK) were injected just before the surgery for analgesia and to reduce potential inflammation. During the surgery, Betadine was used to sterilize the scalp and 70 % (v/v) isopropyl alcohol was used to wipe this area. Lidocaine was injected prior to exposing the skull. A titanium made head-plate was attached and fixed on the bone for fixation of the animal's head during surgery and oxygenation imaging. An area with 3 mm, located over the left barrel cortex (0.5mm posterior to bregma, 3.5mm lateral to the midline), was left uncovered with intact dura mater kept,. In the uncovered area, the skull was thinned gradually to obtain a transparent window. A cover glass was gently pushed against the skull surface and held for a few seconds to allow the glue to dry thoroughly for 15 minutes. On one side of the cover glass, on the thin-skull, a small hole (less than 500 um diameter) was drilled. A drop of biocompatible silicone was then applied on top of this hole to form a self-sealed, durable, tight, and biocompatible access port for awake injection. Right after the surgery, the edge of the cover glass was further glued with dental cement and an injection of Enrofloxacin (IP, 5mg/Kg, Bayer, Germany) was done. The animal was put back in the cage for recovery once awake. After 24 hours following the surgery, the animal was

injected with Ketoprofen (SC), Buprenorphine (SC) and Enrofloxacin (IP) again and then put back in the cage for two more days of recovery. In the following four days, the animal was fixation trained for 10, 20, 30 and 45 minutes, respectively. After this, imaging was performed using OCT and the two-photon systems, respectively.

4.4.4 Two-photon imaging.

A laser-scanning two-photon microscope was built to record imaging data. The MaiTai-XP laser oscillator (Newport corporation, USA) generated a sequence of 820 nm, 80 MHz, 150 fs pulses which were gated by an acousto-optic modulator. The system has an “on” and “off” laser pulse periods for phosphorescence lifetime imaging. Each “on” period lasted for 25 us, and each “off” period lasted for 275 us. The “on” and “off” periods corresponded to excitation of the PtP-C343probe and recording of phosphorescence decay in the brain tissue, respectively. Then the laser pulses went through the galvanometric mirrors (Thorlabs, USA) and the reflected lights were collected by a 20X objective (Olympus XLUMPLFLN-W, NA=1). The excitation laser power was set below 6.5 mW after the objective.

Phosphorescent photons and fluorescent photons were divided into different photomultiplier tubes for quantifying tissue oxygenation and vasculature, respectively. Specifically, the phosphorescent photons went through a filter centered at 680nm and recorded by the first PMT (H7422, Hamamatsu Photonics, Japan), whose output was saved for quantifying tissue oxygenation. The phosphorescence was decayed due to the quenching of oxygen, and the decays were averaged over a large number of cycles (1,000-5,000 decays) with 0.3-1.5 second to quantify each sampling point. Fluorescent light went through a filter centered at 520nm and recorded by the second PMT (R3896, Hamamatsu Photonics, Japan), whose output was processed to quantify vascular measurements.

4.4.5 OCT setup.

A spectral domain OCT was custom-designed for quantifying the blood flow properties in the

cortex of mice. A super luminescent diode (SLD) (LS2000C, Thorlabs) with a bandwidth of 200 nm was used as the light source, and the imaging speed was 50,000 axial scans per second. The light source was firstly passed through a circulator and separated into reference arm and sample arm. In each arm, polarization was implemented to maximize contrast. Samplings in the x-direction (nx=2048, ny=512) were repeatedly performed with the OCT scan in a rate of 24 Hz to compute the phase between adjacent A-lines. The Doppler volumes were repeatedly recorded for ten repetitions and then averaged. Side lobes were eliminated by spectral shaping of the interference signal using a Hanning window (Baraghis et al., 2011) at the expense of broadening axial resolution to ~3.8 μm. Following the procedure proposed by Wojtkowski et al.(Wojtkowski et al., 2004), automatic dispersion compensation was conducted to achieve optimum sharpness, and the dispersion coefficient was obtained based on the first frame of each acquisition and then applied to the rest of acquisitions. A moving-scatterer sensitive technique was used to reconstruct the flow speed (Ren et al., 2006).

4.4.6 Blood flow quantification with OCT.

OCT data were collected over a cortical area of ~700*700μm for all mice groups. Obtained OCT datasets encompassed *en face* planes of flow velocity maps with an interval of ~3.8 μm. In our analyses, we removed the top 50μm of the OCT datasets to eliminate the effects of pial vessels. For each slice in the OCT velocity volume, we measured the projected area of the vessels, and average projected velocity of arterioles and venule over the *en face* planes. Flow in each vessel was computed by the product of the velocity and the area over the projected *en face* plane. This product was further converted to the unit of ml/g/min by corresponding the the estimated cortical mass to the projected area, on the basis of previous assumptions on cortical thickness and density (Kretschmann et al., 1986). Total flow of the cortex was calculated by summing all flows over the *en face* plane (Moeini et al., 2018). In our analyses we excluded the top 50μm of the OCT datasets, and all parameters were averaged within the depth of 50-100 μm.

4.4.7 Cerebral tissue PO_2 measures.

The two-photon enhanced probe (PtP-C343) was injected into the brain tissue through the soft silicon sealed hole. Tissue PO2 was quantified by our custom-designed two-photon phosphorescence and fluorescence lifetime microscopy, as described in previous section 4.4.4. During the animal experiments, the animal' head were constrained by a titanium bar, whereas its limbs were allowed for free movement on the treadmill wheel. An IR camera was used to monitor movement and the corresponding measures were discarded if the mice moved frequently on the wheel during imaging.

PO_2 grid measurements were performed over four 200*200 μm planes with 30-40 μm intervals in depth and up to 350 μm in depth for each animal. The rate of phosphorescence decay, quantified by lifetime, was sensitive to the PO_2 level in the excited tissue; increasing PO_2 made the phosphorescence decay faster (oxygen dependent phosphorescence quenching) which resulted in a shorter lifetime, and vice versa. Averaged phosphorescence decay at each point was transformed to phosphorescence lifetime through a single-exponential curve, followed by converting the lifetime to PO_2 value using a calibration curve.

For all imaging planes, vessels with large diameters were manually labelled as arterioles or venules based on their different properties, as described in Moeini et al. 2018. Each sampling point is labeled with a PO_2 absolute value and a distance from its closest arteriole or venule in adjacent planes. Finally, all sampling points in each group were divided into three categories based on the attribute of distance to corresponding arteriole or venule: (1) "near arteriole", which includeds the points within 100 μm from the neareast arteriole; (2)"near venule", which includes the points within 100 μm from the neareast venule; and (3)"capillary bed", which includes the points with at least 100 μm from any arteriole or venule.

By the end of oxygenation quantification, we collected the vasculature imaging using fluorescent dye. Specifically, the blood plasma was dyed by tail injection with fluorescein isothiocyanate (FITC) with dextran (2MDa). Two-photon microscopy was applied to obtain a

three dimensional microvasculature imaging with multiple 200*200 μm planes with 350 μm in depth.

4.4.8 Thioflavin-S staining.

APP/PS1 mice were euthanized by terminal anesthesia (isoflurane), and the brain sections was obtained following the decapitation of mice and stored property for further analysis. Four sections per animal, located at +1.32 (cortex), -0.82 (cortex), -1.64 and -2.92 (hippocampus and cortex) from Bregma were used for analysis. Fluorescence of Aβ deposits was performed to enable visualization using confocal microscopy (Zeiss LSM 510; Carl Zeiss). A mosaic of the total brain was taken at 10x magnification. Images of amyloid burden were analyzed and quantified with the ImageJ software, and the result was expressed as a thioflavin S-positive area per mm^2.

4.5 Results

We performed measurements of cerebral tissue PO_2 in the left barrel cortex of the following five experimental groups: wild type mice at 3 and 6-month-old (WT3, WT6), transgenic Amyloid Precursor Protein Presenilin-1 (APP/PS1) mice at 3 and 6-month-old (AD3, AD6), and APP/PS1 mice at 6-month-old for which voluntary exercise was initiated at 3-month-old (AD6&EX). The APP/PS1 transgenic mice develop memory dysfunction as amyloid accumulates with pathology onset occurring around 4.5 month old (Cifuentes et al., 2015; Dickey et al., 2003; Radde et al., 2006). Fig. 4-1a depicts the two-photon microscopy setup used to record the oxygenation measurements following tissue injection of the PtP-C343 through a hole close to the cranial window. Imaging recording was performed via a transparent cranial window (see Fig. 4-1b). Multiple PO_2 grid measurements over 200 × 200 μm region were obtained though the depth of 50 - 350 μm to establish a three-dimensional (3D) PO_2 map (Fig. 4-1c, Fig. 4-1e). Angiograms were recorded to obtain the vascular morphology (see Fig. 4-1d) and blood flow properties obtained from OCT. All imaging was

conducted in awake conditions to avoid possible confounding effects from anesthesia.

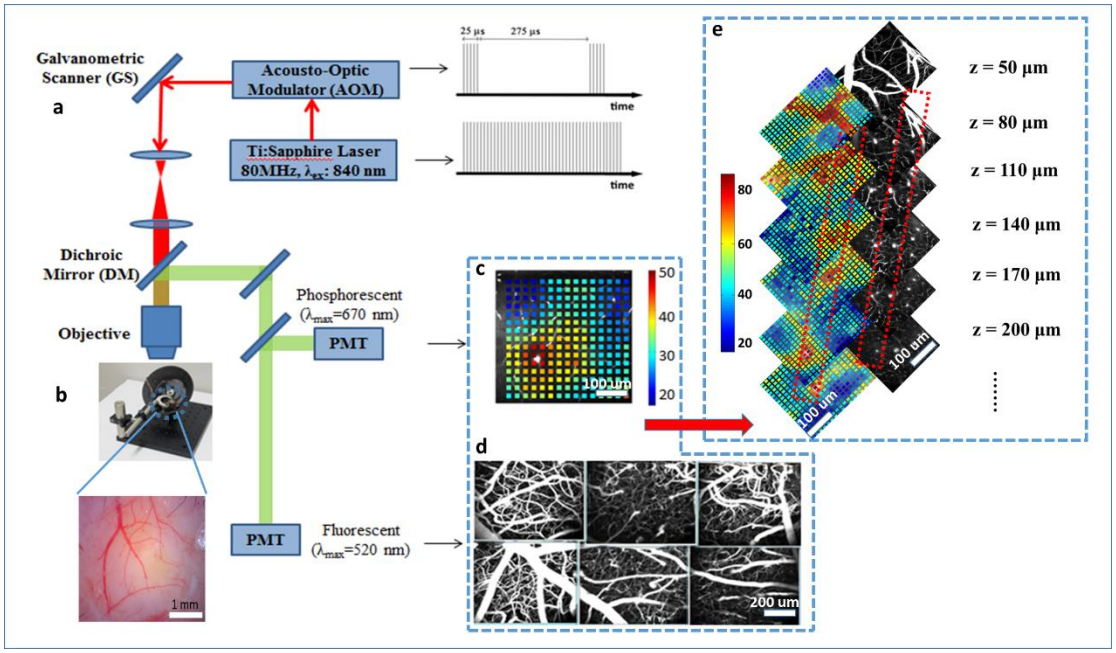

Figure 4-1. Two-photon system setup and measurements. (a) A schematic diagram of fluorescent and phosphorescent two-channel two-photon system. (b) Imaging was performed in the animals' cranial window under awake conditions. The mice could walk freely using a custom-built treadmill wheel with their head restrained by a titanium bar. The scale bar is 1 mm. (c) An example of tissue PO_2 grid measurements over a 200*200 µm region were obtained by phosphorescence lifetime microscopy, exhibiting clear tissue PO_2 gradient around penetrating arterioles. The color bar shows the PO_2 values in mmHg. The scale bar is 100 µm. (d) *En face* maximum intensity projection of six adjacent three-dimensional (3D) fluorescent angiograms through the depth of 50-350µm. The scale bar is 200 µm. (e) Examples of cerebral vascular morphology and tissue PO_2 grid measurements at different depths. Multiple planes were considered to build up a 3D PO_2 map. Top views of the two stacks show diving arterioles with positions marked with red dots lines. The scale bar is 100 µm.

4.5.1 Cerebral tissue PO_2 decreased with AD and was modulated by exercise

PO_2 grid measurements were performed on specific areas of the angiogram figures (Fig. 4-2a and 4-2b). For each sampled PO_2 point, the distance to the closest arteriolar wall was obtained by considering multiple planes in the penetrating direction. PO_2 values exhibited decreasing trend with distance from the arteriolar wall (see Fig. 4-2c). The vascular wall PO_2 values (i.e. within the first 10μm from the wall), hypothesized to be correlated with the input vascular oxygen, were similar in the WT3 group and the AD3 group, but lower in the AD6 group (see Fig. 4-2c). The PO_2 values decayed faster with distance from the arteriole wall in AD groups (both AD3 and AD6), while the PO_2 decay was slower in the AD6&EX group (see Fig. 4-2c). The average tissue PO_2 values, calculated by averaging all the sampled PO_2 values, were 46.4 ± 11.8 mmHg, 44.2 ± 12.3 mmHg, 41.4 ± 10.4 mmHg, 36.7 ± 9.9 mmHg and 45.3 ± 9.3 mmHg in the WT3, AD3, WT6, AD6 and AD6&EX mice groups, respectively (see Fig. 4-2d). The average tissue PO_2 decreased non-significantly from the WT3 group to the AD3 group, indicating potential compromise of O_2 delivery even in the early stage of AD (see Fig. 4-2d). In addition, the average tissue PO_2 was significantly lower in the AD6 group than that in the WT6 group, supporting a decrease of tissue PO_2 after the onset of AD (see Fig. 4-2d). However, the average tissue PO_2 was significantly higher in AD6&EX group than that in the AD6 group demonstrating a modulating effect of exercise on tissue PO_2 (see Fig. 4-2d). In addition, the average tissue PO_2 showed an increasing trend from WT6 to AD6&EX, indicating a potential anti-aging effect of exercises. A similar trend was observed when compartmenting data among different areas, including near arterioles, venules and tissue in the capillary bed (see Supp.Fig. 4-8). We observed an increased heterogeneity of the PO_2 spatial distribution with age (independently in WT and AD groups) and also with AD (see Fig. 4-2e) which could be due to capillary transit time heterogeneity (CTTH) (Jespersen and Østergaard, 2012) as was documented previously in APPswe-PS1ΔE9 mice (Gutierrez-Jimenez, E. Angleys et al., 2018). This heterogeneity was reduced with exercise (see Fig. 4-2e).

The accumulation of Aβ peptides is a hallmark of a pathological diagnosis of AD (Albert et

al., 2011). To further examine the impact of exercise the progression of AD, we performed Aβ staining *ex vivo* (see Fig. 4-3a). We observed that the Aβ accumulation significantly increased in the cortex from the AD3 group (13.8 ± 7.1 Aβ/mm^2) to the AD6 group (35.1 ± 6.9 Aβ/mm^2) and significantly decreased from the AD6 group to the AD6&EX group (28.0 ± 5.2 Aβ/mm^2) (see Fig. 4-3b).

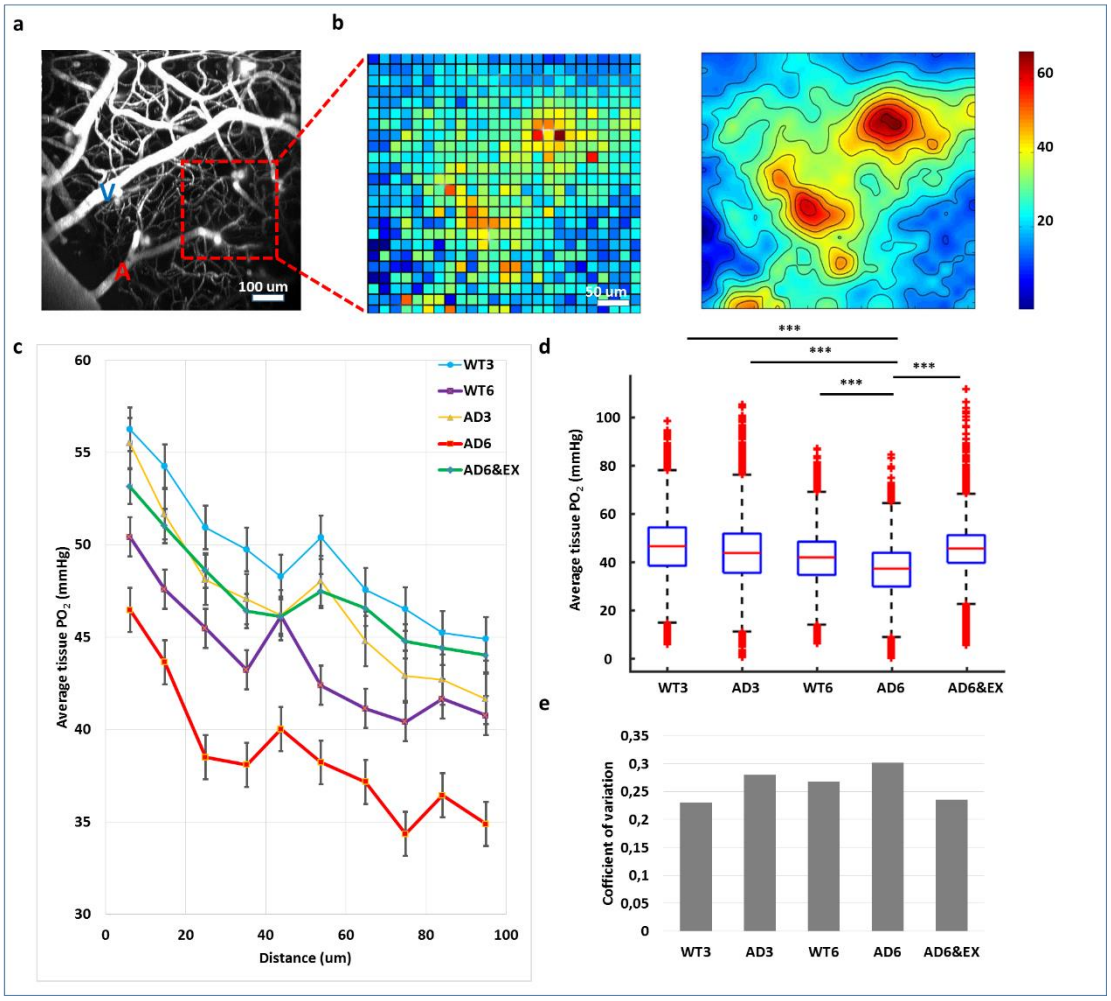

Figure 4-2. An example of vascular angiogram with arterioles (A, red) and venules (V, blue). The scale bar is 100 μm. (b) Left: the PO_2 grid measurement for the area in the red frame; Right: contour plot for the left image. The scale bar is 50 μm. (c) The variation of average tissue PO_2 with distance from the vessel wall in different experimental groups. (d) Average tissue PO_2 in different experimental groups (WT3: n=20391, AD3: n=18038, WT6: n=26124, AD6: n=22171, AD6&EX: n=22272 sampled points). The box represents interquartile range,

the central line indicates the median and the whiskers extend to the most extreme data points; the outliers are plotted individually using the '+' symbol. Statistical significance was computed using ANOVA followed by Tukey HSD post hoc tests, comparisons to AD6 shown. ***: $p < 0.001$. The principle of box plot and significance level also apply to figures in the rest of the paper. (e) Heterogeneity of tissue PO_2 in all experimental groups (calculated as standard deviation of PO_2/mean) (WT3: n=20391, AD3: n=18038, WT6: n=26124, AD6: n=22171, AD6&EX: n=22272 sampled points).

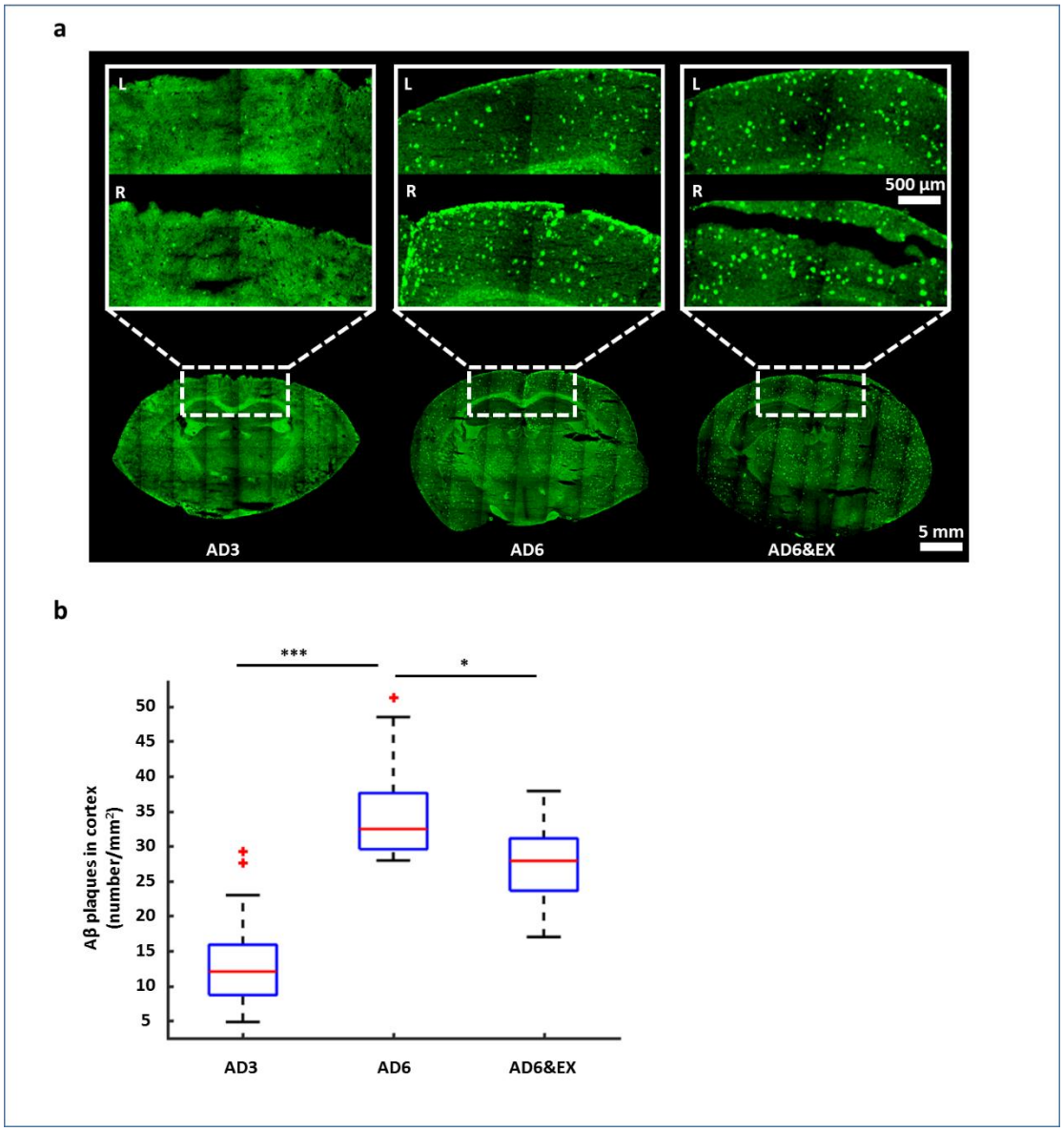

Figure 4-3. (a) Staining of Aβ plaques in the cortex area in mice groups of AD3, AD6, and

AD6&EX with magnified images in solid white frames representing the left and right parts of the areas in white dashed frames in three different groups. The scale bar is 5 mm. (b) Box plot of Aβ plaques in the cortex, quantified by the total number of Aβ plaques divided by the area of imaging (mm^2). Aβ increased with age but decreased with exercise in the AD groups (AD3: n = 17, AD6: n = 17; AD6&EX: n = 22 sampled slices).

4.5.2 Brain tissue hypoxic potential was increased with AD and reduced by exercise

Given observed heterogeneity in PO_2, we then investigated how low PO_2 regions were organized spatially in different experimental groups. Reported values in the literature for critical tissue PO_2 mainly range between 0.01 - 9 mmHg (Chance, 1957; K.A. Kasischke et al., 2011; MacMillan and Siesjo, 1971; Vaupel et al., 2007). Accordingly, we defined near-hypoxic regions as the areas where PO_2 was less than 10 mmHg and regions with hypoxic potential as PO_2 less than 15 mmHg. Fig 4a displays a few regions with low PO_2 at two different depths (120 μm and 220 μm). Despite of the presence of an arteriole, there were areas with low PO_2 values, which were located farther from the arteriole (see Fig. 4-4a), increasing the potential for neuronal loss in these areas. Performing a group analysis and investigating sampled points distributions, we observed that regions with low PO_2 values were more frequent in AD groups (AD3 and AD6) than those in non-AD groups (WT3 and WT6) and the exercise group (AD6&EX) (see Fig. 4-4b). Investigation of the data revealed that the AD6 mice group had around 0.4% of points below the 10 mmHg threshold (see Fig. 4-4c). However, few such points were detected in the other mice groups (see Fig. 4-4c). These trends were confirmed despite raising the threshold to 15 mmHg (see Fig. 4-4d). In the AD6&EX group, voluntary exercise reversed this effect by increasing the level of PO_2 and decreasing the percentage of low PO_2 areas.

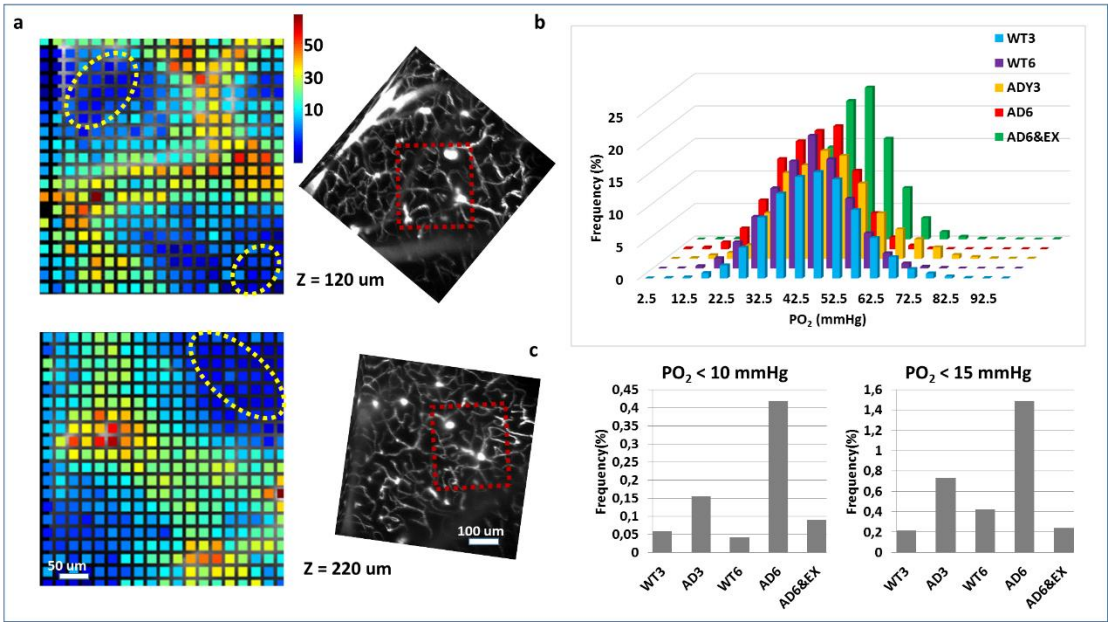

Figure 4-4. Near-hypoxic domains in the AD6 group and the modulation of voluntary exercise. (a) (Right) Two representative near-hypoxic domains observed in the AD6 group (marked with red dots lines). The scale bar is 100 μm. (Left) The corresponding PO_2 3D grid measurement over a 200* 200 μm region at two different depths (120 μm and 220 μm) and the zoomed near-hypoxic domains (marked with yellow dots lines). The scale bar is 50 μm. (b) Frequency of PO_2 value distribution for each group. (c) Frequency of PO_2 values lower than 10 mmHg in each group. The proportion of near-hypoxic points increased sharply with AD. (d) Frequency of PO_2 values lower than 15 mmHg in each group.

4.5.3 AD was associated with lower oxygen input and higher oxygen extraction fraction, reversed by exercise.

We measured vascular-wall PO_2 (within 5 μm from the wall) as a proxy for vascular PO_2 in penetrating arterioles and venules in all mice groups. Specifically, we exploited vascular wall PO_2 to estimate the vascular PO_2 (inside the vessels) using a ratio (PO_2 at vascular wall divided by vascular PO_2) of 0.55, based on the work of Moeini et al.(Moeini et al., 2018) which measured PO_2 values at both wall and inside the vessels and found a mainly constant ratio around 0.55 in all mice groups (young, middle-aged, and old). The PO_2 values next to

the wall of arterioles were 56.2 ± 11.2 mmHg, 55.5 ± 12.0 mmHg, 50.3 ± 10.7 mmHg, 46.5 ± 7.9 mmHg and 53.2 ± 7.9 mmHg in the WT3, AD3, WT6, AD6 and AD6&EX mice groups, respectively. The PO_2 values next to the wall of venules were 42.0 ± 9.7 mmHg, 40.8 ± 12.7 mmHg, 38.6 ± 10.8 mmHg, 34.8 ± 10.3 mmHg and 41.5 ± 8.9 mmHg in the WT3, AD3, WT6, AD6 and AD6&EX mice groups, respectively.

Overall, PO_2 values at the arteriolar wall were significantly lower in the AD6 group than those in the WT6 group (see Fig. 4-5a). However, the PO_2 values at the arteriolar wall was significantly higher in the AD6&EX group than those in the AD6 group (see Fig. 4-5a), suggesting that exercise modulated oxygen input from arterioles. The PO_2 values at the venule wall exhibited similar trend in different mice groups as those at the arteriole wall did (see Fig. 4-5b). Estimated oxygen saturation (SO_2) was then calculated from vascular PO_2 based on the oxygen dissociation curve of mouse hemoglobin suggested by Uchida et al. [40] with Hill coefficients specific for C57BL/6 MICE (h=2.59 and P50 = 40.2 mmHg). Estimations of oxygen extraction fraction (OEF) were then computed by $OEF=(SaO_2-SvO_2)/SaO_2$). The estimated OEF was higher in the AD6 group than that in other groups (see Fig. 4-5c).

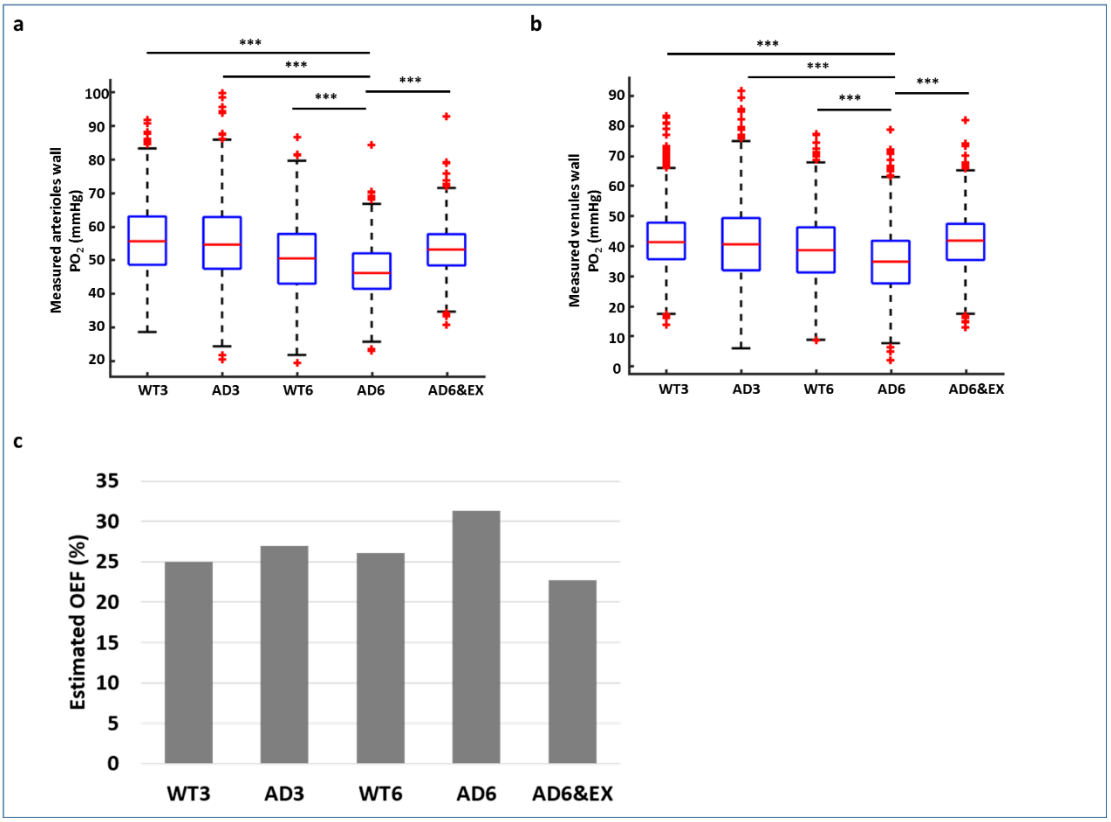

Figure 4-5. Oxygen supply and consumption in different groups. (a) Arterioles wall PO_2 (WT3: n= 30, AD3: n= 26, WT6: n= 36, AD6: n = 32, AD6&EX, n = 40 vessels) in each group. (b) Venules wall PO_2 (WT3, n= 30; AD3, n= 26; WT6, n= 36; AD6, n = 32; AD6&EX, n = 40 vessels) in each group. Wall PO_2 were calculated by the average of PO_2 values within a distance of 10 μm from the arteriole or venule wall. (c) Oxygen extraction fraction (OEF=(SaO_2-SvO_2)/SaO_2) was obtained from averaged arteriolar and venular SO_2 values, which were converted from vascular wall PO_2 values using Hill's equation.

4.5.4 Changes in non-capillary blood flow with AD and exercise

Blood flow in non-capillary vessels (diameter >10 μm) was recorded using Doppler Optical Coherence Tomography (OCT) in all mice groups (see Fig. 4-6a). For each animal, total cerebral blood flows were averaged through the depth of 50-100 μm to obtain the mean total flow near the cortical surface. The CBF values were 1.25± 0.2 ml/g/min, 1.16 ± 0.5 ml/g/min,

1.55 ± 0.3 ml/g/min, 1.46 ± 0.3 ml/g/min, and 1.94 ± 0.4 ml/g/min in the WT3, AD3, WT6, AD6 and AD6&EX mice groups, respectively. We observed that total CBF displayed a decreasing trend from the WT6 group to the AD6 group. However, total CBF increased with voluntary exercise, as the CBF value was significantly higher in AD6&EX group than that in the AD6 group (see Fig. 4-6b). The CBF values showed increasing trend from the 6-month groups (i.e. AD6, WT6) to the 3-month group (i.e., AD3, WT3), which was consistent with findings in previous study (Moeini et al., 2018) showing an increase of CBF from young to middle aged mice due to increase of vascular diameter.

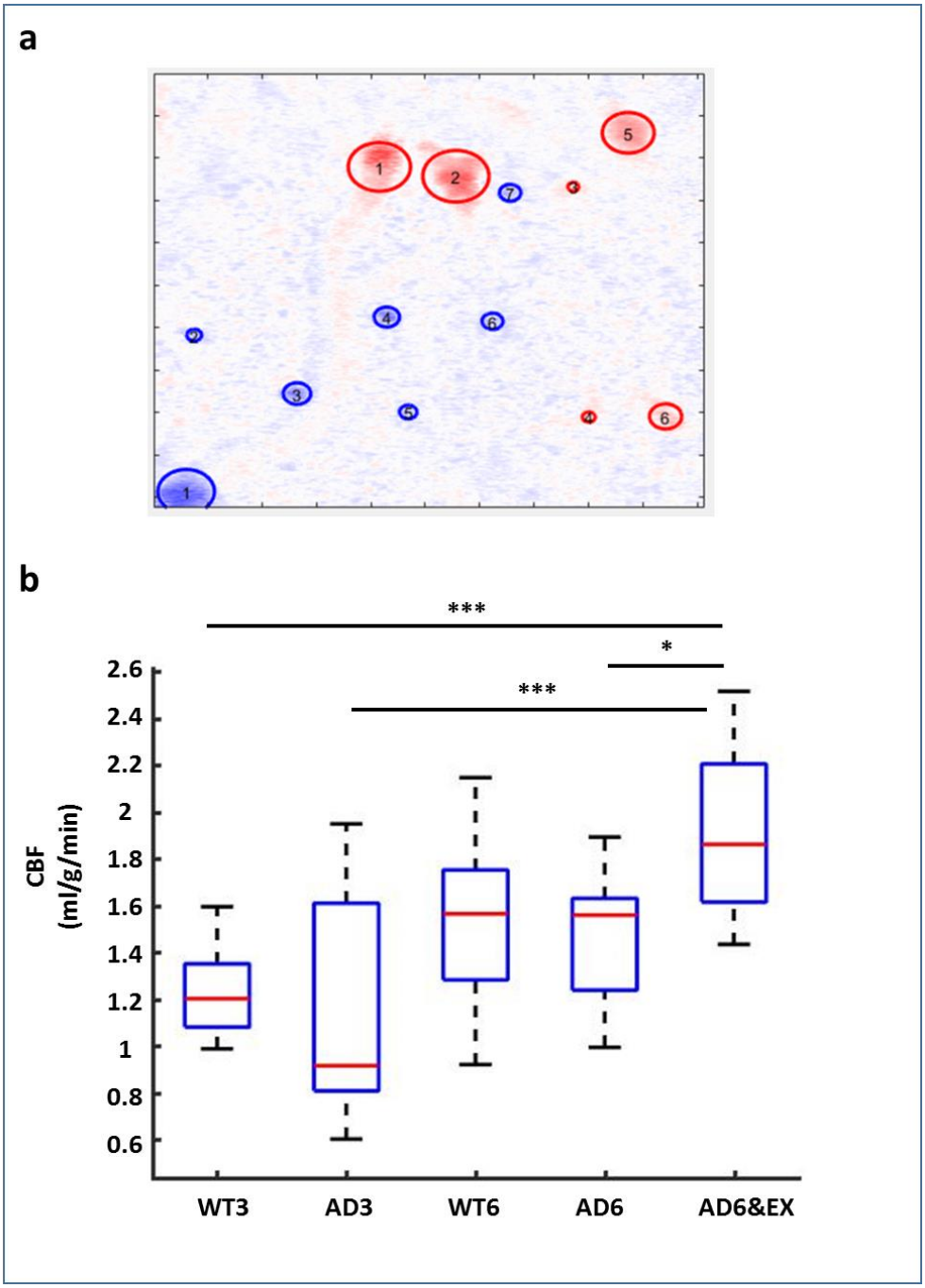

Figure 4-6. Non-capillary blood flow. (a) En face maximum intensity projection of a 3D OCT velocity volume at the depth of 50-100 μm. The top 50 μm volumes were removed to exclude the surface vessels. Positive velocity (red) represents arterioles and negative velocity (blue) represents venules. (b) For each animal, total cerebral blood flows were averaged through the depth of 50-100 μm to obtain the mean total flow near the cortical surface, as an estimate of

regional CBF (WT3:n=11, AD3: n=11, WT6: n=11, AD6: n=11, AD6&EX: n=11 c-scan volumes).

4.5.5 Running distance correlates with brain oxygenation and blood flow

Each mouse in the exercise group displayed different voluntary wheel-running distance over the period of 3 months where they were in the cages equipped with a wheel. To quantify the effect of distance on PO_2, we correlated values with running distance in the AD6&EX group. We also measured the spatial coefficient of variation of PO_2 in the capillary bed, since hypoxia was more likely to occur in areas far away from large vessels. Following Cohen (1988) (Cohen, 1988), which suggests that R^2 greater than 0.37 is considered large in a regression analysis, we used 0.37 as the threshold for R^2 to evaluate the correlation.

Strong correlations were observed between running distance and PO_2 near arterioles, venules and in the capillary bed, with R^2 of 0.62, 0.83 and 0.67, respectively (see Fig. 4-7a, 4-7b, 4-7c). The mean running distance was 2.7 km per day ranging from 2.4 to 4.0 km per day. Additionally, we found that the spatial coefficient of variation of PO_2 in the capillary bed was negatively associated with the running distance in the AD6&EX group (see Fig. 4-7d). Correlation between non-capillary blood flow and running distance was also examined. The arteriole mean flow was positively associated with running distance (R^2= 0.64, see Fig. 4-7e). However, the venule mean flow did not significantly correlate with the running distance ($R^2 <$ 0.37, see Fig. 4-7f).

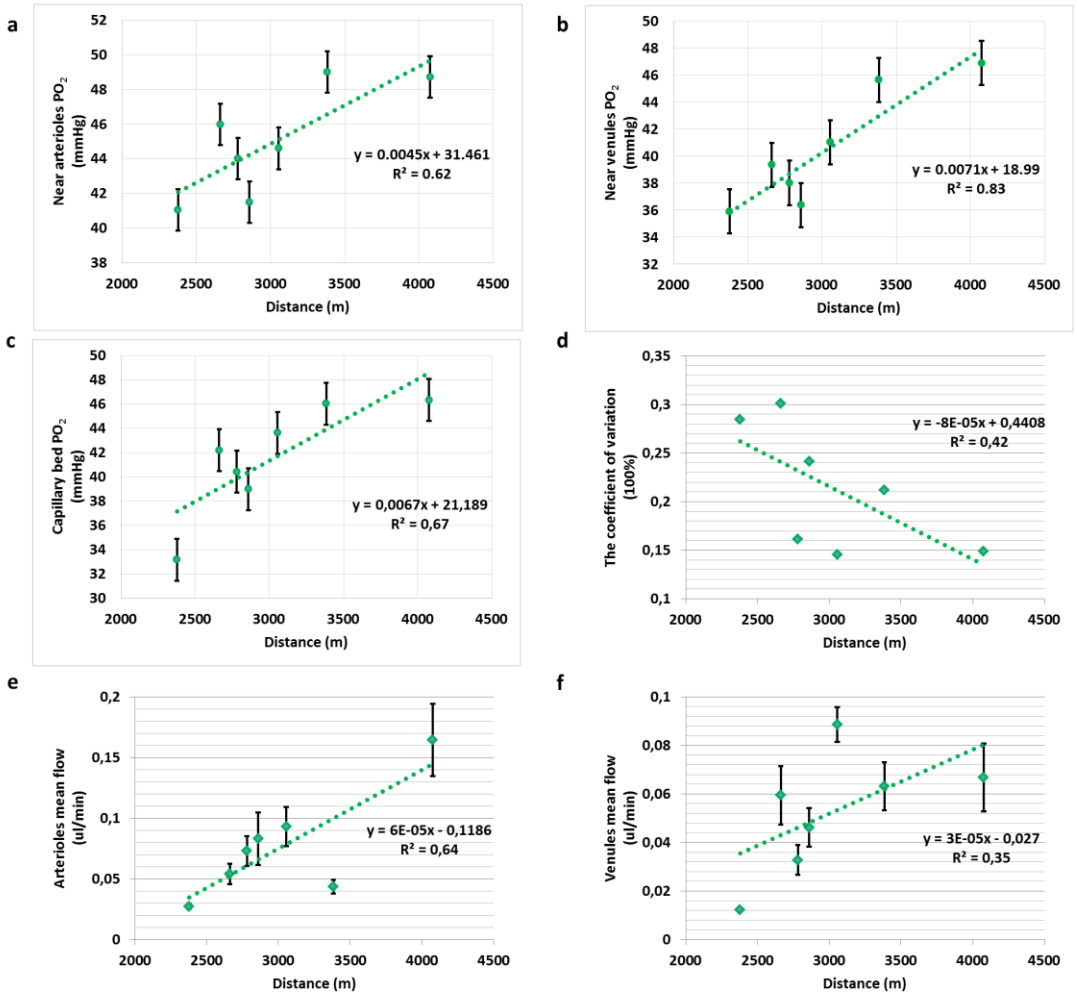

Figure 4-7. Tissue oxygenation and their relationships with running distance. (a, b, c) Strong correlations between running distance and near arterioles/near venules/capillary bed PO_2 values in the AD6&EX group (n=7 mice). The running distance was averaged over 90 days. (d) Spatial heterogeneity of PO_2 in the capillary bed was negatively associated with the running distance in the AD6&EX group. (e) and (f) show the correlation between the mean flow and the running distance for arterioles and venules, respectively (n=7 mice).

4.6 Discussion

In this study, we found AD-related decreases in tissue PO_2 in the mouse cortex *in vivo* and a modulatory effect of voluntary exercise on tissue PO_2 using two-photon phosphorescence

lifetime measurements. Exploiting Doppler-OCT, non-capillary blood flow properties were also quantified in all experimental groups. Specifically, the key findings of the present study include 1) a decrease in average tissue PO_2 with the onset of AD after 4.5 month (Cifuentes et al., 2015) (we used the same mouse model as the study of Cifuentes et al. (Cifuentes et al., 2015) which found that the APP/PS1 mice displayed cognitive impairment in the episodic-like memory task starting from 4.5 month. Thus, in our study, we didn't repeat the memory task to quantify the extent of cognitive decline), 2) higher spatial heterogeneity of tissue PO_2 with both age and AD, 3) a modulatory effect of voluntary exercise on the-above mentioned relationships by increasing tissue PO_2 and decreasing the spatial heterogeneity of tissue oxygenation and reducing the frequency of occurrence of near-hypoxic areas in the AD mice group, 4) a decrease of total blood flow, reversed by exercise, and 5) a dose-response relationship between running distance and brain oxygenation / blood flow. Our results further suggest that the changes in PO_2 had the same trend in different regions, including near arterioles, near venules, and capillary bed, with voluntary exercise having similar modulating effects in these different areas.

Brain physiology gains benefits from voluntary exercise based on both preclinical models and humans (Blurton-Jones et al., 2009; Dorr et al., 2017; Kim et al., 2016; Radak et al., 2010). Prior studies suggest that exercise-induced upregulation of vascularization can ameliorate oxygenation dysfunction in AD subjects (Kim et al., 2016; Radak et al., 2010). Exercise has the capability of inducing the brain-derived neurotrophic factor (BDNF) (Dorr et al., 2017) and nerve growth factor (NGF), which may contribute to decrease the speed of progression of AD (Blurton-Jones et al., 2009; Radak et al., 2010), resulting in enhanced cognitive function. Our study contributes to this stream of research by revealing the beneficial effects of voluntary exercise in the AD mouse model on tissue oxygenation which supports the metabolic demand of neurons and the potential anti-aging effect of exercise on tissue oxygenation.

4.6.1 Hypoxic micro-pockets and AD

Our observation of near-hypoxic areas in the AD mice group relates to previous neuro-pathological studies which found that tiny microinfarcts are common particularly in aging brain samples suffering cognitive decline, such as AD (Grammas, 2011; Smith et al., 2012; Wang et al., 2012). Prior studies reported neuronal loss and cognitive impairment in a mouse model with multiple diffuse microinfarcts (Wang et al., 2012; Zlokovic, 2011). In addition, hypoxia could facilitate the amyloidogenic APP processing by increasing the activity of two key enzymes necessary for Aβ production (Zlokovic, 2011). These and our findings suggest that near-hypoxic areas observed in the AD group may be one of the mechanisms involved in the onset of AD. Whether inhibiting hypoxia-associated pathways could delay or control the progression of AD remains unclear, and future studies may investigate the preventive method for hypoxia and its influence on the onset of AD.

4.6.2 The link between voluntary exercise and Aβ protein in AD

Our *ex vivo* staining study further suggests that voluntary exercise slowed cortical accumulation of Aβ deposits in the ADO&EX group. Although small and potentially with limited biological significance in this very aggressive mouse model, this demonstrates that exercise improves clearance of Aβ deposits and/or reduces their production: in the long term, this suggests that exercise could contribute to delay the onset of AD in patients at risk. A study using the neuron-specific enolase (NSE)/Swedish mutation of amyloid-β protein precursor (Aβ PP) transgenic mice showed that 16 weeks of treadmill running decreased the levels of the Aβ in the AD mice model (Um et al., 2008). Other animal studies also suggest healthy life-style could protect against neurodegeneration associated with AD by decreasing the Aβ levels in the cortex and hippocampus (Walker et al., 2015). Our study showed consistent finding on the potential beneficial effects of voluntary exercise on the control of Aβ deposits accumulation with prior studies. In addition, our study takes a further step to

understand the oxygenation mechanism associated with this change to Aβ deposits. Specifically, the accumulation of Aβ deposits is accompanied by a compromised cerebral tissue oxygenation. Due to the limitation of sample size, we did not establish a link between the running distances and the number of Aβ deposits, a direction to be considered in future studies.

4.6.3 The dose-response relationship between running distance and cerebral tissue oxygenation/blood flow

We observed positive correlations between running distance and tissue PO_2 in different areas. Running distance was also positively associated with arteriolar blood flow. This dose-response finding may provide insight for future studies to explore exercise intensity with the purpose of maximizing benefits for cerebral tissue oxygenation and blood flow in AD patients. Given our limited intervention and maximal total running distance (around 4,000 meters), future research may explore whether an inverted U-shaped relationship will be present after the running distance exceeds 4,000 meters. Prior studies suggest that prolonged exercise in high density reduces muscular fatigue and improves cardiac performance in rats (Di Filippo et al., 2015). Other studies suggest an inverted U-shaped relationship between exercise and cognitive function such that cognitive performance decreases after reaching the optimal intensity of exercise in human subjects (Kamijo et al., 2007; Kashihara et al., 2009; Mekari et al., 2015). Thereby, future study may further examine the impact of the extent of exercise on improving tissue oxygenation/blood flow in AD models.

4.6.4 Awake imaging of cerebral oxygenation

We have developed a technique to image cerebral oxygenation in awake condition to remove the confounding effects from anesthesia, since anesthesia could change physiological and hemodynamic parameters in experimental animals (Schroeter et al., 2014). Our method is based on an angled-wheel that allows mice to walk without signs of stress, while their heads

were restrained below the objective of a two-photon microscope. The relatively modest motion between brain and microscope facilitated brain oxygenation imaging using O_2-sensitive probe in awake mice.

4.7 Conclusion

The present investigation provides evidence that exercise could play a preventive role by adjusting the vascular structure and cerebral oxygenation to facilitate the efficient supply of oxygen. Although AD is associated with compromised brain oxygenation in our mouse model, voluntary exercise could be an important means for preserving neurovascular coupling and slow the rate of neurodegeneration in patients at risk of AD.

4.8 Acknowledgement

The authors thank Marc-Antoine Gillis and Natacha Duquette for their help with the animal preparations. This study was supported with a discovery grant from the Natural Sciences and Engineering Research Council of Canada awarded to Frederic Lesage.

Author contributions

Conceptualizations: X. L, M. M., B. L. and F. L.

Formal analysis: X. L, M. M. and B. L. and O. M.,

Funding acquisition: F. L.

Investigation: X. L. and M. M.

Methodology: X. L., M. M., B. L., O. M., Y. L., S. B., E. T. and F. L.

Project administration: F. L.

Software: X. L, M. M., and F. L.

Supervision: E. T. and F. L.

Writing – original draft: X. L.

Writing – review & editing: X. L., M. M., B. L., O. M., Y. L., S. B., E. T. and F. L.

Conflict of Interests

Dr. Lesage reports a minority ownership in LabeoTech Inc.

4.9 References

Adlard, P.A., Perreau, V.M., Pop, V., Cotman, C.W., 2005. Voluntary exercise decreases amyloid load in a transgenic model of Alzheimer's disease. Journal of Neuroscience 25, 4217–4221.

Albert, M.S., DeKosky, S.T., Dickson, D., Dubois, B., Feldman, H.H., Fox, N.C., Gamst, A., Holtzman, D.M., Jagust, W.J., Petersen, R.C., Snyder, P.J., 2011. The diagnosis of mild cognitive impairment due to Alzheimer's disease: Recommendations from the National Institute on Aging-Alzheimer's Association workgroups on diagnostic guidelines for Alzheimer's disease. Alzheimer's & Dementia 7, 270–279.

Baraghis, E., Bolduc, V., Lefebvre, J., Srinivasan, V.J., Boudoux, C., Thorin, E., Lesage, F., 2011. Measurement of cerebral microvascular compliance in a model of atherosclerosis with optical coherence tomography. Biomedical Optics Express 2, 3079–3093.

Barnes, D.E., Yaffe, K., Satariano, W.A., Tager, I.B., 2003. A longitudinal study of cardiorespiratory fitness and cognitive function in healthy older adults. Journal of the American Geriatrics Society 51, 459–465.

Blurton-Jones, M., Kitazawa, M., Martinez-Coria, H., Castello, N.A., Müller, F.J., Loring, J.F., Yamasaki, T.R., Poon, W.W., Green, K.N., LaFerla, F.M., 2009. Neural stem cells improve cognition via BDNF in a transgenic model of Alzheimer disease. Proceedings of the National Academy of Sciences 106, 13594–13599.

Chance, B., 1957. Cellular oxygen requirements. Fed Proc 16, 671–680.

Cifuentes, D., Poittevin, M., Dere, E., Broquères-You, D., Bonnin, P., Benessiano, J., Pocard, M., Mariani, J., Kubis, N., Merkulova-Rainon, T., Lévy, B.I., 2015. Hypertension accelerates the progression of Alzheimer-like pathology in a mouse model of the disease.

Hypertension 65, 218–224.

Cohen, J., 1988. Statistical power analysis for the behavioral sciences (2nd ed.). Lawrence Erlbaum Associates, Hillsdalle, NJ.

Di Filippo, C., Trotta, M.C., Maisto, R., Siniscalco, D., Luongo, M., Mascolo, L., Alfano, R., Accardo, M., Rossi, C., Ferraraccio, F., D'Amico, M., 2015. Daily oxygen/O3 treatment reduces muscular fatigue and improves cardiac performance in rats subjected to prolonged high intensity physical exercise. Oxidative Medicine and Cellular Longevity.

Dickey, C.A., Loring, J.F., Montgomery, J., Gordon, M.N., Eastman, P.S., Morgan, D., 2003. Selectively reduced expression of synaptic plasticity-related genes in amyloid precursor protein+ presenilin-1 transgenic mice. Journal of Neuroscience 23, 5219–5226.

Dorr, A., Thomason, L.A., Koletar, M.M., Joo, I.L., Steinman, J., Cahill, L.S., Sled, J.G., Stefanovic, B., 2017. Effects of voluntary exercise on structure and function of cortical microvasculature. Journal of Cerebral Blood Flow & Metabolism 37, 1046–1059.

Farkas, E., Luiten, P.G.M., 2001. Cerebral microvascular pathology in aging and Alzheimer's disease, Progress in Neurobiology. https://doi.org/10.1016/S0301-0082(00)00068-X

Finikova, O.S., Lebedev, A.Y., Aprelev, A., Troxler, T., Gao, F., Garnacho, C., Muro, S., Hochstrasser, R.M. Vinogradov, S.A., 2008. Oxygen Microscopy by Two-Photon-Excited Phosphorescence. ChemPhysChem 9, 1673–1679.

Geda, Y.E., Roberts, R.O., Knopman, D.S. Christianson, T.J. Pankratz, V.S., Ivnik, R.J., Boeve, B.F., Tangalos, E.G., Petersen, R.C., Rocca, W.., 2010. Physical exercise, aging, and mild cognitive impairment: a population-based study. Archives of neurology 67, 80–86.

Girouard, H., Iadecola, C., 2006. Neurovascular coupling in the normal brain and in hypertension, stroke, and Alzheimer disease. Journal of Applied Physiology 100, 328–335.

Grammas, P., 2011. Neurovascular dysfunction, inflammation and endothelial activation: implications for the pathogenesis of Alzheimer's disease. Journal of Neuroinflammation

8, 26.

Gutierrez-Jimenez, E. Angleys, H., Rasmussen, P.M., West, M.J., Catalini, L., Iversen, N.K., Jensen, M.S., Frische, S., Østergaard, L., 2018. Disturbances in the control of capillary flow in an aged APPswe/PS1ΔE9 model of Alzheimer's disease. Neurobiology of Aging 62, 82–94.

Heyn, P., Abreu, B.C., Ottenbacher, K.J., 2004. The effects of exercise training on elderly persons with cognitive impairment and dementia: A meta-analysis. Archives of Physical Medicine and Rehabilitation 85, 1694–1704.

Jespersen, S.N., Østergaard, L., 2012. The roles of cerebral blood flow, capillary transit time heterogeneity, and oxygen tension in brain oxygenation and metabolism. Journal of cerebral blood flow & metabolism 32, 264–277.

Kamijo, K., Nishihira, Y., Higashiura, T., Kuroiwa, K., 2007. The interactive effect of exercise intensity and task difficulty on human cognitive processing. International Journal of Psychophysiology 65, 114–121.

Kashihara, K., Maruyama, T., Murota, M., Nakahara, Y., 2009. Positive effects of acute and moderate physical exercise on cognitive function. Journal of Physiological Anthropology 28, 155–164.

Kasischke, K.A., Lambert, E.M., Panepento, B., Sun, A., Gelbard, H.A., Burgess, R.W., Foster, T.H., Nedergaard, M., 2011. Two-photon NADH imaging exposes boundaries of oxygen diffusion in cortical vascular supply regions. Journal of Cerebral Blood Flow & Metabolism 31, 68–81.

Kasischke, K.A., Lambert, E.M., Panepento, B., Sun, A., Gelbard, H.A., Burgess, R.W., Foster, T.H., Nedergaard, M., 2011. Two-photon NADH imaging exposes boundaries of oxygen diffusion in cortical vascular supply regions. Journal of Cerebral Blood Flow and Metabolism 31, 68–81. https://doi.org/10.1038/jcbfm.2010.158

Ke, Z., Yip, S.P., Li, L., Zheng, X.X., Tong, K.Y., 2011. The effects of voluntary, involuntary, and forced exercise on brain-derived neurotrophic factor and motor function recovery: a

rat brain ischemia model. PloS One 6, e16643.

Kim, D.Y., Jung, S.Y., Kim, K., Kim, C.J., 2016. Treadmill exercise ameliorates Alzheimer disease-associated memory loss through the Wnt signaling pathway in the streptozotocin-induced diabetic rats. Journal of Exercise Rehabilitation 12, 276–283.

Kramer, A.F., Hahn, S., Cohen, N.J., Banich, M.T., McAuley, E., Harrison, C.R., Chason, J., Vakil, E., Bardell, L., Boileau, R.A., Colcombe, A., 1999. Ageing, fitness and neurocognitive function. Nature 400, 418.

Kretschmann, H., Kammradt, G., Krauthausen, I., Sauer, B., Wingert, F., 1986. Brain growth in man. Bibl Anat 28, 1–26.

Larson, E.B., Wang, L., Bowen, J.D., Mccormick, W.C., Teri, L., Crane, P., Kukull, W., 2006. Exercise Is Associated with Reduced Risk for Incident Dementia among Persons 65 Years of Age and Older. Annals of Internal Medicine 144, 73–81.

MacMillan, V., Siesjo, B.K., 1971. Critical oxygen tensions in the brain. Acta Physiol Scand 82, 412–414.

Mekari, S., Fraser, S., Bosquet, L., Bonnéry, C., Labelle, V., Pouliot, P., Lesage, F., Bherer, L., 2015. The relationship between exercise intensity, cerebral oxygenation and cognitive performance in young adults. Physiology, European Journal of Applied 115, 2189–2197.

Moeini, M., Lu, X., Avti, P.K., Damseh, R., Bélanger, S., Picard, F., Boas, D., Kakkar, A., Lesage, F., 2018. Compromised microvascular oxygen delivery increases brain tissue vulnerability with age. Scientific Reports 8, 8219.

Montagne, A., Nation, D.A., Pa, J., Sweeney, M.D., Toga, A.W., Zlokovic, B.V., 2016. Brain imaging of neurovascular dysfunction in Alzheimer's disease. Acta Neuropathologica 131, 687–707.

Naylor, A.S., Bull, C., Nilsson, M.K., Zhu, C., Björk-Eriksson, T. Eriksson, P.S., Blomgren, K., Kuhn, H.G., 2008. Voluntary running rescues adult hippocampal neurogenesis after irradiation of the young mouse brain. Proceedings of the National Academy of Sciences 105, 14632–14637.

Paxinos, G., Franklin, K., 2001. The Mouse Brain: In Stereotaxic Coordinates, in: Acadamic Press. p. 296.

Pedersen, L., Idorn, M., Olofsson, G.H., Lauenborg, B., Nookaew, I., Hansen, R.H., Johannesen, H.H., Becker, J.C., Pedersen, K.S., Dethlefsen, C., Nielsen, J., 2016. Voluntary running suppresses tumor growth through epinephrine-and IL-6-dependent NK cell mobilization and redistribution. Cell metabolism 23, 554–562.

Radak, Z., Hart, N., Sarga, L., Koltai, E., Atalay, M., Ohno, H., Boldogh, I., 2010. Exercise plays a preventive role against Alzheimer's disease. Journal of Alzheimer's Disease 20, 777–783.

Radde, R., Bolmont, T., Kaeser, S.A. Coomaraswamy, J. Lindau, D., Stoltze, L., Calhoun, M.E., Jäggi, F., Wolburg, H., Gengler, S., Haass, C., 2006. Aβ42-driven cerebral amyloidosis in transgenic mice reveals early and robust pathology. EMBO Reports, 7, 940–946.

Ren, H., Sun, T., MacDonald, D.J., Cobb, M.J., Li, X., 2006. Real-time in vivo blood-flow imaging by moving-scatterer-sensitive spectral-domain optical Doppler tomography. Optics Express 31, 927–929.

Rozhkov, V., Wilson, D., Vinogradov, S., 2002. Phosphorescent Pd Porphyrin−Dendrimers: Tuning Core Accessibility by Varying the Hydrophobicity of the Dendritic Matrix. Macromolecules 35, 1991–1993.

Sakadži, S., Roussakis, E., Yaseen, M.A., Mandeville, E.T., Srinivasan, J., Arai, K., Ruvinskaya, S., Devor, A., Lo, E.H., Sergei, A., Boas, D.A., 2010. Two-photon high-resolution measurement of partial pressure of oxygen in cerebral vasculature and tissue. Nat Methods 7, 755–759. https://doi.org/10.1038/nmeth.1490.Two-photon

Sakadžić, S., Mandeville, E.T., Gagnon, L., Musacchia, J.J., Yaseen, M.A., Yucel, M.A., Lefebvre, J., Lesage, F., Anders, M., Eikermann-haerter, K., Ayata, C., Srinivasan, V.J., Lo, E.H., Devor, A., Boas, D.A., 2014a. Margin of Oxygen Supply To Cerebral Tissue. Nature communications. https://doi.org/10.1038/ncomms6734.Large

Sakadžić, S., Mandeville, E.T., Gagnon, L., Musacchia, J.J., Yaseen, M.A., Yucel, M.A., Lefebvre, J., Lesage, F., Dale, A.M., Eikermann-Haerter, K., Ayata, C., Srinivasan, V.J., Lo, E.H., Devor, A., Boas, D.A., 2014b. Large arteriolar component of oxygen delivery implies a safe margin of oxygen supply to cerebral tissue. Nature Communications 5. https://doi.org/10.1038/ncomms6734

Schroeter, A., Schlegel, F., Seuwen, A., Grandjean, J., Rudin, M., 2014. Specificity of stimulus-evoked fMRI responses in the mouse: the influence of systemic physiological changes associated with innocuous stimulation under four different anesthetics. Neuroimage 94, 372–384.

Selkoe, D.., Schenk, D., 2003. Alzheimer's disease: molecular understanding predicts amyloid-based therapeutics. Annu Rev Pharmacol Toxicol 43, 545–584.

Singh, M.A.F., 2002. Exercise comes of age: rationale and recommendations for a geriatric exercise prescription. The Journals of Gerontology Series A: Biological Sciences and Medical Sciences 57, 262–282.

Smith, E.E., Schneider, J.A., Wardlaw, J.M., Greenberg, S.M., 2012. Cerebral microinfarcts: The invisible lesions. The Lancet Neurology 11, 272–282. https://doi.org/10.1016/S1474-4422(11)70307-6

Srinivasan, V.J., Mandeville, E.T., Can, A., Blasi, F., Climov, M., Daneshmand, A., Lee, J.H., Yu, E., Radhakrishnan, H., Lo, E.H., Sakadžić, S., Eikermann-Haerter, K., Ayata, C., 2013. Multiparametric, Longitudinal Optical Coherence Tomography Imaging Reveals Acute Injury and Chronic Recovery in Experimental Ischemic Stroke. PLoS ONE 8. https://doi.org/10.1371/journal.pone.0071478

Um, H.S., Kang, E.B., Leem, Y.H., Cho, I.H., Yang, C.H., Chae, K.R., Hwang, D.Y., Cho, J.Y., 2008. Exercise training acts as a therapeutic strategy for reduction of the pathogenic phenotypes for Alzheimer's disease in an NSE/APPsw-transgenic model. International journal of molecular medicine 22, 529–539.

Vaupel, P., Höckel, M., Mayer, A., 2007. Detection and characterization of tumor hypoxia

using pO2 histography. Antioxidants & Redox Signaling 9, 1221–1236.

Vinogradov, S.A., 2005. Arylamide Dendrimers with Flexible Linkers via Haloacyl Halide Method. Org. Lett. 1761–1764.

Voss, M.W., Weng, T.B., Burzynska, A.Z., Wong, C.N., Cooke, G.E., Clark, R., Fanning, J., Awick, E., Gothe, N.P., Olson, E.A., McAuley, E., 2016. Fitness, but not physical activity, is related to functional integrity of brain networks associated with aging. Neuroimage 131, 113–125.

Walker, J.M., Klakotskaia, D., Ajit, D., Weisman, G.A., Wood, W.G., Sun, G.Y., Serfozo, P., Simonyi, A., Schachtman, T.R., 2015. Beneficial effects of dietary EGCG and voluntary exercise on behavior in an Alzheimer's disease mouse model. Journal of Alzheimer's Disease 44, 561–572.

Wang, M., Iliff, J.J., Liao, Y., Chen, M.J., Shinseki, M.S., Venkataraman, A., Cheung, J., Wang, W., Nedergaard, M., 2012. Cognitive Deficits and Delayed Neuronal Loss in a Mouse Model of Multiple Microinfarcts. Journal of Neuroscience 32, 17948–17960. https://doi.org/10.1523/JNEUROSCI.1860-12.2012

Wojtkowski, M., Srinivasan, V.J., Ko, T.H., Fujimoto, J.G., Kowalczyk, A., Duker, J.S., 2004. Ultrahigh-resolution, high-speed, Fourier domain optical coherence tomography and methods for dispersion compensation. Optics Express 12, 2404–2422.

Wong-Goodrich, S.J., Pfau, M.L., Flores, C.T., Fraser, J.A., Williams, C.L., Jones, L.W., 2010. Voluntary running prevents progressive memory decline and increases adult hippocampal neurogenesis and growth factor expression after whole-brain irradiation. Cancer Res. 70, 9329–9338.

Yaffe, K., Barnes, D., Nevitt, M., Lui, L.Y., Covinsky, K., 2001. A prospective study of physical activity and cognitive decline in elderly women: women who walk. Archives of Internal Medicine 161, 1703–1708.

Zhang, Cong, Bélanger, S., Pouliot, P., Lesage, F., 2015. Measurement of local partial pressure of oxygen in the brain tissue under normoxia and epilepsy with

phosphorescence lifetime microscopy. PloS One 10, e0135536.

Zlokovic, B.V., 2011. Neurovascular pathways to neurodegeneration in Alzheimer's disease and other disorders. Nat Rev Neurosci 12, 723–738.

4.10 Suplements

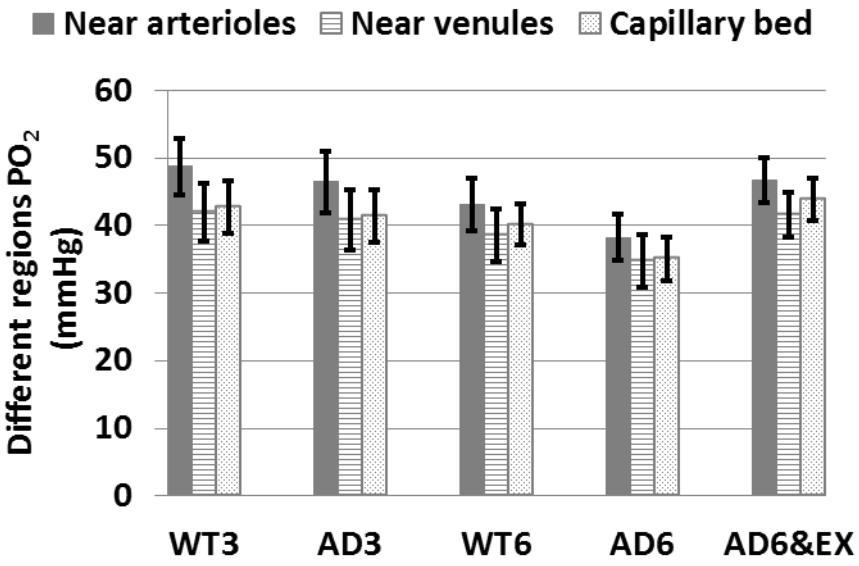

Figure 4-8. Tissue PO2 in different regions.

CHAPTER 5 ARTICLE 2: CHANGES IN CAPILLARY HEMODYNAMICS AND ITS MODULATION BY EXERCISE IN THE APP-PS1 ALZHEIMER MOUSE MODEL

Xuecong Lu[1,2], Mohammad Moeini[4], Baoqiang Li[3], Yuankang Lu[1,2], Rafat Damseh[1,2], Philippe Pouliot[1,2], Éric Thorin[2,5], Frédéric Lesage[1,2,*]

1 Biomedical Engineering Institute, École Polytechnique de Montréal, Montréal, QC, Canada

2 Montreal Heart Institute, Research Center, Montreal, Quebec, Canada.

3 Athinoula A. Martinos Center for Biomedical Imaging, Massachusetts General Hospital, Harvard Medical School, Charlestown, MA 02129, USA

4 Department of Biomedical Engineering, Amirkabir University of Technology (Tehran Polytechnic), Tehran, Iran

5 Department of Surgery, Faculty of Medicine, Université de Montréal, Montreal, Quebec, Canada.

*Corresponding author: Frédéric Lesage, PhD

Address: Biomedical Engineering Institute, École Polytechnique de Montréal, P.O. Box 6079, Succursale Centre-ville, Montréal (QC), H3C 3A7, Canada

Email: frederic.lesage@polymtl.ca, Tel: +1-514-340-4711 ext. 7542, Fax: +1-514-340-4611

Running title: Capillary hemodynamic changes in AD

This paper was submitted to the journal “Frontiers in Neuroscience” on March 28, 2019.

5.1 Abstract

Dysfunction in neurovascular coupling that results in a mismatch between cerebral blood flow and neuronal activity has been suggested to play a key role in the pathogenesis of Alzheimer's disease (AD). Meanwhile, physical exercise is a powerful approach for maintaining cognitive health, and could play a preventive role against the progression of AD. Given the fundamental role of capillaries in the oxygen transport to tissue, our study aimed to characterize changes in capillary hemodynamics with AD and AD supplemented by exercise. Exploiting two-photon microscopy, intrinsic signal optical imaging and magnetic resonance imaging, we found hemodynamic alterations and lower vascular density with AD, reversed by exercise. We further observed that capillary properties were branch order dependent and that stimulation evoked changes were attenuated with AD but increased by exercise. Our study provides novel insights into cerebral microcirculatory disturbances with AD and the modulating role of voluntary exercise on these alterations.

5.2 Keywords

Alzheimer's disease, capillary hemodynamics, voluntary exercise, two-photon imaging

5.3 Introduction

Alzheimer's disease (AD) is the most common cause of cognitive impairement in the erderly (Toledo et al. 2013; Iadecola 2010a). Dysfunction in neurovascular coupling resulting in a mismatch between cerebral blood flow and neuronal activity has long been suggested to play a part in the pathogenesis of AD (Kisler et al. 2017; Zlokovic 2011; Iadecola 2010b; Iadecola 2004). AD also shares many risk factors with cardiovascular diseases (Nielsen et al. 2017; Østergaard et al. 2013), and is associated with alterations in vascular function (Iadecola 2010a). Capillaries are the vessels most proximal to neurons (Stefanovic et al. 2008), and thus play a significant role in modulating oxygen extraction to support neuronal activity (Nielsen et al. 2017; Østergaard et al. 2013; Hall et al. 2014). Characterizing microvascular (dys)function in AD is of vital importance as compromised capillary networks may lead to hypoxia, which in turn damages neurons and precipitates Aβ amyloid retention (Nielsen et al. 2017). The fisrt aim of this study was to quantify the changes in capillary red-blood-cell (RBC) dynamics with AD to provide insights on these questions.

Beyond characterizing hemodynamic dysfunction in microvessels, it is also critical to explore how to mitigate the negative impacts of AD on microcirculation. Physical exercise is a powerful approach for maintaining cognitive health, and is hypothesized to play a preventive role against the progression of AD (Radak et al. 2010). Regular aerobic exercise was found to inhibit the progression of amyloid-related neuropathology in mouse models of AD (Adlard et al. 2005) and enhance cognitive performance in humans (Pereira et al. 2007; Brown et al. 2010; Hayes, Alosco, and Forman 2014). Voluntary exercise has also been shown to improve vascular function in mouse model of atherosclerosis (Shing et al. 2015). Oxidative stress associated with aging has been found to be reduced with exercise in both humans (Pialoux et al. 2009) and rodents (Durrant et al. 2009) studies. Notwithstanding, the hemodynamic changes in microvascular networks in response to physical exercise with the onset of AD has yet to be studied. Despite a number of hypotheses that indicate the beneficial role of exercise,

we still do not have a clear quantification of these changes which can now be done with *in vivo* optical imaging techniques. The second aim of this study was, thus, to quantify the modulation of exercise on cerebral capillaries in AD.

To address these questions, we applied multiple imaging techniques, including two-photon microscopy, intrinsic optical signal imaging (IOSI), and magnetic resonance imaging (MRI), to measure the hemodynamic changes at different spatial scales and the overall stimulus-evoked response and brain perfusion. We found capillary hemodynamic alterations and lower vascular density with AD, modulated by exercise. We further observed that capillary RBC flow properties were branch order dependent and that the stimulation evoked changes were decreased with AD but increased by exercise. By quantifying stimulus-evoked response in IOSI and brain perfusion in MRI, we could examine the association between the hemodynamic changes in capillaries and the global changes of cortex in AD.

5.4 Methods

5.4.1 Animal groups

The experimental animals were handled based on the Animal Research: Reporting of *In Vivo* Experiments guidelines (ARRIVE) and the recommendations of the Canadian Council on Animal Care. The protocol was approved by the ethics committee of the research center of the Montreal Heart Institute. Experiments were performed in male wild type mice at 6-month-old (WT6: n=4), transgenic Amyloid Precursor Protein Presenilin-1 (APP/PS1) mice at 6-month-old (AD6: n=4), and APP/PS1 mice at 6-month-old for which voluntary exercise was initiated at 3-month-old (AD6&EX: n=4). Previous work showed a clear onset of cognitive symptoms in APP/PS1 mice at 4.5-months-old (Cifuentes et al. 2015) and established at 6-month-old (de Montgolfier et al. 2019), and thus, we conducted imaging at 6-month old and investigated the hemodynamic changes in this relatively early stage of AD. For the AD6&EX group, mice started running on wheels at 3-month-old, and continued the

daily exercise till 6-month-old when imaging data were recorded. The wheel (diameter 15 cm, recorded by easy matrix 16 EMKA) was attached outside the cage to ensure enough living space, and the number of wheel running was recorded using the LE907 individual counter on a daily basis. The running distance averaged across mice ranged from ~2 to ~4 km per day in the 3-month exercising period.

5.4.2 Two-photon imaging

To be prepared for two-photon imaging, mice were performed with the craniotomy and adapted to the awake imaging device. On the day of cranial surgery, animals were under anaesthetia with 1.5-2.0% isoflurane mixed in pure oxygen, with their physiological parameters monitored in real time. A fixation bar was attached for awake imaging. At the same time as bar fixation, an imaging cranial window was prepared to allow for two-photon imaging of the mice cortex following well-established guidelines (Shih et al. 2012). A cranial window with 3-mm diameter was made over the left barrel cortex (0.5 mm posterior to bregma, 3.5 mm lateral to the midline). Agarose in artificial cerebral spinal fluid (ACSF) was placed over the exposed skull and then a three-layer cover glass was glued on the skull to generate a transparent cranial window. Ketoprofen (5 mg/Kg, Merial, Canada) and buprenorphine (0.05 mg/Kg, Reckitt Benckiser Healthcare, UK) were injected before the surgery for analgesic and antipyretic effects. Baytril (5 mg/Kg, Bayer, Germany) was injected by completing the surgery and one day after the surgery to control bacterial infection. To adapt to the device during imaging, animals were trained on the imaging wheel in 4 fixation-training sessions beginning after 3 days of recovery following the cranial surgery. The length of fixation time gradually increased from 10 to 45 min over the four sessions.

A home-built two-photon microscope was used to record functional capillary data and vascular density. The MaiTai-BB laser oscillator (Newport Corporation, USA) of the two-photon microscope generated a sequence of 820 nm, 80 MHz, 150 fs pulses modulated by an acousto-optic modulator for power control. The fluorescent dye (dextran-FITC) was injected

through the tail vein to distinguish plasma (in bright colors) and RBCs (appearing as dark shadows) in the recorded images. The line scans were performed both perpendicularly and longitudinally to each measured capillary over 250 ms time intervals to generate space-time images. In consecutive longitudinal scans, the dark shadows move towards the right or left of the scanning beam because of the movement of RBCs, resulting in tilted dark streaks in the space-time image (Kleinfeld et al. 1998). The angle of these dark streaks was used to quantify RBC velocity, with streaks closer to horizontal orientation associated with higher velocity. In perpendicular line scans, the signal is dark when a RBC is passing through the optical focus and RBC flux can be assessed. Following line scanning, 3D angiograms were obtained over four overlapping 600 × 600 μm^2 (400 × 400 pixels) regions at depths of 100 – 550 μm with 5 μm steps at the frame rate of 0.5 Hz. During all measurements, animals were awake, with head fixed by a titanium bar and limbs free to move on the rotating wheel (Moeini et al. 2018; Moeini et al. 2019).

5.4.3 Quantification of capillary properties

The spacetime images were used to obtain the following capillary parameters, following (Moeini et al. 2018): (1) diameter by fitting the perpendicular scans with a Gaussian function with estimated diameter at half maximum of the distribution; (2) RBC velocity from the angle of the streaks in longitudinal scanning; (3) RBC flux, calculated by the number of dark shadows divided by the acquisition time of the images (the flux was obtained from the average of values in longitudinal scan and perpendicular scan); and (4) hematocrit, calculated by RBC flux × RBC volume/ capillary volumetric flow capillary (capillary volumetric flow = RBC velocity × capillary cross-sectional area; RBC volume assumed to be 55 μm^3 for C57Bl/6 mice (Wirth-dzięciołowska and Karaszewska 2009)). The angiogram images were used to compute the vascular density using a deep learning segmentation approach based on the FC-Densenets architecture (Damseh, Cheriet, and Lesage 2018; Damseh et al. 2018). The vascular density was estimated by removing the pial vessels on the top of the imaging area but including the

penetrating arterioles and capillaries.

We also divided the capillaries based on the branching order. The artery region with diving arteriole, precapillary arteriole, and capillaries was labelled with respect to branching order A1, A2, and A3 with A1 branching off directly from the precapillary arterioles. The vein region with surfacing venule and postcapillary venule was labelled with the branching order V1, V2, and V3, with V1 directly linking to veins. In our recordings, the capillary segments ranged from 6 to 12 branch orders. We only labeled and defined the first three branch orders from arterioles (A1, A2, and A3) and venules (V1, V2, and V3). When a capillary path had more than 6 branching orders, these additional branch orders were merged into V3, thus enabling consistent numbering for all capillaries observed.

5.4.4 Magnetic resonance imaging (MRI)

MRI scanning was performed with a 30 cm 7T horizontal MR scanner (Agilent, Palo Alto, CA) before two-photon imaging. The mice were in prone position and imaged with a gradient insert coil (12 cm inner diameter, gradient strength 600 mT/m, and rise-time 130 ms). The brain was imaged with a 2-channel receive-only surface coil and a quadrature transmit/receive birdcage coil (RAPID Biomedical, Germany), while the animal was anesthetized with 1.4-2.2% isoflurane in air with 30% oxygen, with body temperature kept at 37.0°C. Respiration was monitored with a target of ~100 bpm, adjusting the level of isoflurane only whenever the rate was outside 80-120 bpm. Physiological parameter including heart rate was monitored during imaging.

Anatomical images were recorded with a 3D true free induction with steady-state precession (TFISP) sequence (Bowen, Gati, and Menon 2006). Then a 3D amplitude-modulated continuous arterial spin labeling scan (amCASL) was acquired (TR = 3.0 s, labeling duration = 1.0 s, 60 x 54 x 48 matrix, 300 x 333 x 333 μm resolution, 23-min scan time).

The anatomical recordings were first aligned manually to a previously produced anatomic template using ITK-SNAP, and then co-registered non-linearly with the advanced

normalization tools (ANTs) (B.B. Avants et al. 2011; Brian B. Avants et al. 2010), thus producing the ANTs transformations to co-register the perfusion scans to a common referential. Perfusion was calculated voxel-by-voxel as described in (Chugh et al. 2012), with assumed parameters (brain/blood partition coefficient=0.9 mL/g, mouse arterial blood transit time=0.08 s, tagging efficacy=0.67, T_{1b} = 2.3 s, T_1 = 1.53 s, T_{1sat} = 0.57 s, $M_a^z(w)$ = 0.48 s). The MarsBar toolbox in SPM was also used to extract the average perfusion data (Delafontaine-Martel et al. 2018).

5.4.5 Intrinsic signal optical imaging (ISOI)

An ISOI system (Labeo Technologies Inc.) was used to investigate the stimulus-evoked hemodynamic responses in all experimental groups. Whiskers of mice were deflected at a rate of 10 Hz to activate the somatosensory cortex, with 5-second stimulation time and 15-second post-stimulus period. Illumination using green and red lights was positioned to illuminate the exposed skull of the mouse head. Images were acquired by a camera at a rate of 5 Hz per wavelength over a period spanning 10 stimulation repetition. We computed changes in oxy-hemoglobin concentration (Δ[HBO](t)), deoxy-hemoglobin concentration (Δ[HBR](t)), and total hemoglobin concentration (Δ[HBT](t)) as was done in (Dubeau, Desjardins, et al. 2011; Dubeau, Ferland, et al. 2011).

5.5 Results

5.5.1 Capillary RBC flow is altered by AD and modulated by exercise

To better understand the role of exercise and AD on capillary RBC flow properties, we assessed the values of the resting capillary diameter, RBC velocity, RBC flux and capillary hematocrit in all groups and their coefficient of variation (CV) using two-photon microscopy. In Fig 5-1a, we observe that the capillary diameter increased significantly from the WT6 group (4.67 ± 0.06 μm) to the AD6 group (4.98 ± 0.07 um) and to the AD6&EX group

(5.15 ± 0.08 μm). Voluntary exercise led to a trend of increasing for the capillary diameter (see Fig. 1a). A decreasing trend of RBC velocity from WT6 (0.87 ± 0.03 mm/s) to AD6 (0.79 ± 0.03 mm/s) was also observed (see Fig. 5-1a). RBC velocity trended higher with exercise (velocity in the AD6&EX group: 0.91 ± 0.04 mm/s) (see Fig. 5-1a). However, there were no significant differences of RBC flux between groups (see Fig. 1a). Finally, the capillary hematocrit decreased from the WT6 group (39.57 ± 1.15 %) to the AD6 group (35.15 ± 1.30 %) (see Fig. 5-1a). Exercise elevated the hematocrit (AD6&EX group, 37.32 ± 1.19 %) as expected from physiology (see Fig. 5-1a).

Given the hypothesis that capillary heterogeneity is a key element in oxygen delivery, we also computed the CV of these parameters. The CV represents the variations of each property within a capillary as a function of time (5 seconds). In Fig. 5-1b, we show the CV of each parameter to explore the influence of AD and exercise on capillary heterogeneity. There were no significant differences of diameter CV between groups (see Fig. 5-1b). However, we observed significant variations of the velocity CV, flux CV and hematocrit CV. Specifically, the velocity CV increased from the WT6 (18.53 ± 0.66 %) to the AD6 (23.91 ± 1.27 %) significantly (see Fig. 5-1b). Exercise trended to reduce the velocity CV from the AD6 to the AD6&EX (20.97 ± 1.15 %, see Fig. 5-1b). Likewise, flux CV increased from the WT6 (29.17 ± 1.25 %) to the AD6 (40.63 ± 2.13 %) significantly (see Fig. 5-1b). Exercise decreased the flux CV from the AD6 to the AD6&EX (35.50 ± 1.58 %) significantly (see Fig. 5-1b). Finally, hematocrit CV increased from the WT6 (14.65 ± 0.79 %) to the AD6 (20.95 ± 1.41 %, $p<0.001$), while exercise trended towards a reduction of the hematocrit CV from the AD6 to the AD6&EX (18.42 ± 1.08 %, see Fig. 5-1b). Taken together, capillary flux and speed were reduced with AD, associated with increased variations in time while exercise regularized parameters towards values found in WT mice. Capillary diameter was the exception to this. Given the increased heterogeneity in RBC velocity, RBC flux, and hematocrit with AD, we further analyzed the variations of these properties as a function of branch order of capillaries to explore how they varied from the upstream to the downstream

segments.

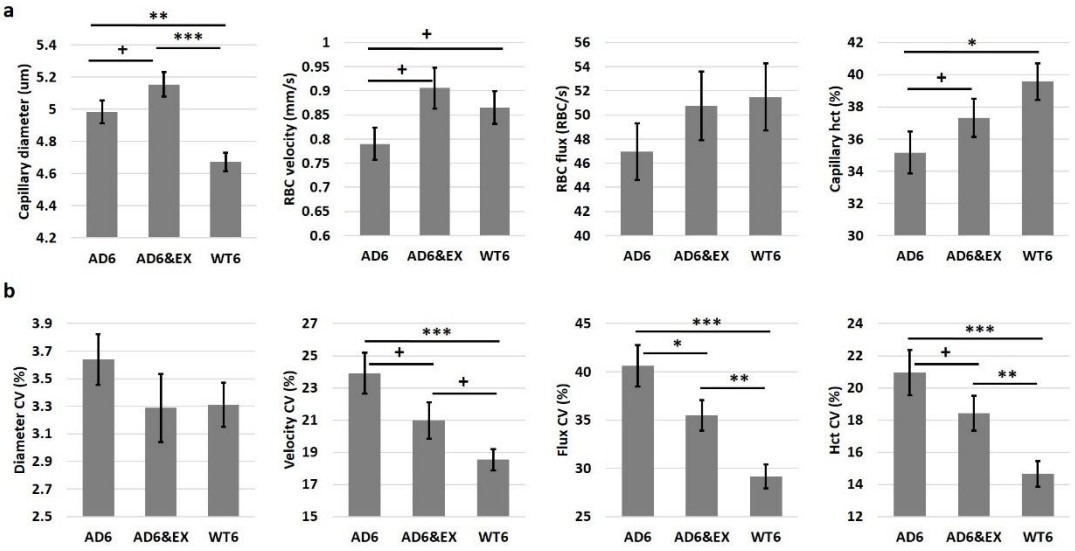

Figure 5-1. Capillary RBC flow characteristics in different groups. (a) Capillary diameter, RBC velocity, flux and hematocrit in different experimental groups (460, 508, and 562 capillaries measured in the AD6, AD6&EX and WT6 groups, respectively). (b) Coefficient of variation (CV) shown for all capillary parameters (460, 508, and 562 capillaries measured in the AD6, AD6&EX and WT6 groups, respectively). The CV in each capillary was computed based on multiple frames recorded each 0.25s within a 5-second time window. Thus CV represents the temporal variations of each property within a capillary. CV was computed by standard deviation devided by mean. Statistical significance was computed using ANOVA followed by Tukey HSD post hoc test. + : $p< 0.1$, *: $p < 0.05$, **: $p < 0.01$, ***, $p < 0.001$. Data are expressed as mean ± s.e.m. . This significance level also applies for the figures below.

5.5.2 Capillary RBC properties are branch order dependent.

We used the 3D angiogram to distinguish different branching orders in capillaries (see Fig. 5-2a). We investigated how capillary hemodynamics varied in different branching orders for

all groups.

We observed that the average diameter showed a slight decreasing trend in WT6 group, while its value remained stable in the AD6 group (see Fig. 5-2b first from the left and Fig. 5-2c first from the left). With exercise, the AD group remained relatively stable with a dip in the downstream capillaries (see Fig. 5-2b first from the left). The smaller diameter in downstream capillaries could be linked to the stalling occuring more in the downstream capillaries (Erdener et al. 2017). The average RBC velocity showed sharp decrease in the upstream capillaries for all groups (see Fig. 5-2b second from the left). The average RBC flux also had sharp reduction in all branches for the AD groups, but had a moderate decrease in the WT group (see Fig. 5-2b third from the left). Finally, all groups showed increasing trends of hematocrit from upper to lower streams (see Fig. 5-2b the fourth from the left and Fig. 5-2c the fourth from left).

Due to the larger reduction in the first three branching orders of capillary RBC velocity and flux, we further calculated the RBC property differences among the initial three orders for each group to explore the differences across branches. We observed that for the initial three orders (from A1 to A3), the RBC velocity dropped at least 62% (calculated by (A1-V3)/A1) (67.28%, 67.70%, 62.25% for AD6, AD6&EX, and WT6, respectively) (see Fig. 5-2c the second from left), suggesting that the RBC velocity was largely modulated in the upper stream of capillaries. Additionally, for the average RBC flux, we observed that in the initial three orders (from A1 to A3), the flux dropped ~ 32% over three groups (calculated by (A1-V3)/A1) (32.74%, 31.87%, 34.83% for AD6, AD6&EX, and WT6, respectively) (see Fig. 5-2c the third from left), indicating that the RBC flux modulation in the upper orders still largely contributed to the variance of overall RBC flux across all capillaries.

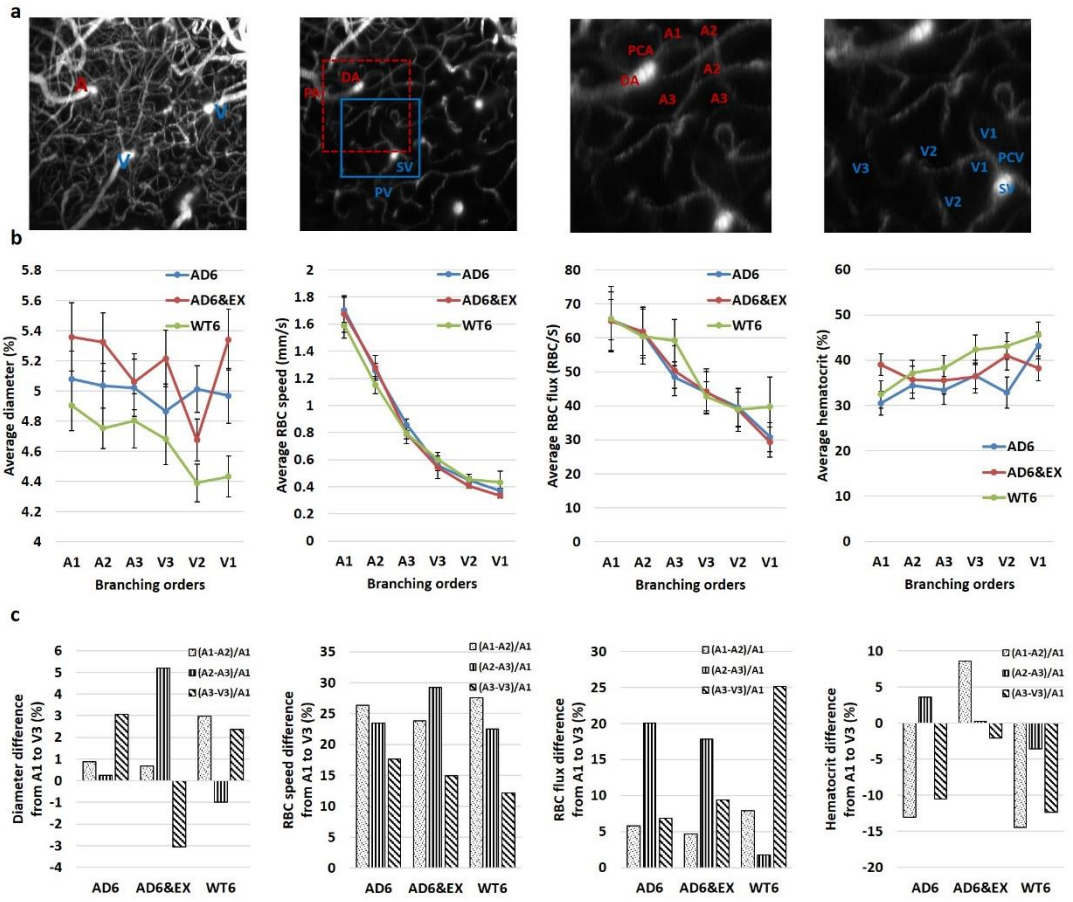

Figure 5-2. Capillary property changes with branching orders. (a) Left : a maximum intensity projection image of the angiogram; Second from the left: an *en face* slice at the depth of ~100 μm. The red square indicates the area used to calculate branching orders from arterioles, and the blue square indicates the area used to calculate branching orders from venules. Third from left: the enlarged artery region with diving arteriole, precapillary arteriole, and capillaries labelled with branching orders. Fourth from left : the enlarged vein region with surfacing venule and postcapillary venule, labelled with the branching orders. (b) The changes of capillary diameter/velocity/flux/hematocrit as a function of branching order (460, 508, and 562 capillaries measured in the AD6, AD6&EX and WT6 groups, respectively). (c) diameter/velocity/flux/hematocrit differences among the first three branching orders in different groups (460, 508, and 562 capillaries measured in the AD6, AD6&EX and WT6 groups, respectively).

5.5.3 High temporal fluctuations of capillary RBC velocity and flux were more frequent with AD.

Previous studies observed spontaneous stalls in capillary red blood cell (RBC) flux in individual capillary segments (Erdener et al. 2017; Hernández et al. 2019). We thus analyzed our data to capture the presence of highly fluctuating RBC properties in capillaries by quantifying the fraction of capillaries with outlier standard deviations of RBC flux or speed within a 5-second recording window (see Fig. 5-3a and 5-3b). Although stalling was not characterized in our experiments, these capillary outliers tend to display highly fluctuating flux and velocity, which may influence oxygen extraction (Gutiérrez-Jiménez et al. 2016; Østergaard et al. 2016). Examples for capillary outliers with temporally high self-fluctuation of RBC flux and velocity were shown in Fig. 5-3a and Fig. 5-3b, respectively. We further calculated and compared the fraction of outliers in all groups, and found that the propotion with high temporal self-fluctuating RBC velocity was highest in the AD6 group (10.43%, 48 outliers in 460 capillaires), followed by the AD6&EX group (9.45%, 48 outliers in 508 capillaries), and lowest in the WT6 group (8.19%, 46 outliers in 562 capillaries) (see Fig. 5-3c). We did the same analysis for RBC flux (see Fig. 5-3d). We also found that the propotion with high temporal self-fluctuating RBC flux was highest in the AD6 group (18.70%, 86 outliers in 460 capillaires), followed by the AD6&EX group (15.35%, 78 outliers in 508 capillaries), and lowest in the WT6 group (13.17%, 74 outliers in 562 capillaries) (see Fig. 5-3d).

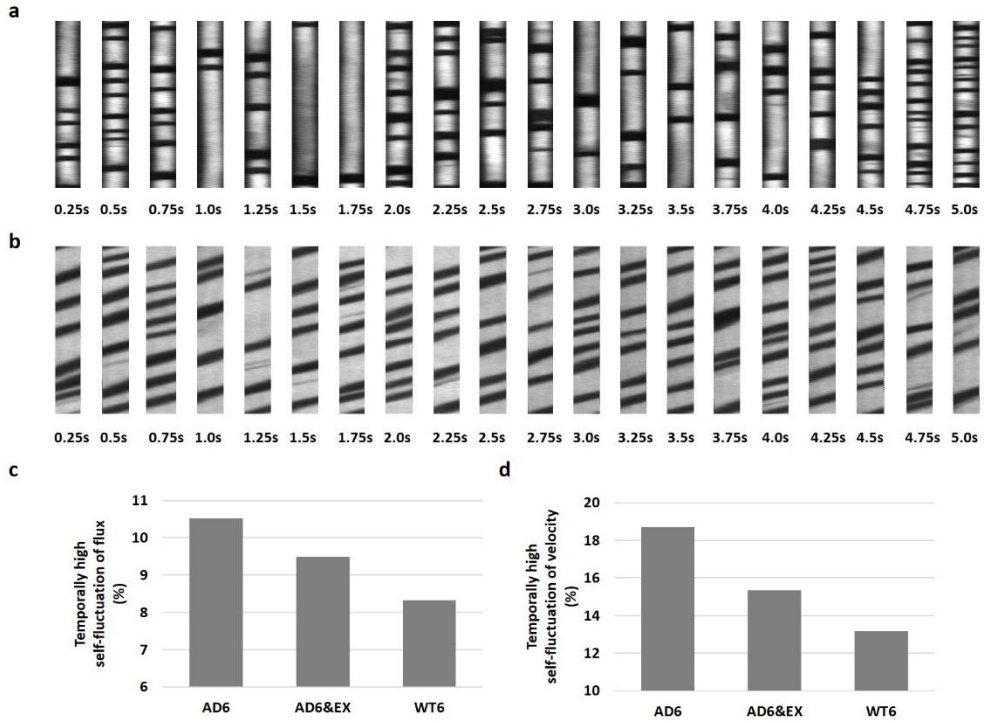

Figure 5-3. High temporal capillary fluctuations of RBC velocity and RBC flux. (a) Imaging snapshots of the RBC trajectory showing high fluctuations of RBC flux in a capillary with 0.25 second as interval during a 5-second recording window. The flux was calculated based on the average value of flux from longitudinal and perpendicular scans. (b) Longitudinal equivalent, RBC velocity was calculated from the angle of dark streaks in a specific frame of recording. (c) The percentage of capillaries with high temporal fluctuations of RBC velocity in all groups. The "isoutlier" method in MATLAB was applied to detect outliers with a standard deviation of RBC velocity exceeding three standard deviations from the mean. (d) Same for RBC flux.

5.5.4 Higher vascular density peak value and lower average vascular density in the AD group.

We calculated the vascular density from two-photon angiograms (see Fig. 5-4a) after binary

segmentation. Interestingly, all experimental groups reached their peak values of vascular density at a depth of ~220 μm, and then gradually decreased with increasing depth under the brain surface (see Fig. 5-4b). The AD groups (both AD6 and AD6&EX) had significant higher peak values (AD: 14.60 ± 0.98%; AD6&EX: 14.48 ± 1.09%), when compared with the peak value of the WT6 (12.74 ± 0.70%) (see Fig. 5-4b). Voluntary exercise did not significantly change the peak value of vascular density (see Fig. 5-4b). When integrating across depths, the AD6 group had signficant lower average value (8.16 ± 0.37%), compared to the WT6 group (8.85 ± 0.29%) (see Fig. 5-4c). With voluntary exercise, the AD6&EX group (8.64 ± 0.34%) exhibited significant higher vascular density than the AD6 group (see Fig. 5-4c). However, there was no significant difference in vascular density between the AD6&EX and WT6 groups (see Fig. 5-4c). Overall, higher vascular density peak value and lower average vascular density were observed in the AD groups, the latter being modulated by exercise.

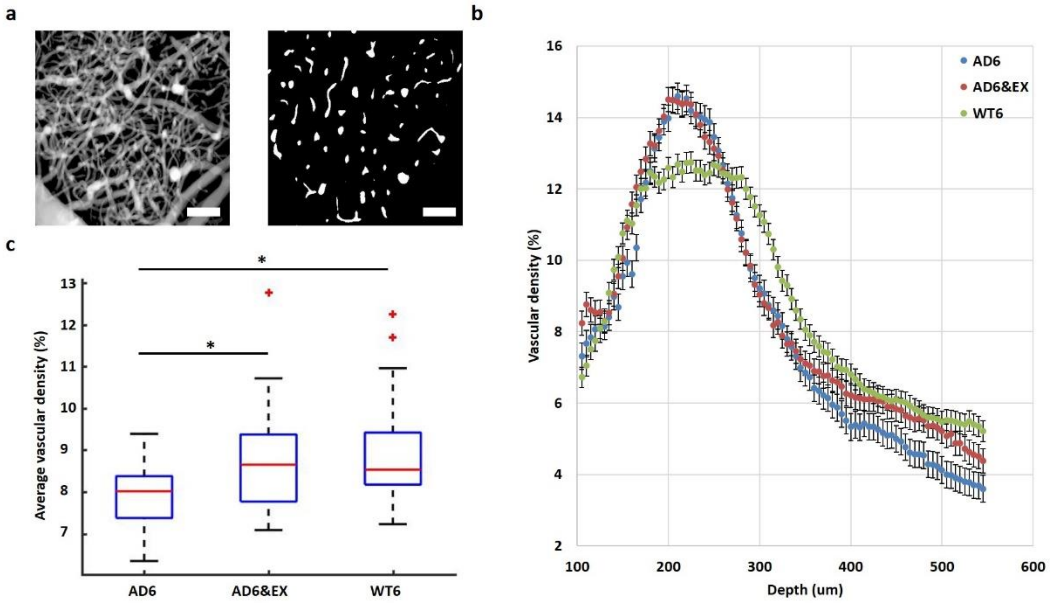

Figure 5-4. Vascular distribution in different experimental groups and different depths. (a) Binarization of microvascular angiograms was applied to calculate the vascular density. Left: MIP image with depths ranging from 100 to 550 μm under the brain surface with 5 μm steps.

Right: an example of a binary segmentation of a single *en face* slice after removing the large horizontal vessels at the depth of 120 um (scale bar : 100 μm). (b) Average vascular density in different experimental groups as a function of depth from 100 to 550 μm under brain surface (14 angiograms in each group). (c) Estimated vascular density (volume%). Results are presented as box plot with the median value (red line).

5.5.5 AD reduced brain perfusion and task-related changes, with the latter modulated by exercise

We used MRI to quantify brain perfusion in each group (see Fig. 5-5a and Fig. 5-5b). We observed that brain perfusion decreased significantly from the WT6 group (2.69 ± 0.15 ml/g/min) to the AD6 group (2.16 ± 0.10 ml/g/min) (see Fig. 5-5c). However, exercise did not significantly modulate brain perfusion in AD groups (AD6&EX: 2.13 ± 0.16 ml/g/min) (see Fig. 5-5c).

ISOI was also used to investigate the response to stimulation to investigate task-related changes of hemoglobin concentration (see Fig. 5-5d and 5-5e). Whiskers of mice were deflected to activate the somatosensory cortex, with 5-second stimulation time and 15-second post-stimulus period. We observed increased HBO with the stimulation for all groups, while HBO had higher peak values in the WT6 group and the AD6&EX group when compared to the AD6 group, as shown in Fig. 5-5d. We found that the Δ[HBO](t) in the AD6 group (10.75 ± 0.64 μM) was significantly lower than that in the WT6 group (15.00 ± 0.85 μM). However, exercise tended to increase the Δ[HBO](t) from the AD6 group to the AD6&EX group (12.69 ± 0.85 μM, see Fig. 5-5f upper panel). Finally, there were no significant differences regarding Δ[HBR](t) between groups (see Fig. 5-5f lower panel). By quantifying stimulus-evoked response in IOSI and brain perfusion in MRI, we found that the disruption in capillary hemodynamics was associated with the global changes in brain cortex in AD.

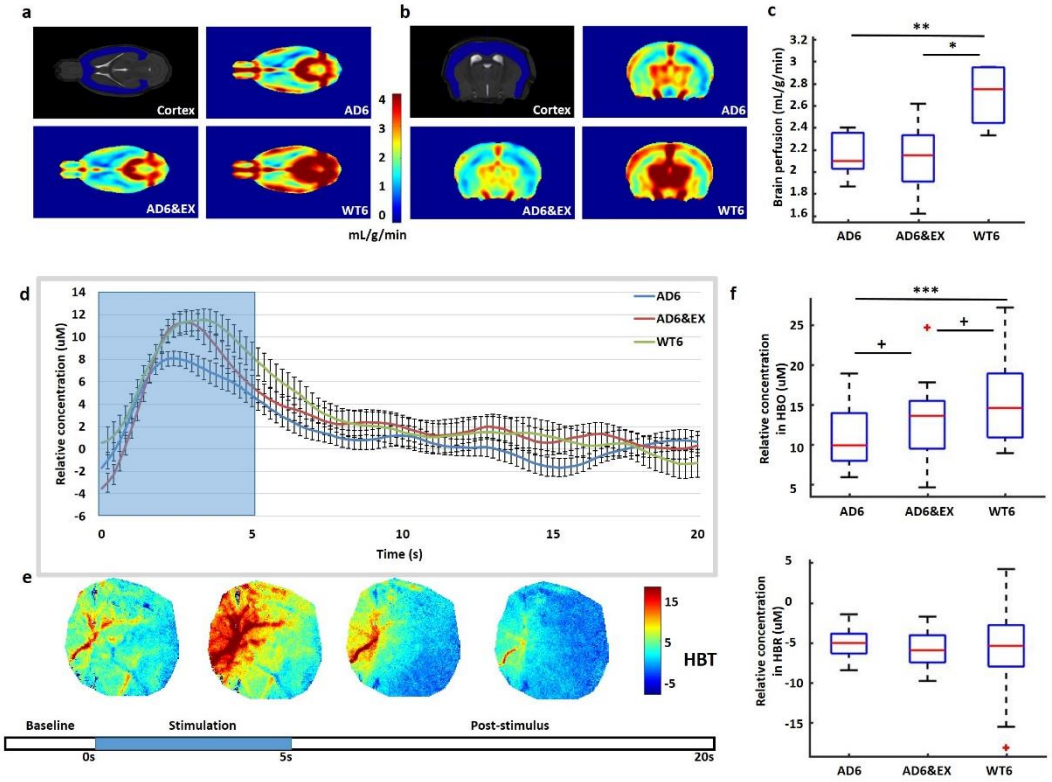

Figure 5-5. (a-b). MRI scans with coronal and axial views of the cortex. (c) Quantification of cerebral perfusion (ml/g/min) by MRI. (d) Averaged temporal response of oxy-hemoglobin (HBO) for all groups with 5-second stimulation (blue background). (e) Temporal dynamics of total hemoglobin (HBT) response to whisker stimulation. Stimulation lasted for 5 seconds, followed with 15-second rest. (f) Averaged results for change of HBO (Δ[HBO](t)) and change of HBR (Δ[HBR](t)) over all mice (28, 24, 30 stimulation curves for the AD6, the AD6&EX, and the WT6, respectively).

5.6 Discussion

In this study, we aimed to quantify hemodynamic properties and the modulation role of exercise on cerebral capillaries in AD, due to the important role of microcirculation in cognitive health (Erdener et al. 2017; Østergaard et al. 2016; Hernández et al. 2019; Zhang et al. 2017). Exploiting awake microscopic vascular imaging and a transgenic mouse model of

AD, we found that in this model (APP-PS1), AD is associated with hemodynamic disruption in capillaries. Voluntary exercise was seen to decrease capillary hemodynamic heterogeneity, potentially through a reduction of microvascular oxidative stress associated with AD (Radak et al. 2010), although exercise did not increase the global cerebral blood flow in the cortex.

5.6.1 Capillary flow property changes to AD and exercise

Blood flow was significantly reduced in AD6 group, compared with WT6 mice, but was partially increased with exercise in the AD6&EX group, compared with the AD6 group. Specifically, RBC velocity was decreased with AD, reversed by exercise. The disrupted RBC velocity could result from the occlusion of vessels due to the amyloid deposition (Arbel-Ornath et al. 2013). The reduced RBC velocity could in turn lead to compromised perfusion in the mice cortex, further slowing the clearance of amyloid and increasing its deposition (Kisler et al. 2017). We further observed that hematocrit was reduced with AD, compared with the WT mice, partially increased by exercise. Previous study (Moeini et al. 2018) found reduced hematocrit in healthy aging, thus disrupting capillary oxygen delivery efficiency. Prior literature has also observed miscrocirculation flow disruption in other cardiovascular disease, such as stroke (Kazmi et al. 2013), hypertension (Pialoux et al. 2009), and even healthy aging (Dubeau, Ferland, et al. 2011). The microvascular flow alterations observed in our study suggest that AD does share many similar microvessel disruptions with cardiovascular pathologies and aging. These microvessel problems could be alleviated by exercise, as the case in other cardiovascular diseaseas (Brown et al. 2010; Pialoux et al. 2009).

We also found that RBC properties, especially velocity and flux, were branch order dependent for all experimental groups. Prior study (Sakadžić et al. 2014) suggests that oxygen is in good proportion extracted in the first few branches after the precapillary arteriole in normal physiological conditions. Our results were related to previous finding and showed that RBC velocity and flux decreased from the upstream capillaries to the downstream

capillaries for all groups to allow for oxygen delivery. Capillaries are responsible for transporting oxygen and nutrients to brain tissue, and clearing metabolic end products from brain to venous circulation (Kisler et al. 2017). In capillary segments close to arterioles, capillaries were observed to have larger RBC velocity and flux, potentially enabling delivery of oxygen and energy metabolites to the brain tissues. Future research may further explore the functioning of different capillary branches and how they play a role in AD.

Capillary obstruction due to flow dysfunction and tissue inflammation has been shown in animal models, and has been found to induce neurodegenerative pathologies (Santisakultarm et al. 2014; Erdener et al. 2017; Hernández et al. 2019). Inflammation and flow disruption are well-recognized features of AD (Gaugler et al. 2018). Inflammation triggers reactive oxygen species, which lead to obstruction in capillaries (Park et al. 2008). Meanwhile, amyloid deposition may also lead to vessel occlusion by disrupting the interstitial fluid drainage pathway (Arbel-Ornath et al. 2013). Although we only focussed on non-stalling capillaries in this study, the highly fluctuating RBC velocity and flux could indicate potential microvascular flow problems. We found higher fraction of capillaries with high self-fluctuations of RBC velocity and flux in AD, slightly decreased with exercise. Previous research suggests that capillary flow patterns should homogenize to support metabolic demands, whereas heterogenous velocities across the capillary network diminishes the oxygen extraction capabilities (Stefanovic et al. 2008; Gutiérrez-Jiménez et al. 2016). Our results suggest more heterogenous flow distribution in the AD group, when compared to WT, but a reduced heterogeneity in the AD&EX group, compared with the AD group which may underly the benefits of exercise in AD.

5.6.2 Vascular morphology alterations in AD

Studies on morphological abnormalities of capillaries in AD reported less dense capillary densities due to deposit of Aβ amyloid (Kitaguchi et al. 2007). Previous work indicated a more rapid loss of vascular density with age, leading to compromised cerebral perfusion

(Farkas and Luiten 2001). Our results indicate that AD is associated with lower vascular density, which could contribute to reduced cerebral perfusion. However, this negative effect was partially mitigated by exercise. Several previous studies have demonstrated the capacity of exercise to improve cognitive function (Hamer and Chida 2008; Durrant et al. 2009; Mekari et al. 2015). Here our data supports the positive role of voluntary exercise on the maintenance of healthy vascular density. The higher peak vascular density and lower average vascular density in AD group may imply the vascular density was more heterogeneous in the AD group, which may influence oxygen and nutrients supply through vessels in areas with loose microvasculature.AD could also influence capillary diameter constriction and dilation which respond to brain demands (Iadecola 2017). Prior studies have shown the pericytes, the multi-functional cells wrapping around the capillaries, are able to influence capillary diameter to adjust the oxygenation levels (Iadecola 2017; Østergaard et al. 2013). Minimal changes in capillary diameter could produce large changes in oxygen delivery, since capillaries are closest to neurons in the vascular network and have large surface area. Interestingly, we observed increased capillary diameters in the AD group and the exercise group. This change of diameters could be due to the compromised flow in AD groups, and the diameters dilate to compensate the hypoperfusion in the AD groups (with or without exercises). Another possible reason for the dilation of capillaries could be the occlusion of capillaries in AD due to amyloid deposition or inflammation (Arbel-Ornath et al. 2013; Park et al. 2008), as occlusion of vessels were shown to lead to vessel dilation in upstream capillaries in stroke disease (Nguyen et al. 2011).

5.6.3 Reduced cerebral perfusion and functional responses in AD

Using ISOI we measured the functional hemodynamic response to stimulation (Sheth et al. 2005). Prior studies used ISOI to investigate pathological departures of neurovascular coupling in diseases such as focal epileptic seizures which exhibit an elevation in HBO (Schwartz et al. 2011). Other study applied ISOI and observed that functional connectivity

was compromised in patients with AD or even normal elderly with increased amyloid accumulation (Bero et al. 2012). Our results corroborate previous finding with a lower response amplitude in AD, suggesting neuro-vascular coupling changes. By contrast, the HBO response further increased with voluntary exercise, suggesting that exercise may increase the regional oxygen delivery efficiency in capillaries but not through global increases in CBF. This finding was supported with MRI results suggesting decreased overal cerebral perfusion in both AD groups.

5.7 Conclusion

Our study provides novel data regarding cerebral microcirculatory disturbances in AD as shown by the hemodynamic changes and the modulating effects of voluntary exercise on these hemodynamic alterations. Our work suggest potential therapy that could alleviate hemodynamic disruption observed in AD.

Author Contributions

X. L. designed the study, carried out the experiments, analyzed the data, and drafted the manuscript. M. M. and P. P. carried out the experiments. M. M., B. L., Y. L., R. D. and P. P. analyzed the data. E. T. participated in designing the study. F. L. conceived, designed and coordinated the study and revised the manuscript. All authors gave final approval for publication.

Funding

This work was supported by a grant from the Natural Sciences and Engineering Research Council of Canada awarded to Frederic Lesage.

Conflict of Interest Statement

Dr. Lesage reports a minority ownership in LabeoTech Inc.

5.8 Acknowledgments

The authors thank Marc-Antoine Gillis and Natacha Duquette for their help with the animal preparations.

5.9 References

Adlard, P.A., V.M. Perreau, V. Pop, and C.W. Cotman. 2005. “Voluntary Exercise Decreases Amyloid Load in a Transgenic Model of Alzheimer’s Disease.” *Journal of Neuroscience* 25 (17): 4217–21.

Arbel-Ornath, M., E. Hudry, K. Eikermann-Haerter, S. Hou, J.L. Gregory, L. Zhao, R.A. Betensky, M.P. Frosch, S.M. Greenberg, and B.J. Bacskai. 2013. “Interstitial Fluid Drainage Is Impaired in Ischemic Stroke and Alzheimer’s Disease Mouse Models.” *Acta Neuropathologica* 126 (3): 353–64. doi:10.1007/s00401-013-1145-2.

Avants, B.B., N.J. Tustison, G. Song, P.A. Cook, A. Klein, and J.C. Gee. 2011. “A Reproducible Evaluation of ANTs Similarity Metric Performance in Brain Image Registration.” *Neuroimage* 54 (3): 2033–44.

Avants, Brian B., Paul Yushkevich, John Pluta, David Minkoff, Marc Korczykowski, John Detre, and James C. Gee. 2010. “The Optimal Template Effect in Hippocampus Studies of Diseased Populations.” *NeuroImage* 49 (3). Elsevier Inc.: 2457–66. doi:10.1016/j.neuroimage.2009.09.062.

Bero, A. W., A. Q. Bauer, F. R. Stewart, B. R. White, J. R. Cirrito, M. E. Raichle, J. P. Culver, and D. M. Holtzman. 2012. “Bidirectional Relationship between Functional Connectivity and Amyloid- Deposition in Mouse Brain.” *Journal of Neuroscience* 32 (13): 4334–40. doi:10.1523/jneurosci.5845-11.2012.

Bowen, Chris V., Joseph S. Gati, and Ravi S. Menon. 2006. “Robust Prescan Calibration for Multiple Spin-Echo Sequences: Application to FSE and b-SSFP.” *Magnetic Resonance Imaging* 24 (7): 857–67. doi:10.1016/j.mri.2006.04.008.

Brown, Allison D., Carly A. McMorris, R. Stewart Longman, Richard Leigh, Michael D. Hill, Christine M. Friedenreich, and Marc J. Poulin. 2010. “Effects of Cardiorespiratory Fitness and Cerebral Blood Flow on Cognitive Outcomes in Older Women.” *Neurobiology of Aging* 31 (12). Elsevier Inc.: 2047–57. doi:10.1016/j.neurobiolaging.2008.11.002.

Chugh, Brige Paul, Jonathan Bishop, Yu Qing Zhou, Jian Wu, R. Mark Henkelman, and John G. Sled. 2012. “Robust Method for 3D Arterial Spin Labeling in Mice.” *Magnetic Resonance in Medicine* 68 (1): 98–106. doi:10.1002/mrm.23209.

Cifuentes, D., M. Poittevin, E. Dere, D. Broquères-You, P. Bonnin, J. Benessiano, M. Pocard, et al. 2015. “Hypertension Accelerates the Progression of Alzheimer-like Pathology in a Mouse Model of the Disease.” *Hypertension* 65 (1): 218–24.

Damseh, Rafat, Farida Cheriet, and Frederic Lesage. 2018. “Fully Convolutional DenseNets for Segmentation of Microvessels in Two-Photon Microscopy∗.” *Proceedings of the Annual International Conference of the IEEE Engineering in Medicine and Biology Society, EMBS* 2018–July: 661–65. doi:10.1109/EMBC.2018.8512285.

Damseh, Rafat, Philippe Pouliot, Louis Gagnon, Sava Sakadzic, David Boas, Farida Cheriet, and Frederic Lesage. 2018. “Automatic Graph-Based Modeling of Brain Microvessels Captured with Two-Photon Microscopy.” *IEEE Journal of Biomedical and Health Informatics*, no. c: 1–1. doi:10.1109/jbhi.2018.2884678.

Delafontaine-Martel, Patrick, Joel Lefebvre, Pier-Luc Tardif, Bernard I. Lévy, Philippe Pouliot, and Frédéric Lesage. 2018. “Whole Brain Vascular Imaging in a Mouse Model of Alzheimer’s Disease with Two-Photon Microscopy.” *Journal of Biomedical Optics* 23 (07): 1. doi:10.1117/1.jbo.23.7.076501.

Dubeau, S., M. Desjardins, P. Pouliot, E. Beaumont, P. Gaudreau, G. Ferland, and F. Lesage. 2011. “Biophysical Model Estimation of Neurovascular Parameters in a Rat Model of Healthy Aging.” *NeuroImage* 57 (4). Elsevier Inc.: 1480–91. doi:10.1016/j.neuroimage.2011.04.030.

Dubeau, S., G. Ferland, P. Gaudreau, E. Beaumont, and F. Lesage. 2011. “Cerebrovascular Hemodynamic Correlates of Aging in the Lou/c Rat: A Model of Healthy Aging.” *NeuroImage* 56 (4). Elsevier Inc.: 1892–1901. doi:10.1016/j.neuroimage.2011.03.076.

Durrant, Jessica R., Douglas R. Seals, Melanie L. Connell, Molly J. Russell, Brooke R. Lawson, Brian J. Folian, Anthony J. Donato, and Lisa A. Lesniewski. 2009. “Voluntary Wheel Running Restores Endothelial Function in Conduit Arteries of Old Mice: Direct Evidence for Reduced Oxidative Stress, Increased Superoxide Dismutase Activity and down-Regulation of NADPH Oxidase.” *Journal of Physiology* 587 (13): 3271–85. doi:10.1113/jphysiol.2009.169771.

Erdener, Şefik Evren, Jianbo Tang, Amir Sajjadi, Kıvılcım Kılıç, Sreekanth Kura, Chris B. Schaffer, and David A. Boas. 2017. “Spatio-Temporal Dynamics of Cerebral Capillary Segments with Stalling Red Blood Cells.” *Journal of Cerebral Blood Flow and Metabolism*. doi:10.1177/0271678X17743877.

Farkas, Eszter, and Paul G.M. Luiten. 2001. *Cerebral Microvascular Pathology in Aging and Alzheimer’s Disease*. *Progress in Neurobiology*. Vol. 64. doi:10.1016/S0301-0082(00)00068-X.

Gaugler, Joseph, Bryan James, Tricia Johnson, Ken Scholz, and Jennifer Weuve. 2018. “2018 Alzheimer’s Disease Facts and Figures.” *Alzheimer’s and Dementia* 12 (4). Elsevier Inc.: 459–509. doi:10.1016/j.jalz.2016.03.001.

Gutiérrez-Jiménez, Eugenio, Changsi Cai, Irene Klærke Mikkelsen, Peter Mondrup Rasmussen, Hugo Angleys, Mads Merrild, Kim Mouridsen, et al. 2016. “Effect of Electrical Forepaw Stimulation on Capillary Transit-Time Heterogeneity (CTH).” *Journal of Cerebral Blood Flow and Metabolism* 36 (12): 2072–86. doi:10.1177/0271678X16631560.

Hall, Catherine N., Clare Reynell, Bodil Gesslein, Nicola B. Hamilton, Anusha Mishra, Brad A. Sutherland, Fergus M. Oâ Farrell, Alastair M. Buchan, Martin Lauritzen, and David Attwell. 2014. “Capillary Pericytes Regulate Cerebral Blood Flow in Health and

Disease.” *Nature* 508 (1). Nature Publishing Group: 55–60. doi:10.1038/nature13165.

Hamer, M., and Y. Chida. 2008. “Physical Activity and Risk of Neurodegenerative Disease: A Systematic Review of Prospective Evidence.” *Psychological Medicine* 39 (1): 3–11. doi:10.1017/S0033291708003681.

Hayes, Scott M., Michael L. Alosco, and Daniel E. Forman. 2014. “The Effects of Aerobic Exercise on Cognitive and Neural Decline in Aging and Cardiovascular Disease.” *Current Geriatrics Reports* 3 (4): 282–90. doi:10.1007/s13670-014-0101-x.

Hernández, Jean C. Cruz, Oliver Bracko, Calvin J. Kersbergen, Victorine Muse, Mohammad Haft-Javaherian, Maxime Berg, Laibaik Park, et al. 2019. “Neutrophil Adhesion in Brain Capillaries Reduces Cortical Blood Flow and Impairs Memory Function in Alzheimer’s Disease Mouse Models.” *Nature Neuroscience*. doi:10.1038/s41593-018-0329-4.

Iadecola, Costantino. 2004. “Neurovascular Regulation in the Normal Brain and in Alzheimer’s Disease.” *Nature Reviews Neuroscience* 5 (5): 347–60. doi:10.1038/nrn1387.

———. 2010a. “The Overlap between Neurodegenerative and Vascular Factors in the Pathogenesis of Dementia.” *Acta Neuropathologica* 120 (3): 287–96. doi:10.1007/s00401-010-0718-6.

———. 2010b. “The Overlap between Neurodegenerative and Vascular Factors in the Pathogenesis of Dementia.” *Acta Neuropathologica* 120 (3): 287–96. doi:10.1007/s00401-010-0718-6.

———. 2017. “The Neurovascular Unit Coming of Age: A Journey through Neurovascular Coupling in Health and Disease.” *Neuron* 96 (1). Elsevier Inc.: 17–42. doi:10.1016/j.neuron.2017.07.030.

Kazmi, Syed Mohammad Shams, Ashwin B. Parthasarthy, Nelly E. Song, Theresa A. Jones, and Andrew K. Dunn. 2013. “Chronic Imaging of Cortical Blood Flow Using Multi-Exposure Speckle Imaging.” *Journal of Cerebral Blood Flow and Metabolism* 33 (6): 798–808. doi:10.1038/jcbfm.2013.57.

Kisler, Kassandra, Amy R. Nelson, Axel Montagne, and Berislav V. Zlokovic. 2017. "Cerebral Blood Flow Regulation and Neurovascular Dysfunction in Alzheimer Disease." *Nature Reviews Neuroscience* 18 (7). Nature Publishing Group: 419–34. doi:10.1038/nrn.2017.48.

Kitaguchi, Hiroshi, Masafumi Ihara, Hidemoto Saiki, Ryosuke Takahashi, and Hidekazu Tomimoto. 2007. "Capillary Beds Are Decreased in Alzheimer's Disease, but Not in Binswanger's Disease." *Neuroscience Letters* 417 (2): 128–31. doi:10.1016/j.neulet.2007.02.021.

Kleinfeld, D., P. P. Mitra, F. Helmchen, and W. Denk. 1998. "Fluctuations and Stimulus-Induced Changes in Blood Flow Observed in Individual Capillaries in Layers 2 through 4 of Rat Neocortex." *Proceedings of the National Academy of Sciences* 95 (26): 15741–46. doi:10.1073/pnas.95.26.15741.

Mekari, S., S. Fraser, L. Bosquet, C. Bonnéry, V. Labelle, P. Pouliot, F. Lesage, and L. Bherer. 2015. "The Relationship between Exercise Intensity, Cerebral Oxygenation and Cognitive Performance in Young Adults." *Physiology, European Journal of Applied* 115 (10): 2189–97.

Moeini, M., X. Lu, P.K. Avti, R. Damseh, S. Bélanger, F. Picard, D. Boas, A. Kakkar, and F. Lesage. 2018. "Compromised Microvascular Oxygen Delivery Increases Brain Tissue Vulnerability with Age." *Scientific Reports* 8 (1): 8219.

Moeini, M., X. Lu, S. Bélanger, F. Picard, D. Boas, A. Kakkar, and F. Lesage. 2019. "Cerebral Tissue PO2 Response to Stimulation Is Preserved with Age in Awake Mice." *Neuroscience Letters* 699: 160–66.

Montgolfier, O. de, A. Pinçon, P. Pouliot, M.A. Gillis, J. Bishop, J.G. Sled, L. Villeneuve, et al. 2019. "High Systolic Blood Pressure Induces Cerebral Microvascular Endothelial Dysfunction, Neurovascular Unit Damage, and Cognitive Decline in Mice." *Hypertension* 73 (1): 217–28.

Nguyen, John, Nozomi Nishimura, Robert N. Fetcho, Costantino Iadecola, and Chris B.

Schaffer. 2011. “Occlusion of Cortical Ascending Venules Causes Blood Flow Decreases, Reversals in Flow Direction, and Vessel Dilation in Upstream Capillaries.” *Journal of Cerebral Blood Flow and Metabolism* 31 (11): 2243–54. doi:10.1038/jcbfm.2011.95.

Nielsen, Rune B., Lærke Egefjord, Hugo Angleys, Kim Mouridsen, Michael Gejl, Arne Møller, Birgitte Brock, et al. 2017. “Capillary Dysfunction Is Associated with Symptom Severity and Neurodegeneration in Alzheimer’s Disease.” *Alzheimer’s and Dementia* 13 (10). Elsevier Inc.: 1143–53. doi:10.1016/j.jalz.2017.02.007.

Østergaard, Leif, Rasmus Aamand, Eugenio Gutiérrez-Jiménez, Yi Ching L. Ho, Jakob U. Blicher, Søren M. Madsen, Kartheeban Nagenthiraja, et al. 2013. “The Capillary Dysfunction Hypothesis of Alzheimer’s Disease.” *Neurobiology of Aging* 34 (4). Elsevier Ltd: 1018–31. doi:10.1016/j.neurobiolaging.2012.09.011.

Østergaard, Leif, Thorbjørn S. Engedal, Fiona Moreton, Mikkel B. Hansen, Joanna M. Wardlaw, Turgay Dalkara, Hugh S. Markus, and Keith W. Muir. 2016. “Cerebral Small Vessel Disease: Capillary Pathways to Stroke and Cognitive Decline.” *Journal of Cerebral Blood Flow and Metabolism* 36 (2): 302–25. doi:10.1177/0271678X15606723.

Park, L, P Zhou, R Pitstick, C Capone, J Anrather, E H Norris, L Younkin, et al. 2008. “Nox2-Derived Radicals Contribute to Neurovascular and Behavioral Dysfunction in Mice Overexpressing the Amyloid Precursor Protein.” *Proceedings of the National Academy of Sciences* 105 (1091–6490 (Electronic)): 1347–52.

Pereira, Ana C, Dan E Huddleston, Adam M Brickman, Alexander A Sosunov, Rene Hen, Guy M Mckhann, Richard Sloan, Fred H Gage, Truman R Brown, and Scott A Small. 2007. “An in Vivo Correlate of Exercise-Induced Neurogenesis in the Adult Dentate Gyrus.” *Proceedings of the National Academy of Sciences of the United States of America* 104 (13): 5638–43. doi:10.1073/pnas.0611721104.

Pialoux, Vincent, Allison D. Brown, Richard Leigh, Christine M. Friedenreich, and Marc J. Poulin. 2009. “Effect of Cardiorespiratory Fitness on Vascular Regulation and Oxidative Stress in Postmenopausal Women.” *Hypertension* 54 (5): 1014–20.

doi:10.1161/HYPERTENSIONAHA.109.138917.

Radak, Z., N. Hart, L. Sarga, E. Koltai, M. Atalay, H. Ohno, and I. Boldogh. 2010. “Exercise Plays a Preventive Role against Alzheimer’s Disease.” *Journal of Alzheimer’s Disease* 20 (3): 777–83.

Sakadžić, Sava, Emiri T. Mandeville, Louis Gagnon, Joseph J. Musacchia, Mohammad A. Yaseen, Meryem A. Yucel, Joel Lefebvre, et al. 2014. “Large Arteriolar Component of Oxygen Delivery Implies a Safe Margin of Oxygen Supply to Cerebral Tissue.” *Nature Communications* 5. doi:10.1038/ncomms6734.

Santisakultarm, T. P., C. Q. Paduano, T. Stokol, T. L. Southard, N. Nishimura, R. C. Skoda, W. L. Olbricht, A. I. Schafer, R. T. Silver, and C. B. Schaffer. 2014. “Stalled Cerebral Capillary Blood Flow in Mouse Models of Essential Thrombocythemia and Polycythemia Vera Revealed by in Vivo Two-Photon Imaging.” *Journal of Thrombosis and Haemostasis* 12 (12): 2120–30. doi:10.1111/jth.12738.

Schwartz, Theodore H., Seung Bong Hong, Andrew P. Bagshaw, Patrick Chauvel, and Christian G. Bénar. 2011. “Preictal Changes in Cerebral Haemodynamics: Review of Findings and Insights from Intracerebral EEG.” *Epilepsy Research* 97 (3): 252–66. doi:10.1016/j.eplepsyres.2011.07.013.

Sheth, Sameer A., Masahito Nemoto, Michael W. Guiou, Melissa A. Walker, and Arthur W. Toga. 2005. “Spatiotemporal Evolution of Functional Hemodynamic Changes and Their Relationship to Neuronal Activity.” *Journal of Cerebral Blood Flow and Metabolism* 25 (7): 830–41. doi:10.1038/sj.jcbfm.9600091.

Shih, Andy Y., Celine Mateo, Patrick J. Drew, Philbert S. Tsai, and David Kleinfeld. 2012. “A Polished and Reinforced Thinned-Skull Window for Long-Term Imaging of the Mouse Brain.” *Journal of Visualized Experiments*, no. 61: 4–9. doi:10.3791/3742.

Shing, Cecilia M., Robert G. Fassett, Jonathan M. Peake, and Jeff S. Coombes. 2015. “Voluntary Exercise Decreases Atherosclerosis in Nephrectomised ApoE Knockout Mice.” *PLoS ONE* 10 (3): 1–12. doi:10.1371/journal.pone.0120287.

Stefanovic, Bojana, Elizabeth Hutchinson, Victoria Yakovleva, Vincent Schram, James T. Russell, Leonardo Belluscio, Alan P. Koretsky, and Afonso C. Silva. 2008. “Functional Reactivity of Cerebral Capillaries.” *Journal of Cerebral Blood Flow and Metabolism* 28 (5): 961–72. doi:10.1038/sj.jcbfm.9600590.

Toledo, Jon B., Steven E. Arnold, Kevin Raible, Johannes Brettschneider, Sharon X. Xie, Murray Grossman, Sarah E. Monsell, Walter A. Kukull, and John Q. Trojanowski. 2013. “Contribution of Cerebrovascular Disease in Autopsy Confirmed Neurodegenerative Disease Cases in the National Alzheimer’s Coordinating Centre.” *Brain* 136 (9): 2697–2706. doi:10.1093/brain/awt188.

Wirth-dzięciołowska, Elżbieta, and Jadwiga Karaszewska. 2009. “Selected Peripheral Blood Cell Parameters in Twelve Inbred Strains of Laboratory Mice.” *Animal Science Papers ...* 27 (1): 69–77. http://www.ighz.edu.pl/files/objects/7509/66/strona69-80.pdf.

Zhang, Cong, Maryam Tabatabaei, Samuel Bélanger, Hélène Girouard, Mohammad Moeini, Xuecong Lu, and Frédéric Lesage. 2017. “Astrocytic Endfoot Ca2+ Correlates with Parenchymal Vessel Responses during 4-AP Induced Epilepsy: An in Vivo Two-Photon Lifetime Microscopy Study.” *Journal of Cerebral Blood Flow and Metabolism* 39 (2): 260–71. doi:10.1177/0271678X17725417.

Zlokovic, B.V. 2011. “Neurovascular Pathways to Neurodegeneration in Alzheimer’s Disease and Other Disorders.” *Nat Rev Neurosci* 12: 723–38.

CHAPTER 6 ARTICLE 3: HYPERTENSION ACCELERATES CEREBRAL TISSUE PO_2 DISRUPTION IN ALZHEIMER'S DISEASE

Xuecong Lu[1,2], Mohammad Moeini[3], Baoqiang Li[4], Éric Thorin[2,5], Frédéric Lesage[1,2*]

1 Biomedical Engineering Institute, École Polytechnique de Montréal, Montréal, QC, Canada

2 Montreal Heart Institute, Research Center, Montreal, Quebec, Canada.

3 Department of Biomedical Engineering, Amirkabir University of Technology (Tehran Polytechnic), Tehran, Iran

4 Athinoula A. Martinos Center for Biomedical Imaging, Massachusetts General Hospital, Harvard Medical School, Charlestown, MA 02129, USA

5 Department of Surgery, Faculty of Medicine, Université de Montréal, Montreal, Quebec, Canada.

*Corresponding author: Frédéric Lesage, PhD

Address: Biomedical Engineering Institute, École Polytechnique de Montréal, P.O. Box 6079, Succursale Centre-ville, Montréal (QC), H3C 3A7, Canada

Email: frederic.lesage@polymtl.ca, Tel: +1-514-340-4711 ext. 7542, Fax: +1-514-340-4611

Running headline: Hypertension modulates arteriolar PO_2 delivery

This article was submitted to the journal "Neuroscience Letters" on May 29, 2019.

6.1 Abstract

This study measured stimulus-evoked brain tissue oxygenation changes in a mouse model of Alzheimer disease (AD) and further explored the influence of exercise and angiotensin II-induced hypertension on these changes. *In vivo* two-photon phosphorescence lifetime microscopy was used to investigate local changes in brain tissue oxygenation following whisker stimulation. During rest periods, PO_2 values close to the arteriolar wall were lower in the AD groups. The PO_2 spatial decay as a function of distance to arteriole was increased by hypertension. During stimulation, tissue PO_2 response had a similar peak response across groups. Post-stimulation dynamics of tissue PO_2 was larger in AD groups (e.g., AD6 and ADH6) than in the controls (WT6 and WTH6). After a 3-month voluntary exercise period, some of these changes were reversed in AD mice. This provides novel insight into tissue oxygen delivery and the impact of blood pressure control and exercise on brain tissue oxygenation in AD.

6.2 Keywords

Alzheimer’s disease, cerebral tissue oxygenation, stimulation, hypertension, exercises, Two-photon microscopy

6.3 Introduction

The brain requires oxygen to maintain its metabolic demand and normal function (Kisler et al., 2017; Sakadžić et al., 2014; A.L. Vazquez et al., 2010) while the dynamics of oxygen depends on neuronal vitality (Masamoto et al., 2003; A.L. Vazquez et al., 2010). Prior studies documented stimulus-evoked tissue oxygenation changes as a function of distance from feeding vascular sources (Devor et al., 2011), as a function of age (Moeini et al., 2019), during transient and sustained stimulation (Ances et al., 2001), and in healthy anesthetized rats (Alberto L. Vazquez et al., 2010). Nonetheless, these studies were all investigated in a normal brain, despite the fact that brain pathology and neurodegenerative diseases have long been recognized to compromise cerebral oxygenation (Iadecola, 2010, 2004).

Here, we examine a model of Alzheimer's disease (AD), since AD is a neurodegenerative disease involving neuron damage (Gaugler et al., 2018), which may further disrupt the neurovascular coupling in the brain and thus compromise delivery of oxygen and other nutrients to neurons (Iadecola, 2004; Kisler et al., 2017). While a subset of the AD pathology can be attributed to specific genetic variations, its onset in older population is in most cases associated with cardiovascular risk factors. Among vascular risk factors, hypertension exhibits a significant link with AD (Barnes and Yaffe, 2011). Recent evidence suggests that AD animal models, which co-express the KM670/671NL 'Swedish' mutated amyloid precursor protein (APP) and the Leu to Pro mutated presenilin-1 (APP-PS1), display faster progression of AD following the injection of angiotensin II to induce hypertension, as early as at the age of 4.5 months, through cerebral vasculature impairment (Diana Cifuentes et al., 2015). While this work confirmed that vascular changes, induced by hypertension, accelerated AD progression, its role on oxygen delivery to tissue, a potential contributor to damage, was not explored. Hence, our work examines the potential modulating role of hypertension on tissue oxygen response to stimulation in AD models.

As opposed to hypertension, regular physical training has been shown to reduce the risk of

cardiovascular disease and improve cognitive function (Hamer and Chida, 2008). Multiple mechanisms help explain the beneficial effects of exercise, including a control of age-related blood pressure elevation and aortic stiffness (Liu et al., 2014) and an alleviation of oxidative stress (Durrant et al., 2009). Thus, we also explored how exercise may modulate stimulus-evoked tissue oxygenation changes in the same AD model.

Using two-photon phosphorescence lifetime microscopy, we quantified changes in tissue partial pressure of oxygen (PO_2) in response to somatosensory stimulation. Our findings suggest altered tissue PO_2 delivery and response to stimulation in AD pathology, and its combination with hypertension while exercise has the potential to modulate this disruption. These novel data provide insight into tissue oxygen changes associated with blood pressure control and exercise and their cross-talk with AD.

6.4 Methods

6.4.1 Animal preparation

Animals were handled according to the Animal Research: Reporting of In Vivo Experiments (ARRIVE) guidelines and the recommendations of the Canadian Council on Animal Care (CCAC). Experimental protocols were reviewed and approved by the ethics committee of the research center of the Montreal Heart Institute. Experiments were conducted on five mice groups: wild type mice at 6-month-old (C57BL/6J, WT6: N=8), transgenic Amyloid Precursor Protein Presenilin-1 (APP/PS1) mice at 6-month-old (AD6: N=8), APP/PS1 mice at 6-month-old for which voluntary exercise was initiated at 3-month-old (ADE6: N=8), hypertensive mice induced by infusing hypertensive doses of angiotensin II initiated at 3-month old (WTH6: N=8), and mice with dual pathology of AD and induced hypertension (ADH6: N=8).

Previous work (D. Cifuentes et al., 2015) showed a clear onset of cognitive deficit in APP/PS1 mice at 4.5 months, and thus we anticipated that mice at 6-month-old should allow us to

explore oxygen delivery changes in early phases of disease progression. For the exercise group, mice started voluntary exercise on running wheels at 3-month-old and continued the exercise till 6-month-old when brain imaging was performed. The time interval of 3 months was sufficient to observe the effects of voluntary running (Adlard et al., 2005; Pedersen et al., 2016). In hypertensive mice, Angiotensin II was infused at a rate of 1000 ng/kg/min by the mini pumps a 3-month period. To alleviate pain, buprenorphine (at 0.1 mg/kg) was injected before the surgery.

In preparation for two-photon imaging, a craniotomy was performed about ten days before measurements, following the procedure of (Shih et al., 2012). A transparent thin-skull window was created under anesthesia (2% isoflurane in pure oxygen) over the left barrel cortex. A titanium bar was fixed on the skull using dental cement to allow for fixation during surgery and imaging. The skull over the somatosensory area was then slowly thinned to transparency using a micro-drill (OmniDrill 35, World Precision, USA). Then a cover glass was attached to the thinned skull to form the imaging window. The edges of the window were sealed with dental cement to hinder bone growth. A small thinned region (~0.5mm) was left uncovered to allow for injection of phosphorescent dye PtP-C343 into tissue. During the surgery, mice were fixed on a system (LabeoTech, Canada) which allowed for monitoring of physiological parameters.

6.4.2 Awake imaging

All imaging was conducted in awake condition to avoid confounding effects from anesthesia (Schroeter et al., 2014). For two-photon phosphorescence lifetime imaging, mice were fixed on a 3-D printed and angled treadmill wheel allowing for free movement of limbs whereas constraining the head via the titanium bar fixed on the skull (Moeini et al., 2018). To adapt to the fixation device, animals were trained on the imaging wheel in 4 sessions beginning 3 days after the cranial surgery. The training time slowly increased from 10 to 45 minutes in the four sessions.

6.4.3 Whisker stimulation

Air puffs were utilized to stimulate the right whiskers of experimental animals via pulses of compressed air with a pressure of 25 psi, a frequency of 5 Hz, and a pulse width of 100 ms enabled by a pressure microinjection device. Each stimulation lasted for 5 seconds with interstimulus intervals of ~35 s.

6.4.4 PtP-C343 probe

The PtP-C343 probe was synthesized and prepared as described by (Finikova et al., 2008). It is a two-photon enhanced phosphorescent probe for oxygen imaging in which coumarin-343 (C343) in the external circle of the probe acts as antennas to channel the excitation energy from two-photon to the PtP core via a process of Forster-type resonance energy transfer. This probe overcomes the conventional shortcomings of probes based on Pt and Pd porphyrins which are disadvantageous due to low two-photon absorption. The calibration plot for converting phosphorescence decay to PO_2 values was acquired by titration experiments at 37 ^oC and 7.2 pH (Rozhkov et al., 2002).

6.4.5 Two-photon phosphorescence lifetime imaging of tissue PO2 response to stimulation

Tissue PO_2 response to stimulation was recorded using a custom-built two-photon laser microscope, as described in (Moeini et al., 2018). The MaiTai-XP laser oscillator (Newport corporation, USA) generated consecutive sequences of 820 nm, 80 MHz, 150 fs pulses which were gated by an acousto-optic modulator that allowed for “on” and “off” laser pulse periods for microsecond lifetime imaging. Each “on” period lasted for 25 us, and each “off” period lasted for 275 us. The “on” and “off” periods corresponded to periods of excitation of phosphorescence and recording for the lifetime of two-photon enhanced phosphorescent probe PtP-C343 (Finikova et al., 2008) in the brain tissue.

Photons emitted via phosphorescence were detected by a photomultiplier tube (PMT) with a filter centered at 680 nm, and the phosphorescence decays detected were averaged. Fluorescent light was transmitted through a filter centered at 520 nm and passed through the other PMT. The point measurements contained 10 points surrounding diving arterioles, up to a distance of 100 μm from the arteriole with an interval of 10 μm. At each sampling point, 150 phosphorescence decays were imaged, and this sampling process was repeated for 600 times for all stimulation cycles. For each PO_2 measurement, a corresponding "reference" vascular image was acquired immediately after for co-registration of the PO_2 measurements points in the vascular network. For all imaging planes, vessels with large diameters (40 to 250 μm) (Auer, 2016) were manually graphed and labeled as arterioles or venules based on their unique attributes.

6.4.6 Statistical analysis

All image analysis was conducted using custom-designed algorithms in MATLAB. Averaged phosphorescence decay was converted in to tissue oxygenation value using the calibration curve of the corresponding probe (Moeini et al., 2018). The results are presented as bar plots (representing mean±s.e.m.). Statistical significance is denoted as: * $p<0.05$, ** $p<0.01$, ***, $p<0.001$. The sample size is provided in the figure legends. Comparisons across AD and/or hypertension groups were carried out using a two-way ANOVA, with mouse species (AD,WT) and condition (healthy/hypertension) as factors.

6.5 Results

6.5.1 Hypertension leads to faster PO_2 decay from arterioles with distance

To investigate PO_2 delivery to tissue from arterioles, we imaged lines of PO_2 measurements surrounding diving arterioles for each experimental group. Arterioles are known to contribute oxygen to tissue from previous studies (Devor et al., 2011; Sakadžić et al., 2014). As shown

in Fig. 6-1, we measured the behavior of the PO_2 values as a function of radial distance from the corresponding sourcing arteriole. When comparing groups, a two-way ANOVA test showed a significant main effect of AD on tissue PO_2 at rest. Tissue PO_2 close to the arteriole wall was lower in the AD6 group (43.97±0.75 mmHg), when compared to the WT6 group (49.15±0.92 mmHg) and tissue PO_2 close to the arteriole wall was lower in the ADH6 group (40.19±0.94 mmHg) when compared to the WTH6 group (42.52±0.76 mmHg) (Fig. 6-1b). Exercise had a potential modulating effect by elevating the tissue PO_2, while hypertension slightly lowered the tissue PO_2 at rest (Fig. 6-1b). Although tissue PO_2 had decreasing trends with distance for all groups, the hypertensive ADH6 and WTH6 group saw faster spatial decay (Fig. 6-1c), with PO_2 decreasing below longer-distance capillary bed tissue level. Measuring the total decrease between PO_2 at the arterial wall and the longest distance values, we found a main effect of AD (Fig. 6-1d). During stimulation, the change in PO_2 between stimulation and rest also decayed with distance from the arteriole (Fig. 6-1e), showing that stimulation induced larger changes in regions near arterioles than regions far from arterioles.

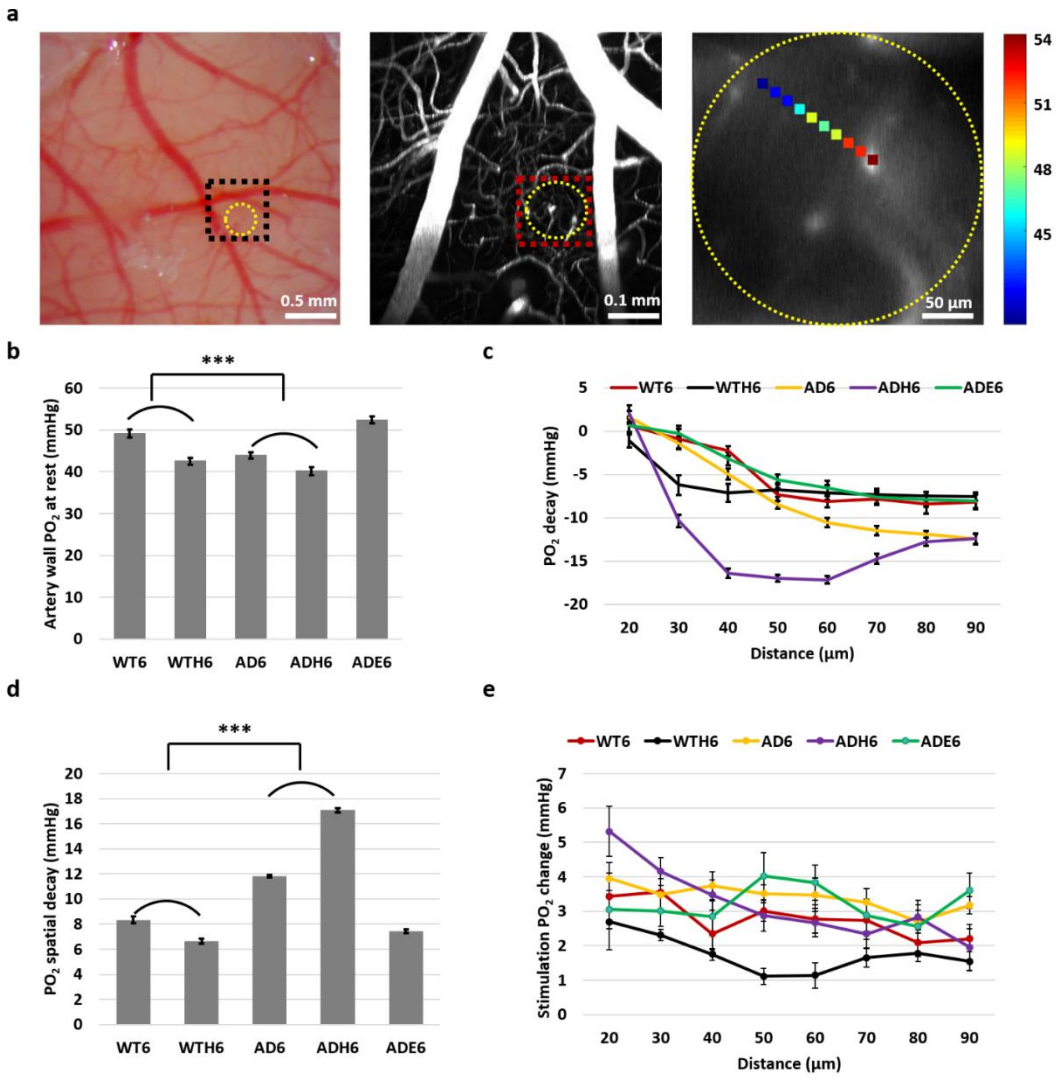

Figure 6-1. Tissue PO_2 decay from arterioles was measured during rest and stimulation (0 – 5 second) for all groups: WT6: wild-type (n=12 arterioles), WTH6: hypertensive WT (n=14 arterioles), AD6: APP-PS1 (n=16 arterioles), ADH6: APP-PS1 with hypertension (n=17 arterioles), ADE6: APP-PS1 with exercise (n=17 arterioles). a) Left panel: an example of the brain area (the yellow circle) where tissue PO_2 was measured. Middle panel: corresponding zoomed vasculature image of the area. Right panel: an example of line point measurements from an arteriole (up to 100 µm from the arteriole). The color of the points denotes different levels of tissue PO_2. b) Arteriole wall PO_2 at rest for each group, estimated by points located within 10 µm from the arterioles during the rest period. c) Tissue PO_2 decay vs distance

(20-90 μm) normalized to wall-PO2. d) PO_2 decay during rest, estimated as (tissue PO_2 with a distance of 90 μm - tissue PO_2 with a distance of 10 μm). e) Difference of tissue PO_2 between stimulation and rest as a function of distance (20-90 μm) from arterioles.

6.5.2 The temporal tissue PO_2 response to stimulation had a larger undershoot in AD

We measured the time course of PO_2 changes integrated over radial distance (an example is shown in Fig. 6-2a). Fig. 6-2b shows the time course of averaged tissue PO_2 for all groups while Fig. 6-2c provides the same data normalized to baseline PO_2. The WT6 and ADE6 groups had higher averaged tissue PO_2 values than other groups (i.e., AD6, WTH6, and ADH6) throughout the entire time course (see Fig. 6-2b). To better understand the PO_2 dynamics, we divided the time course into two periods: stimulation and post-stimulation. A comparison of PO_2 values for the two periods are illustrated in Fig. 6-2d and 6-2e. During stimulation, a two-way ANOVA test did not show statistical differences in PO_2 responses despite an increasing trend for the AD group (2.55±0.22 mmHg) and the group with dual pathology (2.58±0.22 mmHg) compared to the control group (2.26±0.16 mmHg). When investigating the post-stimulation dynamics (Fig. 6-2e), we found the main effect of AD on the undershoot.

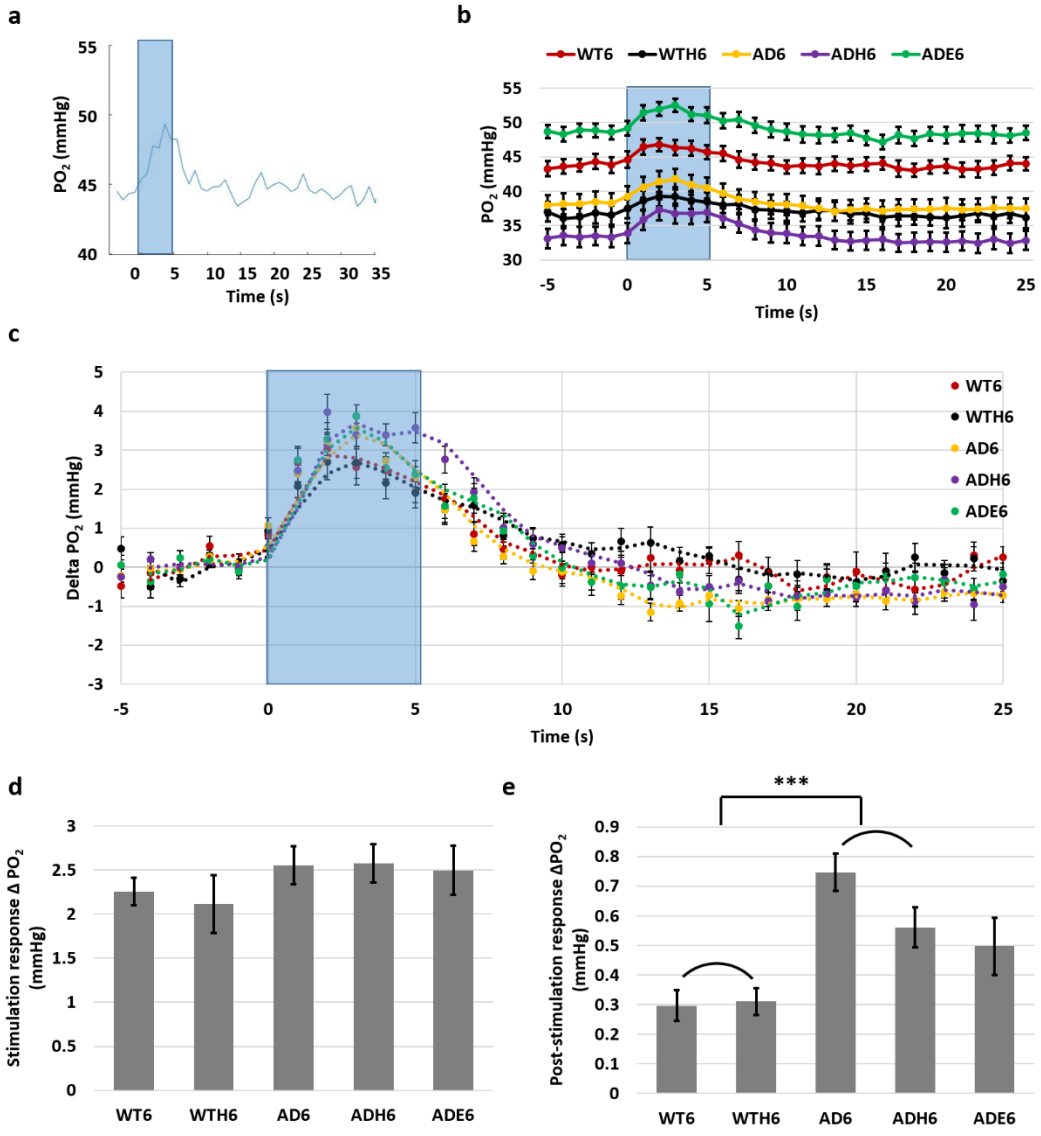

Figure 6-2. Tissue PO_2 response to stimulation for all groups. a) An example of a single time course of PO_2 change during stimulation. The blue area represents the 5-second stimulation window. b) The time course of averaged tissue PO_2 for each experimental group. c) The time course of Δ PO_2 (PO_2 – baseline PO_2) for each group. d) Stimulation response magnitude for all groups, estimated as average response through 0-5 second from the stimulation onset. e) Absolute value of the post-stimulation dynamics estimated by points located 10-25 second from the stimulation onset.

6.6 Discussion

The main objective of this work was to quantify alteration in tissue PO_2 during neural activity in AD mouse models. We used two-photon phosphorescence lifetime microscopy to measure cerebral tissue oxygenation in both WT and AD mice, combined with hypertension and exercise. A prior study (Metzger et al., 2016) investigated the AD patients' response to stimulation at the vascular level, quantifying level of oxygenated hemoglobin using the functional near-infrared spectroscopy (fNIRS) (Metzger et al., 2016). Our data provide unbiased high-resolution sampling of tissue oxygenation changes during neuronal activity in pathological condition of AD and hypertension. Stimulation of the mice whisker induced measurable increases in tissue PO_2 throughout all experimental groups.

The tissue PO2 decay surrounding arterioles

The tissue PO_2 decays observed in the tissue areas near a diving arterioles suggest that oxygen diffuses into the tissue from the sourcing arterioles across all groups (Fig. 1c and 1e). During rest, the AD group is associated with significantly larger tissue PO_2 decay when compared with the healthy control (Fig. 1d).

Based on the modified Krogh model of (Moeini et al., 2018), steeper gradients around arterioles could arise from reduced diffusivity of oxygen in tissue, which could arise from amyloid deposition, increased $CMRO_2$ or decreased O_2 delivery from the capillary bed. While we are unable to validate changes in oxygen diffusion, previous work (X Lu et al., 2019; Xuecong Lu et al., 2019) has shown that AD is associated with a more heterogeneous oxygen delivery from capillaries. This effect was more pronounced in the hypertensive groups which saw large early decays with distance (Fig. 1c). A decreased diameter associated with blood pressure regulation and hypertrophy of the arteriolar wall could lead to both a reduction of the O_2 diffusion surface and impede diffusion through the vascular wall (Baumbach and Heistad, 1989; Didion et al., 2005; Didion and Faraci, 2003; Faraco et al., 2016; Kazama et al., 2004; Ryan et al., 2004). Likewise, changes in tissue PO_2 during

stimulation also led to larger decay with distance in the group of dual pathology (Fig. 1e). Results on PO_2 during rest suggest that hypertension could lead to increased PO_2 decay compared to the healthy control and exacerbate the PO_2 decay associated with AD, consistent with previous findings (Feihl et al., 2006; Gorelick et al., 2011; Pialoux et al., 2009) of the negative impact of hypertension on vasculature and oxygen supply. Meanwhile, the AD group which performed exercise had the trend of lower decay than the AD group during both rest and stimulation (Fig. 1c, 1d and 1e). The later data is in agreement with previous literature (Hamer and Chida, 2008; Radak et al., 2010) which consistently suggested the positive role of exercise on tissue oxygen supply in AD.

The tissue oxygenation response during stimulation

All experimental groups exhibited stimulus-evoked peak responses (Fig. 2b, Fig. 2c), suggesting that the "overshoot" pattern of tissue oxygen is maintained despite the presence of AD and hypertension. Prior studies (Devor et al., 2011; Masamoto et al., 2003) showed that neural activation triggered a tissue PO_2 increase accompanied with cerebral blood flow increase in wild-type mice, which may serve to prevent oxygenation drop during neuronal activity or at locations remote from vascular feeding source. This general pattern of PO_2 increase in response to stimulation was preserved in all groups in our study. The magnitude of the PO_2 increase in response to stimulation had increasing trend in the AD group and the group with dual pathology (Fig. 2d) but no significant differences were seen. On the other hand, the AD group had higher post-stimulus undershoot compared with the healthy controls (Fig. 2e), this could be correlated to changes in neurovascular coupling and the hemodynamic response with AD, and further studies are needed to elucidate the origin of this difference.

6.7 Conclusion

Direct assessment of tissue PO_2 response to functional stimulation could be useful in analyzing how the brain suffers from oxygen supply disruptions in neurogenerative diseases such as AD and how vascular factors (e.g. hypertension) and lifestyle changes (exercise)

could influence the oxygenation response. Our data provides insights into tissue oxygen parameters through which the impact of blood pressure control and exercise on the brain can be quantified. It may help define a role for oxygen delivery in the progression of AD.

Author Contributions

X. L. designed the study, carried out the experiments, analyzed the data, and drafted the manuscript. M. M. carried out the experiments and analyzed the data. B. L. analyzed the data. E. T. participated in designing the study. F. L. conceived, designed and coordinated the study and revised the manuscript. All authors gave final approval for publication.

Funding

This work was supported by a grant from the Natural Sciences and Engineering Research Council of Canada awarded to Frederic Lesage.

6.8 Acknowledgement

The authors thank Marc-Antoine Gillis and Natacha Duquette for their help with the animal preparations.

Conflict of interest

Dr. Lesage reports a minority ownership in LabeoTech Inc.

6.9 References

Adlard, P.A., Perreau, V.M., Pop, V., Cotman, C.W., 2005. Voluntary exercise decreases amyloid load in a transgenic model of Alzheimer's disease. J. Neurosci. 25, 4217–4221.

Ances, B.M., Buerk, D.G., Greenberg, J.H., Detre, J.A., 2001. Temporal dynamics of the partial pressure of brain tissue oxygen during functional forepaw stimulation in rats. Neurosci. Lett. 306, 106–110. https://doi.org/10.1016/S0304-3940(01)01868-7

Auer, R.N., 2016. 4 - Histopathology of Brain Tissue Response to Stroke and Injury, in: Stroke (Sixth Edition) Pathophysiology, Diagnosis, and Management. pp. 47–59.

Barnes, D.E., Yaffe, K., 2011. The projected effect of risk factor reduction on Alzheimer's disease prevalence. Lancet Neurol. 10, 819–828. https://doi.org/10.1016/S1474-4422(11)70072-2

Baumbach, G.L., Heistad, D.D., 1989. Remodeling of Cerebral Arterioles in Chronic Hypertension. Hypertension 13, 968–972.

Cifuentes, Diana, Poittevin, M., Dere, E., Broquères-You, D., Bonnin, P., Benessiano, J., Pocard, M., Mariani, J., Kubis, N., Merkulova-Rainon, T., Lévy, B.I., 2015. Hypertension accelerates the progression of Alzheimer-like pathology in a mouse model of the disease. Hypertension 65, 218–224. https://doi.org/10.1161/HYPERTENSIONAHA.114.04139

Cifuentes, D., Poittevin, M., Dere, E., Broquères-You, D., Bonnin, P., Benessiano, J., Pocard, M., Mariani, J., Kubis, N., Merkulova-Rainon, T., Lévy, B.I., 2015. Hypertension accelerates the progression of Alzheimer-like pathology in a mouse model of the disease. Hypertension 65, 218–224.

Devor, A., Sakadzic, S., Saisan, P.A., Yaseen, M.A., Roussakis, E., Srinivasan, V.J., Vinogradov, S.A., Rosen, B.R., Buxton, R.B., Dale, A.M., Boas, D.A., 2011. "Overshoot" of O2 Is Required to Maintain Baseline Tissue Oxygenation at Locations Distal to Blood Vessels. J. Neurosci. 31, 13676–13681.

https://doi.org/10.1523/JNEUROSCI.1968-11.2011

Didion, S.P., Faraci, F.M., 2003. Angiotensin II produces superoxide-mediated impairment of endothelial function in cerebral arterioles. Stroke 34, 2038–2042. https://doi.org/10.1161/01.STR.0000081225.46324.AA

Didion, S.P., Kinzenbaw, D.A., Faraci, F.M., 2005. Critical role for CuZn-superoxide dismutase in preventing angiotensin II-induced endothelial dysfunction. Hypertension 46, 1147–1153. https://doi.org/10.1161/01.HYP.0000187532.80697.15

Durrant, J.R., Seals, D.R., Connell, M.L., Russell, M.J., Lawson, B.R., Folian, B.J., Donato, A.J., Lesniewski, L.A., 2009. Voluntary wheel running restores endothelial function in conduit arteries of old mice: Direct evidence for reduced oxidative stress, increased superoxide dismutase activity and down-regulation of NADPH oxidase. J. Physiol. 587, 3271–3285. https://doi.org/10.1113/jphysiol.2009.169771

Faraco, G., Park, L., Zhou, P., Luo, W., Paul, S.M., Anrather, J., Iadecola, C., 2016. Hypertension enhances A β -induced neurovascular dysfunction, promotes β -secretase activity, and leads to amyloidogenic processing of APP. J. Cereb. Blood Flow Metab. 36, 241–252. https://doi.org/10.1038/jcbfm.2015.79

Feihl, F., Liaudet, L., Waeber, B., Levy, B.I., 2006. Hypertension A Disease of the Microcirculation? Hypertension 48, 1012–1017. https://doi.org/10.1161/01.HYP.0000249510.20326.72

Finikova, O.S., Lebedev, A.Y., Aprelev, A., Troxler, T., Gao, F., Garnacho, C., Muro, S., Hochstrasser, R.M. Vinogradov, S.A., 2008. Oxygen Microscopy by Two-Photon-Excited Phosphorescence. ChemPhysChem 9, 1673–1679.

Gaugler, J., James, B., Johnson, T., Scholz, K., Weuve, J., 2018. 2018 Alzheimer's disease facts and figures. Alzheimer's Dement. 12, 459–509. https://doi.org/10.1016/j.jalz.2016.03.001

Gorelick, P.B., Scuteri, A., Black, S.E., DeCarli, C., Greenberg, S.M., Iadecola, C., Launer, L.J., Laurent, S., Lopez, O.L., Nyenhuis, D., Petersen, R.C., 2011. Vascular

contributions to cognitive impairment and dementia. Stroke 42, 2672–2713. https://doi.org/10.1016/j.bbadis.2016.02.010

Hamer, M., Chida, Y., 2008. Physical activity and risk of neurodegenerative disease: A systematic review of prospective evidence. Psychol. Med. 39, 3–11. https://doi.org/10.1017/S0033291708003681

Iadecola, C., 2010. The overlap between neurodegenerative and vascular factors in the pathogenesis of dementia. Acta Neuropathol. 120, 287–296. https://doi.org/10.1007/s00401-010-0718-6

Iadecola, C., 2004. Neurovascular regulation in the normal brain and in Alzheimer's disease. Nat. Rev. Neurosci. 5, 347–360. https://doi.org/10.1038/nrn1387

Kazama, K., Anrather, J., Zhou, P., Girouard, H., Frys, K., Milner, T.A., Iadecola, C., 2004. Angiotensin II impairs neurovascular coupling in neocortex through NADPH oxidase-derived radicals. Circ. Res. 95, 1019–1026. https://doi.org/10.1161/01.RES.0000148637.85595.c5

Kisler, K., Nelson, A.R., Montagne, A., Zlokovic, B. V., 2017. Cerebral blood flow regulation and neurovascular dysfunction in Alzheimer disease. Nat. Rev. Neurosci. 18, 419–434. https://doi.org/10.1038/nrn.2017.48

Liu, Junxiu, Sui, X., Lavie, C.J., Zhou, H., Mark Park, Y.M., Cai, B., Liu, Jihong, Blair, S.N., 2014. Effects of cardiorespiratory fitness on blood pressure trajectory with aging in a cohort of healthy men. J. Am. Coll. Cardiol. 64, 1245–1253. https://doi.org/10.1016/j.jacc.2014.06.1184

Lu, X, Moeini, M., Li, B., Lu, Y., Damseh, R., Pouliot, P., Thorin, E., Lesage, F., 2019. Changes in capillary hemodynamics and its modulation by exercise in the APP-PS1 Alzheimer mouse model.

Lu, Xuecong, Moeini, M., Li, B., Montgolfier, O. de, Lu, Y., Bélanger, S., Thorin, É., Lesage, F., 2019. Voluntary exercise increases brain tissue oxygenation and spatially homogenizes oxygen delivery in a mouse model of Alzheimer's Disease.

Masamoto, K., Takizawa, N., Kobayashi, H., Oka, K., Tanishita, K., 2003. Dual responses of tissue partial pressure of oxygen after functional stimulation in rat somatosensory cortex. Brain Res. 979, 104–113. https://doi.org/10.1016/S0006-8993(03)02882-8

Metzger, F.G., Schopp, B., Haeussinger, F.B., Dehnen, K., Synofzik, M., Fallgatter, A.J., Ehlis, A.C., 2016. Brain activation in frontotemporal and Alzheimer's dementia: A functional near-infrared spectroscopy study. Alzheimer's Res. Ther. 8, 1–12. https://doi.org/10.1186/s13195-016-0224-8

Moeini, M., Lu, X., Avti, P.K., Damseh, R., Bélanger, S., Picard, F., Boas, D., Kakkar, A., Lesage, F., 2018. Compromised microvascular oxygen delivery increases brain tissue vulnerability with age. Sci. Rep. 8, 8219.

Moeini, M., Lu, X., Bélanger, S., Picard, F., Boas, D., Kakkar, A., Lesage, F., 2019. Cerebral tissue pO2 response to stimulation is preserved with age in awake mice. Neurosci. Lett. 699, 160–166.

Pedersen, L., Idorn, M., Olofsson, G.H., Lauenborg, B., Nookaew, I., Hansen, R.H., Johannesen, H.H., Becker, J.C., Pedersen, K.S., Dethlefsen, C., Nielsen, J., 2016. Voluntary running suppresses tumor growth through epinephrine-and IL-6-dependent NK cell mobilization and redistribution. Cell Metab. 23, 554–562.

Pialoux, V., Brown, A.D., Leigh, R., Friedenreich, C.M., Poulin, M.J., 2009. Effect of cardiorespiratory fitness on vascular regulation and oxidative stress in postmenopausal women. Hypertension 54, 1014–1020. https://doi.org/10.1161/HYPERTENSIONAHA.109.138917

Radak, Z., Hart, N., Sarga, L., Koltai, E., Atalay, M., Ohno, H., Boldogh, I., 2010. Exercise plays a preventive role against Alzheimer's disease. J. Alzheimer's Dis. 20, 777–783.

Rozhkov, V., Wilson, D., Vinogradov, S., 2002. Phosphorescent Pd Porphyrin−Dendrimers: Tuning Core Accessibility by Varying the Hydrophobicity of the Dendritic Matrix. Macromolecules 35, 1991–1993.

Ryan, M.J., Didion, S.P., Mathur, S., Faraci, F.M., Sigmund, C.D., 2004. Angiotensin

II-Induced Vascular Dysfunction is Mediated by the AT 1A Receptor in Mice. Hypertension 43, 1074–1079. https://doi.org/10.1161/01.HYP.0000123074.89717.3d

Sakadžić, S., Mandeville, E.T., Gagnon, L., Musacchia, J.J., Yaseen, M.A., Yucel, M.A., Lefebvre, J., Lesage, F., Dale, A.M., Eikermann-Haerter, K., Ayata, C., Srinivasan, V.J., Lo, E.H., Devor, A., Boas, D.A., 2014. Large arteriolar component of oxygen delivery implies a safe margin of oxygen supply to cerebral tissue. Nat. Commun. 5. https://doi.org/10.1038/ncomms6734

Schroeter, A., Schlegel, F., Seuwen, A., Grandjean, J., Rudin, M., 2014. Specificity of stimulus-evoked fMRI responses in the mouse: the influence of systemic physiological changes associated with innocuous stimulation under four different anesthetics. Neuroimage 94, 372–384.

Shih, A.Y., Mateo, C., Drew, P.J., Tsai, P.S., Kleinfeld, D., 2012. A Polished and Reinforced Thinned-skull Window for Long-term Imaging of the Mouse Brain. J. Vis. Exp. 4–9. https://doi.org/10.3791/3742

Vazquez, Alberto L., Fukuda, M., Tasker, M.L., Masamoto, K., Kim, S.G., 2010. Changes in cerebral arterial, tissue and venous oxygenation with evoked neural stimulation: Implications for hemoglobin-based functional neuroimaging. J. Cereb. Blood Flow Metab. 30, 428–439. https://doi.org/10.1038/jcbfm.2009.213

Vazquez, A.L., Masamoto, K., Fukuda, M., Kim, S.G., 2010. Cerebral oxygen delivery and consumption during evoked neural activity. Front. Neuroenergetics 2, 1–12. https://doi.org/10.3389/fnene.2010.00011

CHAPTER 7 GENERAL DISCUSSION

This chapter reviews the objectives introduced in chapter 1 and responds to the validation of the hypotheses based on the results of the three peer-reviewed articles presented in chapter 4, 5 and 6.

7.1 Objective 1

The first objective of this research was to monitor the changes of brain tissue oxygenation in a mouse model of AD and explore the modulating effect of voluntary exercise on oxygenation. Accordingly, we hypothesized that brain tissue oxygenation is compromised by the onset of AD, expressed by attenuated tissue PO2, the presence of hypoxia, and heterogeneity of tissue PO2, and that exercise could modulate the tissue oxygenation alteration in AD, thus alleviating the oxidative stress in the mouse model of AD.

In first article, we did find AD-related decreases in tissue PO_2 in the mouse cortex using two-photon phosphorescence lifetime measurements in vivo and in awake condition. Our key findings include a decrease in average tissue PO_2 with the onset of AD, higher spatial heterogeneity of tissue PO_2 with AD, a modulatory effect of voluntary exercise by increasing average tissue PO_2 and decreasing the spatial heterogeneity of tissue oxygenation and reducing the frequency of hypoxia in the AD, a decrease of total blood flow in AD which was also reversed by exercise, and a dose-response relationship between running distance and brain oxygenation / blood flow.

To verify these hypotheses, we developed a technique to image cerebral oxygenation in awake conditions, thus eliminating the effects of anesthesia, since anesthesia may affect physiological parameters, such as oxygen, in the experimental subjects (Schroeter et al., 2014). In our experiments, we used an angled-wheel through which mice could walk, while their heads were fixed below the two-photon microscope for imaging. We designed training sessions for the mice to adapt to the angled-wheel such that the animals were under minimum

stress when used for imaging.

Our article suggests that although AD leads to compromised brain oxygenation, voluntary exercise could preserve neurovascular coupling and potentially slow the rate of neurodegeneration in patients at risk of AD.

7.2 Objective 2

The second objective is to quantify the changes in capillary RBC dynamics with AD and the modulation of exercise on cerebral capillaries in AD. Accordingly, we hypothesized that capillary hemodynamic changes are associated with the presence of AD and that exercise could play a modulating role on the alterations of capillary RBC dynamics in the mouse model of AD.

In the second article, we found that blood flow was significantly reduced in AD group, partially increased with exercise. RBC velocity was decreased with AD, which could lead to compromised perfusion in the mice cortex and compromised clearance of beta-amyloid in brain. Hematocrit was reduced with AD, partially increased by exercise. These microvascular changes observed suggest that AD does share many similar microvessel disruptions with cardiovascular pathologies and aging, disruptions that could be alleviated by exercise, as the case in other cardiovascular diseaseas.

This article also suggests that RBC properties, such as velocity and flux, were branch order dependent. In particular, RBC velocity and flux largely decreased from the upstream capillaries to the downstream capillarie, suggesting possible occlusion in capillaries. Functional hemodynamic response to stimulation was also disrupted in AD, and reversed by exercise. ISOI data suggests that AD mice had weaker oxy-hemoglobin response to stimulation, which could be improved by exercise.

In general, this study provides novel insights into the hemodynamic mechanisms of cerebral microcirculatory disturbances in AD and the benefits of voluntary exercise on these hemodynamic changes. Our work suggests the potential theraputic target for alleving the

microvascular compromise in AD via lifestyle changes of exercise.

7.3 Objective 3

The third objective was to investigate the stimulus-evoked tissue oxygenation changes in the model of AD and further examine modulating factors, including exercise and hypertension for these changes. Accordingly, we propose that the stimulus-evoked tissue oxygenation changes differ in AD mice and control mice and that hypertension and exercise may modulate these changes in opposite directions.

Our data, for the first time to our knowledge, provide information of tissue oxygenation change during neuronal activity in pathological condition of AD and hypertension. All experimental groups exhibited "overshoot" patterns of tissue oxygen, while the magnitude of the PO_2 increase in response to stimulation was significantly higher in the group with both AD and hypertension, which may serve as a response toward deteriorated tissue hypoxia under elevated neuronal activity. AD is associated with an attenuated baseline tissue PO_2, an attenuation worsened by hypertension and reversed by exercise. This finding extends the first article of average tissue oxygenation state under resting state. Hypertension could exacerbate the attenuated baseline PO_2 in AD, in agreement with previous findings of the negative impact of hypertension on vasculature and oxygen supply. The AD group took longer time for its response to increase during the stimulation periods, with the time further prolonged by hypertension, suggesting slower response toward stimulation.

These novel data provide insight into tissue oxygen parameters through which the impact of blood pressure control and exercise on the progression of AD can be quantified simultaneously for further clinical studies. Our results also offer insights for functional imaging techniques which depend on oxygen response toward neuronal stimulation.

7.4 Limitations and future studies

Despite the novel insights provided by these studies, there are several limitations regarding

the experimental animals, the imaging techniques, and the data collection.

Firstly, there are limitations with the use of experimental animals used in our studies. Although the transgenic mice carrying mutant amyloid precursor protein and presenilin 1(APP-PS1) transgenes used in our studies have been well-established as an AD model and have been used in numerous studies (Götz et al., 2018; Hernández et al., 2019; Holcomb et al., 1998), our studies do not consider alternative AD animal models (e.g., 5xFAD mice which express human APP and PSEN1 transgenes with a total of five AD-linked mutations). Some of our findings could be specific to the model and future studies may image cerebral oxygenation in different types of AD mouse models (Götz et al., 2018), which will help improve the robustness and ensure the generalizability of our results. Additionally, the mice used in our studies were males. Prior studies (Hirata-Fukae et al., 2008; Howlett et al., 2004) documented that female mice were associated with more extensive amyloid deposition than male mice, and thus our sample did not represent female subjects with AD. Future studies may use both female and male subjects for the imaging of cerebral oxygenation to provide information for both sexes.

Secondly, there are limitations with the imaging technique. In the first article, although cerebral tissue oxygenation was quantified in vivo in awake condition, the amyloid plaques were quantified ex vivo, limiting our capacity to analyze the connection between cerebral tissue oxygen and the level of amyloid deposition. A previous study (Michaud et al., 2013) adopted a Congo Red dye to stain amyloid aggregates and imaged amyloid deposition in vivo using two-photon microscopy. Future work may combine the advantage of our two-photon phosphorescence laser microscopy and the Congo Red dye to quantify cerebral tissue oxygen and amyloid deposition in AD animal models in vivo simultaneously. Comparison of amyloid deposition between hypoxic area and normal tissue area could be conducted to examine the relationship between cerebral tissue oxygen and the accumulation of amyloid beta. In the second article, capillary blood flow properties were quantified, while the information of cerebral tissue oxygenation was omitted. Future study may improve the imaging technique to

quantify capillary flow and tissue oxygenation simultaneously, which provide information on potential changes of the connection between cerebral blood flow and tissue oxygenation in AD. In the third article, our study was limited by not quantifying CBF during stimulation in AD models. Quantifying CBF and cerebral oxygenation simultaneously would enable measurement of tissue oxygen consumption during stimulation (Devor et al., 2011; Moeini et al., 2019), offering unprecedented opportunities for our understanding of cerebral metabolism changes in AD. Future work may set up a multimodal microscope combining two-photon imaging and OCT. To take full advantage of each imaging modality, separate scanning arms and probing optical beams need to be combined into the same microscope objective (Sakadžić et al., 2014).

Thirdly, our data collection was cross-sectional. Specifically, data collection was conducted only once in each experimental group. Given that AD is sporadic in the early stage, longitudinal data regarding the progressive change of cerebral oxygenation plays a key role in understanding the development of the disease. To achieve longitudinal data collection, long-term optical cranial windows have been suggested to support two-photon microscopy imaging (Desjardins et al., 2019). These long-term windows provide opportunities for sampling oxygenation parameters repeatedly in the same animal over days to weeks and months (Berthiaume et al., 2018). Future work may consider longitudinal in vivo two-photon imaging of cerebral oxygenation in AD animal models, which will enable us to understand how cerebral oxygenation is compromised over time.

CHAPTER 8 CONCLUSION

This thesis aimed to explore cerebral oxygenation by exploiting two photon phosphorescence microscopy for better spatial and temporal resolution of oxygen. The two-photon technique was also complemented by other imaging techniques, including ISOI, MRI, and OCT to provide information on cerebral oxygenation alteration in AD. APP-PS1 mice were used in all experiments, and this type of mice have been shown to develop early syptoms of AD at around 4.5 months of age.

The first endeavor showed that cerebral average tissue PO2 decreased with the onset of AD, suggesting compromised oxygen state in AD mice. Reduced average tissue PO2 was associated with the presence of small near-hypoxic areas, which may threaten cell survival. Ex vivo staining also confirmed more amyloid-β (Aβ) deposits in AD. However, these alterations in AD could be alleviated by exercise. Interestingly, there is a dose-response relationship between running and cerebral tissue oxygenation, suggesting the benefits of active lifestyle.

The tissue oxygenation state is highly influenced by the cerebral blood flow to supply oxygen to tissue. In the second attempt, capillary hemodynamics was explored in AD mice, given the fundamental role of capillaries in the oxygen transport to tissue. Our data show that hemodynamic properties, such as velocity and hematocrit, were reduced with AD, and that exercise counter-acted to re-establish homeostatis. The oxygen-hemoglobin response in capillaries was also compromised in AD, although improved by exercise.

Given that cortex is an energy-demanding region in the brain due to neuronal activity during cognitive tasks, investigating the oxygenation state under stimulation is essential, as neurons may demand more oxygen and nutrients with elevated activity. Thus, the last paper aimed to explore the stimulus-evoked tissue oxygenation changes in the model of AD and further explore the modulating factors including exercise and hypertension for these changes. Our results showed that lower baseline tissue PO2 value in the AD group, exacerbated by

hypertension while reversed by exercise, and more fluctuations of oxygenation state under stimulation in AD.

Overall, these studies suggest that compromised brain oxygenation is potential biomarker AD, with the exercise having potential to preserve cerebral oxygenation while hypertension exacerbating the oxygenation compromise in AD.

REFERENCES

Adlard, P.A., Perreau, V.M., Pop, V., Cotman, C.W., 2005. Voluntary exercise decreases amyloid load in a transgenic model of Alzheimer's disease. J. Neurosci. 25, 4217–4221.

Alata, W., Ye, Y., St-Amour, I., Vandal, M., Calon, F., 2015. Human apolipoprotein E ε4 expression impairs cerebral vascularization and blood-brain barrier function in mice. J. Cereb. Blood Flow Metab. 35, 86–94. https://doi.org/10.1038/jcbfm.2014.172

Ances, Beau M., Buerk, D.G., Greenberg, J.H., Detre, J.A., 2001. Temporal dynamics of the partial pressure of brain tissue oxygen during functional forepaw stimulation in rats. Neurosci. Lett. 306, 106–110. https://doi.org/10.1016/S0304-3940(01)01868-7

Ances, B.M., Wilson, D.F., Greenberg, J.H., Detre, J.A., 2001. Dynamic changes in cerebral blood flow, O2 tension, and calculated cerebral metabolic rate of O2 during functional activation using oxygen phosphorescence quenching. J. Cereb. Blood Flow Metab. 21, 511–516.

Attwell, D., Buchan, A.M., Charpak, S., Lauritzen, M., MacVicar, B.A., Newman, E.A., 2010. Glial and neuronal control of brain blood flow. Nature 468, 232–243. https://doi.org/10.1038/nature09613.Glial

Bell, R.D., Deane, R., Chow, N., Long, X., Sagare, A., Streb, J.W., Guo, H., Rubio, A., Nostrand, W.Van, Joseph, M., Zlokovic, B.V, 2009. SRF and myocardin regulate LRP-mediated amyloid-β clearance in brain vascular cells. Nat. Cell Biol. 11, 143–153. https://doi.org/10.1038/ncb1819.SRF

Bero, A.W., Bauer, A.Q., Stewart, F.R., White, B.R., Cirrito, J.R., Raichle, M.E., Culver, J.P., Holtzman, D.M., 2012. Bidirectional Relationship between Functional Connectivity and Amyloid- Deposition in Mouse Brain. J. Neurosci. 32, 4334–4340. https://doi.org/10.1523/jneurosci.5845-11.2012

Berthiaume, A.A., Grant, R.I., McDowell, K.P., Underly, R.G., Hartmann, D.A., Levy, M., Bhat, N.R., Shih, A.Y., 2018. Dynamic Remodeling of Pericytes In Vivo Maintains

Capillary Coverage in the Adult Mouse Brain. Cell Rep. 22, 8–16. https://doi.org/10.1016/j.celrep.2017.12.016

Brantigan, J.W., Gott, V.L., Martz, M.N., 1972. A Teflon membrane for measurement of blood and intramyocardial gas tensions by mass spectroscopy. J. Appl. Physiol. 32, 276–282.

Buxton, R.B., 2010. Interpreting oxygenation-based neuroimaging signals: the importance and the challenge of understanding brain oxygen metabolism. Front. Neuroenergetics 2, 1–16. https://doi.org/10.3389/fnene.2010.00008

Cahill, L.S., Bishop, J., Gazdzinski, L.M., Dorr, A., Stefanovic, B., Sled, J.G., 2017. Altered cerebral blood flow and cerebrovascular function after voluntary exercise in adult mice. Brain Struct. Funct. 222, 3395–3405. https://doi.org/10.1007/s00429-017-1409-z

Chance, B., 1957. Cellular oxygen requirements. Fed Proc 16, 671–680.

Chance, B., Cohen, P., Jobsis, F., Schoener, B., 1962. Intracellular oxidation- reduction states in vivo. Science (80-.). 137, 499–508.

Cifuentes, D., Poittevin, M., Dere, E., Broquères-You, D., Bonnin, P., Benessiano, J., Pocard, M., Mariani, J., Kubis, N., Merkulova-Rainon, T., Lévy, B.I., 2015. Hypertension accelerates the progression of Alzheimer-like pathology in a mouse model of the disease. Hypertension 65, 218–224. https://doi.org/10.1161/HYPERTENSIONAHA.114.04139

Damseh, R., Pouliot, P., Gagnon, L., Sakadzic, S., Boas, D., Cheriet, F., Lesage, F., 2018. Automatic Graph-based Modeling of Brain Microvessels Captured with Two-Photon Microscopy. IEEE J. Biomed. Heal. Informatics 1–1. https://doi.org/10.1109/jbhi.2018.2884678

Delafontaine-Martel, P., Lefebvre, J., Tardif, P.-L., Lévy, B.I., Pouliot, P., Lesage, F., 2018. Whole brain vascular imaging in a mouse model of Alzheimer's disease with two-photon microscopy. J. Biomed. Opt. 23, 1. https://doi.org/10.1117/1.jbo.23.7.076501

Desjardins, M., Kılıç, K., Thunemann, M., Mateo, C., Holland, D., Ferri, C.G.L., Cremonesi,

J.A., Li, B., Cheng, Q., Weldy, K.L., Saisan, P.A., Kleinfeld, D., Komiyama, T., Liu, T.T., Bussell, R., Wong, E.C., Scadeng, M., Dunn, A.K., Boas, D.A., Sakadžić, S., Mandeville, J.B., Buxton, R.B., Dale, A.M., Devor, A., 2019. Awake Mouse Imaging: From Two-Photon Microscopy to Blood Oxygen–Level Dependent Functional Magnetic Resonance Imaging. Biol. Psychiatry Cogn. Neurosci. Neuroimaging 1–10. https://doi.org/10.1016/j.bpsc.2018.12.002

Devor, A., Sakadzic, S., Saisan, P.A., Yaseen, M.A., Roussakis, E., Srinivasan, V.J., Vinogradov, S.A., Rosen, B.R., Buxton, R.B., Dale, A.M., Boas, D.A., 2011. "Overshoot" of O2 Is Required to Maintain Baseline Tissue Oxygenation at Locations Distal to Blood Vessels. J. Neurosci. 31, 13676–13681. https://doi.org/10.1523/JNEUROSCI.1968-11.2011

Devor, A., Sakadžić, S., Srinivasan, V.J., Yaseen, M.A., Nizar, K., Saisan, P.A., Tian, P., Dale, A.M., Vinogradov, S.A., Franceschini, M.A., Boas, D.A., 2012. Frontiers in optical imaging of cerebral blood flow and metabolism. J. Cereb. Blood Flow Metab. 32, 1259–1276. https://doi.org/10.1038/jcbfm.2011.195

Dorr, A., Thomason, L.A., Koletar, M.M., Joo, I.L., Steinman, J., Cahill, L.S., Sled, J.G., Stefanovic, B., 2017. Effects of voluntary exercise on structure and function of cortical microvasculature. J. Cereb. Blood Flow Metab. 37, 1046–1059.

Farkas, E., Luiten, P.G.M., 2001. Cerebral microvascular pathology in aging and Alzheimer's disease, Progress in Neurobiology. https://doi.org/10.1016/S0301-0082(00)00068-X

Finikova, O.S., Lebedev, A.Y., Aprelev, A., Troxler, T., Gao, F., Garnacho, C., Muro, S., Hochstrasser, R.M. Vinogradov, S.A., 2008. Oxygen Microscopy by Two-Photon-Excited Phosphorescence. ChemPhysChem 9, 1673–1679.

Gallez, B., Baudelet, C., Jordan, B.F., 2004. Assessment of tumor oxygenation by electron paramagnetic resonance: Principles and applications. NMR Biomed. 17, 240–262. https://doi.org/10.1002/nbm.900

Gaugler, J., James, B., Johnson, T., Scholz, K., Weuve, J., 2018. 2018 Alzheimer's disease

facts and figures. Alzheimer's Dement. 12, 459–509. https://doi.org/10.1016/j.jalz.2016.03.001

Girouard, H., Iadecola, C., 2006. Neurovascular coupling in the normal brain and in hypertension, stroke, and Alzheimer disease. J. Appl. Physiol. 100, 328–335. https://doi.org/10.1152/japplphysiol.00966.2005

Gorelick, P.B., Scuteri, A., Black, S.E., DeCarli, C., Greenberg, S.M., Iadecola, C., Launer, L.J., Laurent, S., Lopez, O.L., Nyenhuis, D., Petersen, R.C., 2011. Vascular contributions to cognitive impairment and dementia. Stroke 42, 2672–2713. https://doi.org/10.1016/j.bbadis.2016.02.010

Götz, J., Bodea, L.G., Goedert, M., 2018. Rodent models for Alzheimer disease. Nat. Rev. Neurosci. 19, 583–598. https://doi.org/10.1038/s41583-018-0054-8

Grammas, P., 2011. Neurovascular dysfunction, inflammation and endothelial activation: implications for the pathogenesis of Alzheimer's disease. J. Neuroinflammation 8, 26.

Hachinski, V., 2015. Stroke and Potentially Preventable Dementias Proclamation. Stroke 46, 3039–3040. https://doi.org/10.1161/strokeaha.115.011237

Hall, C.N., Reynell, C., Gesslein, B., Hamilton, N.B., Mishra, A., Sutherland, B.A., Oâ Farrell, F.M., Buchan, A.M., Lauritzen, M., Attwell, D., 2014. Capillary pericytes regulate cerebral blood flow in health and disease. Nature 508, 55–60. https://doi.org/10.1038/nature13165

Hernández, J.C.C., Bracko, O., Kersbergen, C.J., Muse, V., Haft-Javaherian, M., Berg, M., Park, L., Vinarcsik, L.K., Ivasyk, I., Rivera, D.A., Kang, Y., Cortes-Canteli, M., Peyrounette, M., Doyeux, V., Smith, A., Zhou, J., Otte, G., Beverly, J.D., Davenport, E., Davit, Y., Lin, C.P., Strickland, S., Iadecola, C., Lorthois, S., Nishimura, N., Schaffer, C.B., 2019. Neutrophil adhesion in brain capillaries reduces cortical blood flow and impairs memory function in Alzheimer's disease mouse models. Nat. Neurosci. https://doi.org/10.1038/s41593-018-0329-4

Heyn, P., Abreu, B.C., Ottenbacher, K.J., 2004. The effects of exercise training on elderly

persons with cognitive impairment and dementia: A meta-analysis. Arch. Phys. Med. Rehabil. 85, 1694–1704.

Hirata-Fukae, C., Li, H.F., Hoe, H.S., Gray, A.J., Minami, S.S., Hamada, K., Niikura, T., Hua, F., Tsukagoshi-Nagai, H. Horikoshi-Sakuraba, Y. and Mughal, M., 2008., 2008. Females exhibit more extensive amyloid, but not tau, pathology in an Alzheimer transgenic model. Brain Res. 1216, 92–103.

Holcomb, L., Gordon, M.N., Mcgwan, E., Yu, X.I.N., Benkovic, S., Antzen, P., Wright, K., Saad, I., Mueller, R., Morgan, D., Sanders, S., Zehr, C., Campa, K.O., Hardy, J., Prada, C., Eckman, C., Younkin, S., Hsia, K., Duff, K., 1998. Accelerated Alzheimer-type phenotype in transgenic mice carrying both mutant amyloid precursor protein and presenilin 1 transgenes. Nat Methods 4, 97–100.

Howlett, D.R., Richardson, J.C., Austin, A., Parsons, A.A., Bate, S.T., Davies, D.C., Gonzalez, M.I., 2004. Cognitive correlates of Aβ deposition in male and female mice bearing amyloid precursor protein and presenilin-1 mutant transgenes. Brain Res. 1017, 130–136.

Iadecola, C., 2017. The Neurovascular Unit Coming of Age: A Journey through Neurovascular Coupling in Health and Disease. Neuron 96, 17–42. https://doi.org/10.1016/j.neuron.2017.07.030

Iadecola, C., 2013. The Pathobiology of Vascular Dementia. Neuron 80, 844–866. https://doi.org/10.1016/j.neuron.2013.10.008

Iadecola, C., 2010a. The overlap between neurodegenerative and vascular factors in the pathogenesis of dementia. Acta Neuropathol. 120, 287–296. https://doi.org/10.1007/s00401-010-0718-6

Iadecola, C., 2010b. The overlap between neurodegenerative and vascular factors in the pathogenesis of dementia. Acta Neuropathol. 120, 287–296. https://doi.org/10.1007/s00401-010-0718-6

Iadecola, C., 2004. Neurovascular regulation in the normal brain and in Alzheimer's disease.

Nat. Rev. Neurosci. 5, 347–360. https://doi.org/10.1038/nrn1387

Iturria-Medina, Y., Sotero, R.C., Toussaint, P.J., Mateos-Pérez, J.M., Evans, A.C., Initiative, T.A.D.N., 2016. Early role of vascular dysregulation on late-onset Alzheimer's disease based on multifactorial data-driven analysis. Nat. Commun. 7, 11934. https://doi.org/10.1038/ncomms11934

Khajehpour, M., Rietveld, I., Vinogradov, S., Prabhu, N.V, Sharp, K.A., Vanderkooi, J.M., 2003. Accessibility of Oxygen With Respect to the Heme Pocket in Horseradish Peroxidase. PROTEINS Struct. Funct. Genet. 53, 656–666.

Kisler, K., Nelson, A.R., Montagne, A., Zlokovic, B.V., 2017a. Cerebral blood flow regulation and neurovascular dysfunction in Alzheimer disease. Nat. Rev. Neurosci. 18, 419–434. https://doi.org/10.1038/nrn.2017.48

Kisler, K., Nelson, A.R., Rege, S.V, Ramanathan, A., Wang, Y., Ahuja, A., Lazic, D., Tsai, P.S., Zhao, Z., Zhou, Y., Baos, D.A., Sakadzic, S., Zlokovic, B.V, 2017b. Pericyte degeneration leads to neurovascular uncoupling and limits oxygen supply to brain. Nat. Neurosci. 20, 406–416. https://doi.org/10.1038/nn.4489

Kitaguchi, H., Ihara, M., Saiki, H., Takahashi, R., Tomimoto, H., 2007. Capillary beds are decreased in Alzheimer's disease, but not in Binswanger's disease. Neurosci. Lett. 417, 128–131. https://doi.org/10.1016/j.neulet.2007.02.021

Langan, L.M., Dodd, N.J.F., Owen, S.F., Purcell, W.M., Jackson, S.K., Jha, A.N., 2016. Direct Measurements of Oxygen Gradients in Spheroid Culture System Using Electron Parametric Resonance Oximetry. PLoS One 11, e0149492. https://doi.org/10.1371/journal.pone.0149492

Larson, E.B., Wang, L., Bowen, J.D., Mccormick, W.C., Teri, L., Crane, P., Kukull, W., 2006. Exercise Is Associated with Reduced Risk for Incident Dementia among Persons 65 Years of Age and Older. Ann. Intern. Med. 144, 73–81.

Latest information and statistics [WWW Document], 2018. . Alzheimer's Soc. Canada. URL https://alzheimer.ca/en/Home/Get-involved/Advocacy/Latest-info-stats

Laurent, S., Ejtehadi, M.R., Rezaei, M., Kehoe, P.G., Mahmoudi, M., 2012. Interdisciplinary challenges and promising theranostic effects of nanoscience in Alzheimer's disease. RSC Adv. 2, 5008–5033. https://doi.org/10.1039/c2ra01374f

Lecoq, J., Parpaleix, A., Roussakis, E., Ducros, M., Houssen, Y.G., Vinogradov, S.A., Charpak, S., 2011. Simultaneous two-photon imaging of oxygen and blood flow in deep cerebral vessels. Nat Med. 17, 893–898. https://doi.org/10.1016/j.pain.2013.06.005.Re-Thinking

Lecoq, J., Tiret, P., Najac, M., Shepherd, G.M., Greer, C.A., Charpak, S., 2009. Odor-Evoked Oxygen Consumption by Action Potential and Synaptic Transmission in the Olfactory Bulb. J. Neurosci. 29, 1424–1433. https://doi.org/10.1523/jneurosci.4817-08.2009

Lévy, B.I., Lesage, F., Lefebvre, J., Tardif, P.-L., Pouliot, P., Delafontaine-Martel, P., 2018. Whole brain vascular imaging in a mouse model of Alzheimer's disease with two-photon microscopy. J. Biomed. Opt. 23, 1. https://doi.org/10.1117/1.jbo.23.7.076501

Lin, A.-L., Fox, P.T., Hardies, J., Duong, T.Q., Gao, J.-H., 2010. Nonlinear coupling between cerebral blood flow, oxygen consumption, and ATP production in human visual cortex. Proc. Natl. Acad. Sci. 107, 8446–8451. https://doi.org/10.1073/pnas.0909711107

Lyons, D., 2015. Mapping oxygen in the awake mouse brain. Universit_e Pierre et Marie Curie - Paris VI.

Masamoto, K., Takizawa, N., Kobayashi, H., Oka, K., Tanishita, K., 2003. Dual responses of tissue partial pressure of oxygen after functional stimulation in rat somatosensory cortex. Brain Res. 979, 104–113. https://doi.org/10.1016/S0006-8993(03)02882-8

Michaud, J.P., Bellavance, M.A., Préfontaine, P., Rivest, S., 2013. Real-time in vivo imaging reveals the ability of monocytes to clear vascular amyloid beta. Cell Rep. 5, 646–653. https://doi.org/10.1016/j.celrep.2013.10.010

Michels, L., Warnock, G., Buck, A., Macauda, G., Leh, S.E., Kaelin, A.M., Riese, F., Meyer, R., O'gorman, R., Hock, C., Kollias, S., Gietl, A.F., 2016. Arterial spin labeling imaging

reveals widespread and Aβ-independent reductions in cerebral blood flow in elderly apolipoprotein epsilon-4 carriers. J. Cereb. Blood Flow Metab. 36, 581–595. https://doi.org/10.1177/0271678X15605847

Moeini, M., Lu, X., Avti, P.K., Damseh, R., Bélanger, S., Picard, F., Boas, D., Kakkar, A., Lesage, F., 2018. Compromised microvascular oxygen delivery increases brain tissue vulnerability with age. Sci. Rep. 8, 8219.

Moeini, M., Lu, X., Bélanger, S., Picard, F., Boas, D., Kakkar, A., Lesage, F., 2019. Cerebral tissue pO2 response to stimulation is preserved with age in awake mice. Neurosci. Lett. 699, 160–166.

Montine, T.J., Koroshetz, W.J., Babcock, D., Dickson, D.W., Galpern, W.R., Maria Glymour, M., Greenberg, S.M., Hutton, M.L., Knopman, D.S., Kuzmichev, A.N., Manly, J.J., Marder, K.S., Miller, B.L., Phelps, C.H., Seeley, W.W., Sieber, B.A., Silverberg, N.B., Sutherland, M., Torborg, C.L., Waddy, S.P., Zlokovic, B.V., Corriveau, R.A., 2014. Recommendations of the alzheimer's disease-related dementias conference. Neurology 83, 851–860. https://doi.org/10.1212/WNL.0000000000000733

Mueggler, T., Baumann, D., Rausch, M., Staufenbiel, M., Rudin, M., 2003. Age-dependent impairment of somatosensory response in the amyloid precursor protein 23 transgenic mouse model of Alzheimer's disease. J. Neurosci. 23, 8231–6. https://doi.org/23/23/8231 [pii]

Nazem, A., Sankowski, R., Bacher, M., Al-Abed, Y., 2015. Rodent models of neuroinflammation for Alzheimer's disease. J. Neuroinflammation 12, 1–15. https://doi.org/10.1186/s12974-015-0291-y

Ndubuizu, O., LaManna, J.C., 2007. Brain Tissue Oxygen Concentration Measurements. Antioxid. Redox Signal. 9, 1207–1220. https://doi.org/10.1089/ars.2007.1634

Nguyen, N., Myllylä, E., Shan, C.-E., Gerasimenko, O., Nyári, J., 2014. Dissolved Oxygen Sensors [WWW Document]. Sens. Technol. URL https://wiki.metropolia.fi/display/sensor/Dissolved+Oxygen+Sensors

Nielsen, R.B., Egefjord, L., Angleys, H., Mouridsen, K., Gejl, M., Møller, A., Brock, B., Brændgaard, H., Gottrup, H., Rungby, J., Eskildsen, S.F., Østergaard, L., 2017. Capillary dysfunction is associated with symptom severity and neurodegeneration in Alzheimer's disease. Alzheimer's Dement. 13, 1143–1153. https://doi.org/10.1016/j.jalz.2017.02.007

Nippert, A.R., Mishra, A., Newman, E.A., 2018. Keeping the Brain Well Fed: The Role of Capillaries and Arterioles in Orchestrating Functional Hyperemia. Neuron 99, 248–250. https://doi.org/10.1016/j.neuron.2018.07.011

Niwa, K., Younkin, L., Ebeling, C., Turner, S.K., Westaway, D., Younkin, S., Ashe, K.H., Carlson, G.A., Iadecola, C., 2000. Abeta 1-40-related reduction in functional hyperemia in mouse neocortex during somatosensory activation. Proc. Natl. Acad. Sci. 97, 9735–9740. https://doi.org/10.1073/pnas.97.17.9735

Østergaard, L., Aamand, R., Gutiérrez-Jiménez, E., Ho, Y.C.L., Blicher, J.U., Madsen, S.M., Nagenthiraja, K., Dalby, R.B., Drasbek, K.R., Møller, A., Brændgaard, H., Mouridsen, K., Jespersen, S.N., Jensen, M.S., West, M.J., 2013. The capillary dysfunction hypothesis of Alzheimer's disease. Neurobiol. Aging 34, 1018–1031. https://doi.org/10.1016/j.neurobiolaging.2012.09.011

Quaranta, M., Borisov, S.M., Klimant, I., 2012. Indicators for optical oxygen sensors. Bioanal Rev 4, 115–157. https://doi.org/10.1007/s12566-012-0032-y

R.L., R., J.S., M., K.F., M., 1990. After reaching retirement age physical activity sustains cerebral perfusion and cognition. J. Am. Geriatr. Soc. 38, 123–128.

Radak, Z., Hart, N., Sarga, L., Koltai, E., Atalay, M., Ohno, H., Boldogh, I., 2010. Exercise plays a preventive role against Alzheimer's disease. J. Alzheimer's Dis. 20, 777–783.

Reusch, W., 2013. Mass spectrometry [WWW Document]. URL https://www2.chemistry.msu.edu/faculty/reusch/virttxtjml/spectrpy/massspec/masspec1.htm

Rigaud-Monnet, A.S., Pinard, E., Borredon, J., Seylaz, J., 1994. Blockade of nitric oxide synthesis inhibits hippocampal hyperemia in kainic acid-induced seizures. J. Cereb.

Blood Flow Metab. 14, 581–590. https://doi.org/10.1038/jcbfm.1994.72

Rozhkov, V., Wilson, D., Vinogradov, S., 2002. Phosphorescent Pd Porphyrin−Dendrimers: Tuning Core Accessibility by Varying the Hydrophobicity of the Dendritic Matrix. Macromolecules 35, 1991–1993.

Ruitenberg, A., denHeijer, T., Bakker, S.L.M., vanSwieten, J.C., Koudstaal, P.J., Hofman, A., Breteler, M.M.B., 2005. Cerebral hypoperfusion and clinical onset of dementia: The Rotterdam study. Ann. Neurol. 57, 789–794. https://doi.org/10.1002/ana.20493

Rungta, R.L., Chaigneau, E., Osmanski, B.F., Charpak, S., 2018. Vascular Compartmentalization of Functional Hyperemia from the Synapse to the Pia. Neuron 99, 362-375.e4. https://doi.org/10.1016/j.neuron.2018.06.012

Sakadži, S., Roussakis, E., Yaseen, M.A., Mandeville, E.T., Srinivasan, J., Arai, K., Ruvinskaya, S., Devor, A., Lo, E.H., Sergei, A., Boas, D.A., 2010. Two-photon high-resolution measurement of partial pressure of oxygen in cerebral vasculature and tissue. Nat Methods 7, 755–759. https://doi.org/10.1038/nmeth.1490.Two-photon

Sakadžić, S., Mandeville, E.T., Gagnon, L., Musacchia, J.J., Yaseen, M.A., Yucel, M.A., Lefebvre, J., Lesage, F., Dale, A.M., Eikermann-Haerter, K., Ayata, C., Srinivasan, V.J., Lo, E.H., Devor, A., Boas, D.A., 2014. Large arteriolar component of oxygen delivery implies a safe margin of oxygen supply to cerebral tissue. Nat. Commun. 5. https://doi.org/10.1038/ncomms6734

Sakadžic, S., Yaseen, M.A., Jaswal, R., Roussakis, E., Dale, A.M., Buxton, R.B., Vinogradov, S.A., Boas, D.A., Devor, A., 2016. Two-photon microscopy measurement of cerebral metabolic rate of oxygen using periarteriolar oxygen concentration gradients. Neurophotonics 3, 045005. https://doi.org/10.1117/1.nph.3.4.045005

Santisakultarm, T.P., Paduano, C.Q., Stokol, T., Southard, T.L., Nishimura, N., Skoda, R.C., Olbricht, W.L., Schafer, A.I., Silver, R.T., Schaffer, C.B., 2014. Stalled cerebral capillary blood flow in mouse models of essential thrombocythemia and polycythemia vera revealed by in vivo two-photon imaging. J. Thromb. Haemost. 12, 2120–2130.

https://doi.org/10.1111/jth.12738

Shen, J., Sood, R., Weaver, J., Timmins, G.S., Schnell, A., Miyake, M., Kao, J.P.Y., Rosen, G.M., Liu, K.J., 2009. Direct visualization of mouse brain oxygen distribution by electron paramagnetic resonance imaging: Application to focal cerebral ischemia. J. Cereb. Blood Flow Metab. 29, 1695–1703. https://doi.org/10.1038/jcbfm.2009.89

Shonat, R.D., Kight, A.C., 2003. Oxygen tension imaging in the mouse retina. Ann. Biomed. Eng. 31, 1084–1096. https://doi.org/10.1114/1.1603256

Snyder, H.M., Carrillo, M.C., Grodstein, F., Henriksen, K., Jeromin, A., Lovestone, S., Mielke, M.M., O'Bryant, S., Sarasa, M., Sjøgren, M., Soares, H., Teeling, J., Trushina, E., Ward, M., West, T., Bain, L.J., Shineman, D.W., Weiner, M., Fillit, H.M., 2014. Developing novel blood-based biomarkers for Alzheimer's disease. Alzheimer's Dement. 10, 109–114. https://doi.org/10.1016/j.jalz.2013.10.007

Stefanovic, B., Hutchinson, E., Yakovleva, V., Schram, V., Russell, J.T., Belluscio, L., Koretsky, A.P., Silva, A.C., 2008. Functional reactivity of cerebral capillaries. J. Cereb. Blood Flow Metab. 28, 961–972. https://doi.org/10.1038/sj.jcbfm.9600590

Swartz, H., Williams, B., Zaki, B., Hartford, A., Jarvis, L., Chen, E., Comi, R., Ernstoff, M., Hou, H., Khan, N., Swarts, S., Flood, A., Kuppusamy, P., 2014. Clinical EPR: unique opportunities and some challenges. Acad. Radiol. 21, 197–206. https://doi.org/10.1016/j.acra.2013.10.011.Clinical

Sweeney, M.D., Sagare, A.P., Zlokovic, B.V., 2011. Cerebrospinal fluid biomarkers of neurovascular dysfunction in mild dementia and Alzheimer's disease. J. Cereb. Blood Flow Metab. 42, 1055–1068. https://doi.org/10.1038/jcbfm.2015.76

Toledo, J.B., Arnold, S.E., Raible, K., Brettschneider, J., Xie, S.X., Grossman, M., Monsell, S.E., Kukull, W.A., Trojanowski, J.Q., 2013. Contribution of cerebrovascular disease in autopsy confirmed neurodegenerative disease cases in the National Alzheimer's Coordinating Centre. Brain 136, 2697–2706. https://doi.org/10.1093/brain/awt188

Vazquez, A.L., Masamoto, K., Fukuda, M., Kim, S.G., 2010. Cerebral oxygen delivery and

consumption during evoked neural activity. Front. Neuroenergetics 2, 1–12. https://doi.org/10.3389/fnene.2010.00011

Vinogradov, S.A., Lo, L., Wilson, D.F., 1999. Dendritic Polyglutamic Porphyrins : Probing Porphyrin Protection by Oxygen-Dependent Quenching of Phosphorescence. Chem Eur. J. 5, 1338–1347.

Wang, M., Iliff, J.J., Liao, Y., Chen, M.J., Shinseki, M.S., Venkataraman, A., Cheung, J., Wang, W., Nedergaard, M., 2012. Cognitive Deficits and Delayed Neuronal Loss in a Mouse Model of Multiple Microinfarcts. J. Neurosci. 32, 17948–17960. https://doi.org/10.1523/JNEUROSCI.1860-12.2012

Wardlaw, J.M., Smith, E.E., Biessels, G.J., Cordonnier, C., Fazekas, F., Frayne, R., Lindley, R.I., O'Brien, J.T., Barkhof, F., Benavente, O.R., Black, S.E., Brayne, C., Breteler, M., Chabriat, H., DeCarli, C., deLeeuw, F.E., Doubal, F., Duering, M., Fox, N.C., Greenberg, S., Hachinski, V., Kilimann, I., Mok, V., Oostenbrugge, R.van, Pantoni, L., Speck, O., Stephan, B.C.M., Teipel, S., Viswanathan, A., Werring, D., Chen, C., Smith, C., vanBuchem, M., Norrving, B., Gorelick, P.B., Dichgans, M., 2013. Neuroimaging standards for research into small vessel disease and its contribution to ageing and neurodegeneration. Lancet Neurol. 12, 822–838. https://doi.org/10.1016/S1474-4422(13)70124-8

Weaver, J., Liu, K., 2017. In vivo electron paramagnetic resonance oximetry and applications in the brain. Med. Gas Res. 7, 56. https://doi.org/10.4103/2045-9912.202911

Wong-Goodrich, S.J., Pfau, M.L., Flores, C.T., Fraser, J.A., Williams, C.L., Jones, L.W., 2010. Voluntary running prevents progressive memory decline and increases adult hippocampal neurogenesis and growth factor expression after whole-brain irradiation. Cancer Res. 70, 9329–9338.

YSI, 2009. The Dissolved Oxygen Handbook, YSI.

Zhang, Cong, Bélanger, S., Pouliot, P., Lesage, F., 2015. Measurement of local partial pressure of oxygen in the brain tissue under normoxia and epilepsy with

phosphorescence lifetime microscopy. PLoS One 10, e0135536.

Zhang, F., Eckman, C., Younkin, S., Hsiao, K.K., Iadecola, C., 1997. Increased Susceptibility to Ischemic Brain Damage in Transgenic Mice Overexpressing the Amyloid Precursor Protein. J. Neurosci. 17, 7655–7661. https://doi.org/10.1523/jneurosci.17-20-07655.1997

Zlokovic, B.V., 2011. Neurovascular pathways to neurodegeneration in Alzheimer's disease and other disorders. Nat Rev Neurosci 12, 723–738.